



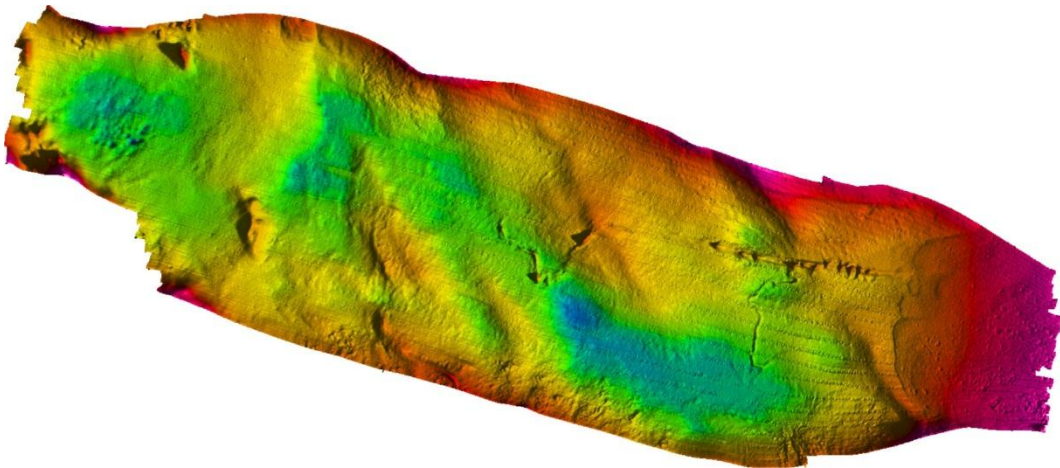
GEO-3900

MASTER'S THESIS IN GEOLOGY

Sedimentary Processes and Palaeoenvironment in Van Keulenfjorden,
Spitsbergen

Philipp Kempf

May, 2011



Faculty of Science and Technology

Department of Geology

University of Tromsø

GEO-3900
MASTER'S THESIS IN GEOLOGY

Sedimentary Processes and Palaeoenvironment in Van Keulenfjorden,
Spitsbergen

Philipp Kempf

May, 2011

Abstract

Swath bathymetry, high resolution seismic and core data are analysed to describe the Late Weichselian and Holocene sedimentary processes and palaeoenvironment in Van Keulenfjorden, Spitsbergen.

Bottom currents, the bathymetry of the fjord and the distance from sediment sources are the controlling factors for the sediment distribution as indicated by isopach maps. Sandur deltas at the mouth of tributary valleys cause repeated mass-transport along the slopes. Rapid postglacial isostatic uplift reactivated faults of the West Spitsbergen fold and thrust belt, which acted as pathways for thermogenic gas creating pockmarks.

The results from this study confirm previous indications that an ice stream drained the Late Weichselian Barents Sea Ice Sheet through Van Keulenfjorden. The deglaciation of the fjord began ~ 11.2 cal. ka BP with a retreat rate of ~ 160 m a⁻¹. A hiatus between 10.7 cal. ka BP and 7.0 cal. ka BP in the outer part of the fjord was most likely caused by bottom currents.

Following a warm period between 10.7 cal. ka BP and min. 7.0 cal. ka BP increasing IRD content indicates slow but steady cooling. Glacial activity in the Holocene peaked at 2.8 cal. ka BP, resulting in the deposition of morainal banks. Adjacent to these morainal banks two debris flow lobes were deposited. They are interpreted to be the product of two consecutive surges. This contradicts the conclusions of previous investigations, where the upper lobe is interpreted to be from the Little Ice Age. Since 2.8 cal. ka BP the glacial activity was relatively constant. The terminal position of the Nathorstbreen from 2.8 cal. ka BP was reached in the late 19th century. While the work of this study was conducted Nathorstbreen surged and almost reached the front position from 2.8 cal. ka BP again.

Acknowledgements

In March 2010 I began to work on this master thesis. Since then I lived to see a summer that was not a summer, I saw nights without darkness and days without light. In contrast to these unreal experiences I met very real people to whom I send out my very real gratitude.

First and foremost I want to thank my supervisor Dr. Matthias Forwick. Matze, you have been supportive in every single way possible. If it was a scientific problem, a writer's block, a motivational low, the search for a PhD position or even the acute need of biscuits to nibble on during periods of major sea sickness, you have always helped me out. Every master student can consider him- or herself lucky to have you as a supervisor. For this and more: Vielen Dank!

Prof. Dr. Tore O. Vorren is thanked for inspiring discussions. I often got the feeling that you always knew where the discussions would lead to. Thank you for bearing with me. I think it takes a well-structured and patient mind to follow my winding train of thought, especially if you are already waiting at the terminal stop. Your genuine interest besides the studies was most appreciated. One does not leave Tores office without an "og ellers, går det bra med deg?". Tusen hjertelig takk.

Dr. Jan Sverre Laberg deserves my gratitude for giving me the opportunity to repeatedly prove that I am not a born sailor man and work as a student assistant on R/V Jan Mayen in summer 2010. You make science look simple in a matter-of-factly manner, especially when it is not. For the inspiring talk that launched my discussion chapter I want to thank you dearly. I needed it. Tusen hjertelig takk.

Steinar Iversen made sure the geophysical data were correctly obtained. Trine Dahl, Kristina Hansen and Edel Ellingsen always knew the tricks in the lab. Nicole J. Baeten, Noortje Dijkstra, Diane Groot and Tom Arne Rydningen corrected my very first drafts of the introductory chapters and searched for typos in the almost finished version. Prof. Stefan Bünz, Lilja Run Bjarnadóttir and Jan Petter Holm were greatly helpful with software issues.

Acknowledgements

All these helping hands made me take the speed bumps that you are bound to come across in course of a master thesis so much smoother. Takk, bedankt, danke.

The fellow students are thanked for a fantastic time in the blå brakka. Elisabeth, Lene, Kenneth and Kjetil and more always had an ear for useless but fun rants when the stress was peaking.

My dear friends are thanked for taking care of my sometimes lost self. They are responsible for my most productive and most unproductive times. Nicole J. Baeten, Noortje Dijkstra and Marianne Negrini shall here be named representatively for many more.

To my parents I owe everything. You are my role model for leading a good life. How you manage to be outstanding to all intents and purposes is beyond me. You ensure I keep my perspective and encourage me to take the road less travelled by.

Yours sincerely

Philipp Kempf

Table of Content

1	Preface	1
1.1	Objectives.....	1
1.2	Project Affiliation.....	1
2	Introduction	3
2.1	Glacial History of Spitsbergen	3
2.2	Holocene Palaeoclimate of Spitsbergen	4
2.3	Previous Investigations of the Study Area	6
2.4	Physiographic Setting	8
2.4.1	Geomorphology.....	9
2.4.2	Climate	11
2.4.3	Oceanography	13
2.4.4	Glaciology	17
2.5	Geology.....	20
2.5.1	Tectonic History	20
2.5.2	Bedrock Geology	23
3	Material and Methods.....	25
3.1	Swath Bathymetry.....	25
3.2	Chirp Sonar	26
3.3	Sediment Cores.....	27
3.4	Laboratory Work on the Sediment Cores.....	29
3.4.1	Multi-Sensor Core Logger	29
3.4.1.1	γ -Ray Attenuation	30
3.4.1.2	P-Wave Velocity System.....	30
3.4.1.3	Magnetic Susceptibility Loop Sensor.....	31
3.4.1.4	Temperature Measurement.....	31
3.4.2	Opening of the Cores.....	31
3.4.3	X-Ray Photography.....	32
3.4.4	XRF-Scanner	32
3.4.5	Sedimentological Logs.....	33
3.4.6	Wet Sieving.....	33
3.4.7	Dry Sieving	33
3.4.8	Sedigraph	33

3.4.9	Shear Strength Analysis	34
3.4.10	Radiocarbon Dating.....	34
3.4.10.1	Basic Principles	34
3.4.10.2	Accelerator Mass Spectrometry (AMS)	35
3.4.10.3	Marine Reservoir Effects.....	35
4	Swath Bathymetry.....	37
4.1	Large Scale Morphology and Bedrock Related Ridges	37
4.2	Short Linear Ridges	40
4.3	Eskers	41
4.4	Mass-Transport Deposits.....	43
4.5	Pockmarks	46
5	Chirp Sonar	49
5.1	Seismostratigraphy and Sedimentary Architecture	49
5.1.1	Unit Vk0.....	53
5.1.2	Unit Vk1	54
5.1.3	Unit Vk2.....	57
5.1.4	Unit Vk3.....	58
5.1.5	Unit Vk4.....	60
5.1.5.1	Sub-Unit Vk4.1	60
5.1.5.2	Sub-Unit Vk4.2	62
6	Lithostratigraphy	65
6.1	Core Site JM07-012.....	66
6.1.1	Box Core JM07-012-BC	66
6.1.1.1	Unit 12BC-1 (25 – 0 cm).....	67
6.1.2	Gravity Core JM07-012-GC.....	69
6.1.2.1	Unit 12GC-1 (270 – 244 cm)	69
6.1.2.2	Unit 12GC-2 (244 – 208 cm)	73
6.1.2.3	Unit 12GC-3 (208 – 0 cm)	74
6.1.2.4	XRF-Data of Core JM07-012-GC	75
6.1.3	Piston Core JM07-012-PC	77
6.1.3.1	Unit 12PC-1 (382 – 339 cm)	77
6.1.3.2	Unit 12PC-2 (339 – 28 cm).....	77
6.1.3.3	Unit 12PC-3 (28 – 0 cm)	81
6.1.3.4	XRF-Data of Core JM07-012-PC.....	82
6.1.3.5	Correlation between Cores JM07-012-GC and JM07-012-PC.....	83

6.1.4	Deductions from the Core Data of Core Site JM07-012	83
6.2	Core Site JM07-014.....	83
6.2.1	Box Core JM07-014-BC	83
6.2.1.1	Unit 14BC-1 (26 – 0 cm).....	84
6.2.2	Gravity Core JM07-014-GC.....	84
6.2.2.1	Unit 14GC-1 (270 – 109 cm)	88
6.2.2.2	Unit 14GC-2 (109 – 0 cm)	88
6.2.2.3	XRF-Data of Core JM07-014-GC.....	89
6.2.3	Piston Core JM07-014-PC	90
6.2.3.1	Unit 14PC-1 (538 – 88 cm).....	91
6.2.3.2	Unit 14PC-2 (88 – 0 cm).....	95
6.2.3.3	XRF-Data of Core JM07-014-PC.....	95
6.2.4	Deductions from the Core Data of Core Site JM07-014	95
7	Discussion.....	97
7.1	Correlation of the Litho- and Seismostratigraphy	97
7.2	Chronology	99
7.3	Sedimentation Rates.....	102
7.4	Sedimentary Processes.....	103
7.4.1	Sub- and Proglacial Processes	103
7.4.2	Suspension Fall-Out	104
7.4.3	Ice Rafted Debris (IRD)	105
7.4.4	Mass-Transport Deposits.....	106
7.4.5	Glacifluvial Sediment Input from Tributary Valleys	108
7.4.6	Hiatus	108
7.5	Deglaciation and Holocene Environment in Van Keulenfjorden.....	110
7.5.1	Deglaciation from Shelf break to Fjord Mouth, from 17400 cal. yrs. BP to 11260 cal. yrs. BP (10400 ¹⁴ C yrs. BP)	110
7.5.2	Deglaciation of Van Keulenfjorden, from 11260 cal. yrs. BP to 10660 cal. yrs. BP	113
7.5.3	Climatic Optimum in Van Keulenfjorden, min. 10660 cal. yrs. BP to 6750 cal. yrs. BP	117
7.5.4	Cooling in Van Keulenfjorden, from ~6750 cal. yrs. BP to 2780 cal. yrs. BP.....	119
7.5.5	Glacial Advances in Van Keulenfjorden, from 2780 cal. yrs. BP to present	121
8	Summary and Conclusions.....	125
	References.....	129

1 Preface

1.1 Objectives

The objectives of this master thesis at the Department of Geology at the University of Tromsø are

- i) to establish a seismostratigraphy of the Late Weichselian to Holocene succession and compare it to recent research results from other fjords on the west coast of Spitsbergen.
- ii) to describe and interpret the assemblage of sedimentary processes and products in order to describe the sedimentary palaeoenvironment
- iii) to paste the entity of this study's conclusions into the bigger picture of the geoscientific research of Svalbard

1.2 Project Affiliation

This study was carried out between September 2009 and May 2011 at the Department of Geology, University of Tromsø (UiTø), Norway. It is part of the strategic university programme *Sedimentary Processes and Palaeoenvironments on Northern Continental Margins* (SPONCOM), funded by the Research Council of Norway. The overall goal of this program is to assess the changes in the physical environment of the seafloor and overlying water and ice in selected fjords and continental margins in northern Norway and West Spitsbergen during the last glacial – interglacial cycle.

Glacial history is very important because of its close relationship to climate change. This relationship is not yet fully understood and needs more investigation

(<http://www.ig.uit.no/sponcom/>).

2 Introduction

2.1 Glacial History of Spitsbergen

The West Spitsbergen fjord systems acted as pathways of fast-flowing ice streams that drained the Late Weichselian Barents Sea ice sheet (Mangerud et al., 1987, Landvik et al., 1998, Landvik et al., 2005, Ottesen et al., 2005, Ottesen and Dowdeswell, 2006, Ottesen et al., 2007, Dowdeswell et al., 2008, Baeten et al., 2010a). The final deglaciation of the ice sheet at the shelf margin started around 17.9 cal. ka BP (thousands of calendar years before present). The retreat from that outermost position was rapid, but it was interrupted by a readvance to the mid-shelf shortly after 14.3 cal. ka BP (Elverhøi et al., 1995a, Svendsen et al., 1996). According to Mangerud et al. (1992) and Svendsen et al. (1996) shortly after 14.3 cal. ka BP the glacier retreated from Bellsund to the fjord basins of Van Mijenfjorden and Van Keulenfjorden (fig. 2.1).

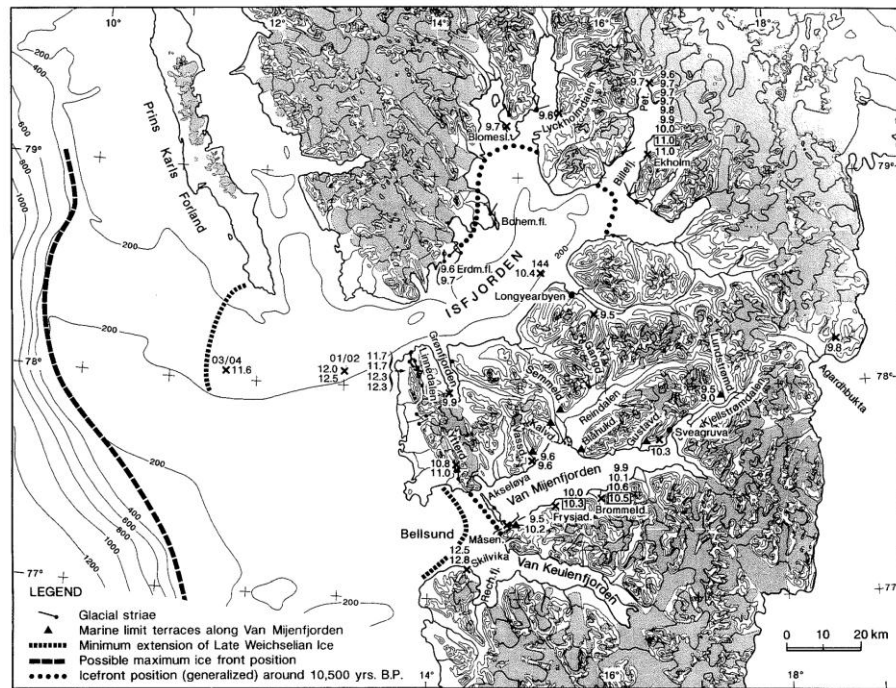


Figure 2.1 Map of central Spitsbergen and the west coast, with Isfjorden trough and Bellsund. Indicated are ice marginal positions at various times, see legend (from Mangerud et al., 1992).

On the Norwegian coast a prominent glacial readvance in the Younger Dryas chronozone from c. 12.9 to 11.6 cal. ka BP (11.0 to 10.0 ¹⁴C ka BP, thousands of radiocarbon years before present) is described (e.g. Mangerud et al., 1974, Plassen and Vorren, 2003). However, the local western Spitsbergen cirque glaciers are thought to have been smaller during the Younger Dryas than at the Little Ice Age maximum extent (~1890 AD; Mangerud and Landvik, 2007). On the basis of lithological analyses Forwick and Vorren (2009) suggested that a period of a relative increase in sea-ice rafted debris and/or decreased iceberg rafted debris within stratified glacial marine sediments might reflect a Younger Dryas readvance. Recently, evidence from 2D seismic lines in form of sediment wedges and moraines correlated to a Younger Dryas readvance of ~25 km have been found in the Isfjorden area (Forwick and Vorren, 2011).

The final retreat into the inner fjord systems, e.g. Van Keulenfjorden, Van Mijenfjorden, Tempelfjorden and Billefjorden, finished c. 10.9 cal. ka BP (Elverhøi et al., 1995a, Svendsen et al., 1996, Mangerud et al., 1998, Lønne, 2005, Forwick and Vorren, 2009, Baeten et al., 2010a). Before 10.9 cal. ka BP the isostatic uplift along the ice-free coast of western Svalbard was low (Landvik et al., 1987, Forman, 1990, Forman et al., 2004). After 10.9 cal. ka BP the entire archipelago, especially on the west coast, emerged rapidly. It was therefore proposed that the glaciers on eastern Spitsbergen might have built up mass undergoing a Younger Dryas readvance synchronously to the Norwegian mainland glaciers, and thus withholding the uplift (Landvik et al., 1987, Svendsen et al., 1996).

2.2 Holocene Palaeoclimate of Spitsbergen

The Holocene climatic development is described by Birks (1991) based on a plant ecology study on mainly seeds and fruits. Between 9.0 and 4.0 cal. ka BP the climate was inferred to be similar to today's climate with at least 1.5 °C higher summer temperatures. The Holocene increase in summer temperature on Spitsbergen was independently backed up by thermophilous shells, *Mytilus edulis* (Salvigsen et al., 1990). Further research has shown that during this time glaciers were small or non-existent (fig. 2.2; Svendsen and Mangerud, 1997). During this loosely defined Holocene Climatic Optimum most, if not all glaciers on the Norwegian mainland have been melted completely at least once (Nesje et al., 2005). For

Bjørnøya the Holocene Climatic Optimum lasted from ~11.2 cal. ka BP to 9.3 cal ka BP (Wohlfarth et al., 1995). Hald et al. (2004) and Forwick & Vorren (2009) suggest a cooling period after a marked warm period between 11.2 and 9.0 cal. ka BP at the West Spitsbergen margin and in Isfjorden, respectively.

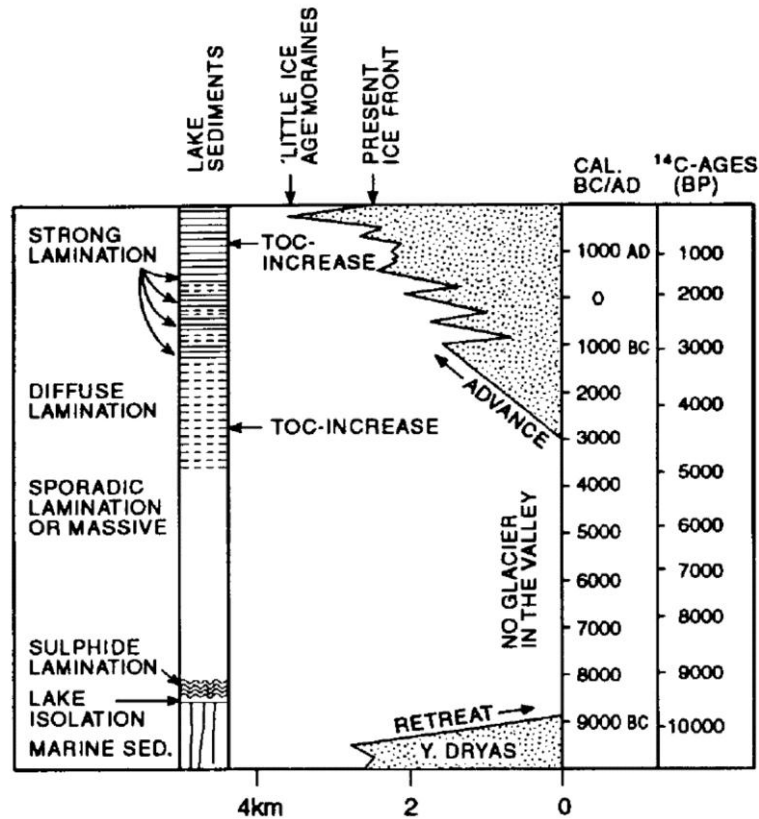


Figure 2.2: Time distance glaciation diagram for the valley glacier Linnébreen, western Spitsbergen, deduced from the stratigraphy in the downstream lake Linnévatnet (from Svendsen and Mangerud, 1997).

From 4.0 to 2.5 cal. ka BP a colder climate is proposed (Birks, 1991, Svendsen and Mangerud, 1997). This colder period is not displayed in the SSTs (Hald et al., 2004). For the last 2.5 cal. ka BP the records show rather constant climatic conditions (Birks, 1991, Baeten et al., 2010a, Forwick et al., 2010).

Ice rafted debris (IRD) is present during the whole Holocene sedimentary succession in Van Mijenfjorden, Isfjorden and tributary fjords indicating that central Spitsbergen has

never been entirely deglaciated during this interglacial period (Hald et al., 2004, Forwick and Vorren, 2009, Baeten et al., 2010a).

2.3 Previous Investigations of the Study Area

Bratlie (1994) focused on denudation rates and glacial activity in Van Keulenfjorden. The total Quaternary sediment succession comprises 120 to 230 ms of two-way-travel-time (TWT). If calculated with an average p-wave velocity of 1600 ms^{-1} this translates into 96 to 184 m thickness (Bratlie, 1994). An AMS-radiocarbon date of a reworked shell fragment *Portlandia arctica* gave an age of $11160 \pm 150 \text{ cal. ka BP}$ ($10263 \pm 122 \text{ }^{14}\text{C yrs. BP}$) from the north-western part of Van Keulenfjorden (Bratlie, 1994). Though the shell fragment is reworked this age indicates that glacial marine sedimentation started as early as c. 11.2 cal. ka BP in Van Keulenfjorden. This goes in line with the start of the postglacial sedimentation for Van Mijenfjorden at c. 11.30 cal. ka BP (Mangerud et al., 1992).

In 1898 a topographic map was made in the Van Keulenfjorden area showing Nathorstbreen (the main tidewater glacier occupying the fjord head) terminating at the lateral moraines that flank the inner fjord (Hamberg, 1905 after Ottesen et al., 2008). A submerged morainal bank ridge crosses the fjord just beyond the western ends of the lateral moraines on land and is interpreted as the contemporary terminal moraine from the Little Ice Age. Within ~30 yrs. Nathorstbreen had advanced ~12 km and then retreated 3 km (fig. 2.3). This strongly suggests a surge advance in the late 19th century (Ottesen et al., 2008).

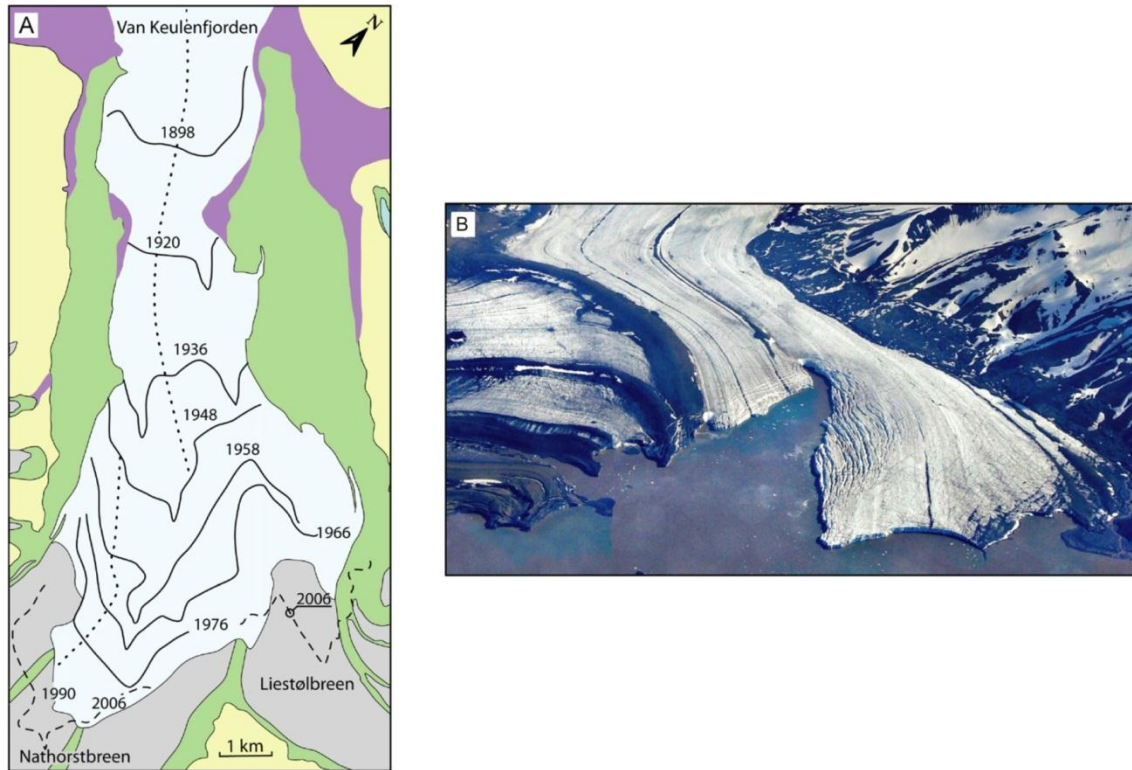


Figure 2.3: a) calving front development map since the Little Ice Age of Nathorstbreen Glacier System reconstructed from maps and aerial photographs (Liestøl, 1977, Ottesen et al., 2008), b) aerial photograph of the calving front of Doktorbreen (left) and Liestølbreen (right) from July 2006. Note the strongly indented tidewater glacier front line, very much like those indicated on the map and the highly turbid water entering the fjord (from Ottesen et al., 2008).

Furthermore, looped moraines are indicated at the southern side of the glacier tongue on the Hamberg map from 1898 (Ottesen et al., 2008), which provides additional evidence for a glacier surge (Meier and Post, 1969). Looped moraines are also visible on aerial photographs of currently quiescent tributaries of Nathorstbreen. They are especially clear on Doktorbreen verifying the surge-type characteristic of the tributary glaciers of the fjord head glacier front (Ottesen et al., 2008).

On the basis of swath bathymetry in the inner basin of Van Keulenfjorden a variety of typical glacial morphologic features is described. In front of Nathorstbreen mega-scale glacial lineation (MSGSL), eskers, De Geer moraines (annual recessional moraines) and

rhombohedral crevasse fill/squeeze ridges are identified (Ottesen et al., 2008). However, this assemblage of subglacial landforms was formed by the Little Ice Age advance, which was restricted to the inner basin of Van Keulenfjorden. This study focuses on the outer fjord basin.

2.4 Physiographic Setting

Spitsbergen is the largest island (~ 39.044 km²) of the Norwegian arctic archipelago of Svalbard and situated between 74° and 81°N and 10° and 35°E. The west coast is dominated by fjord systems facing the Norwegian Sea (fig. 2.4).

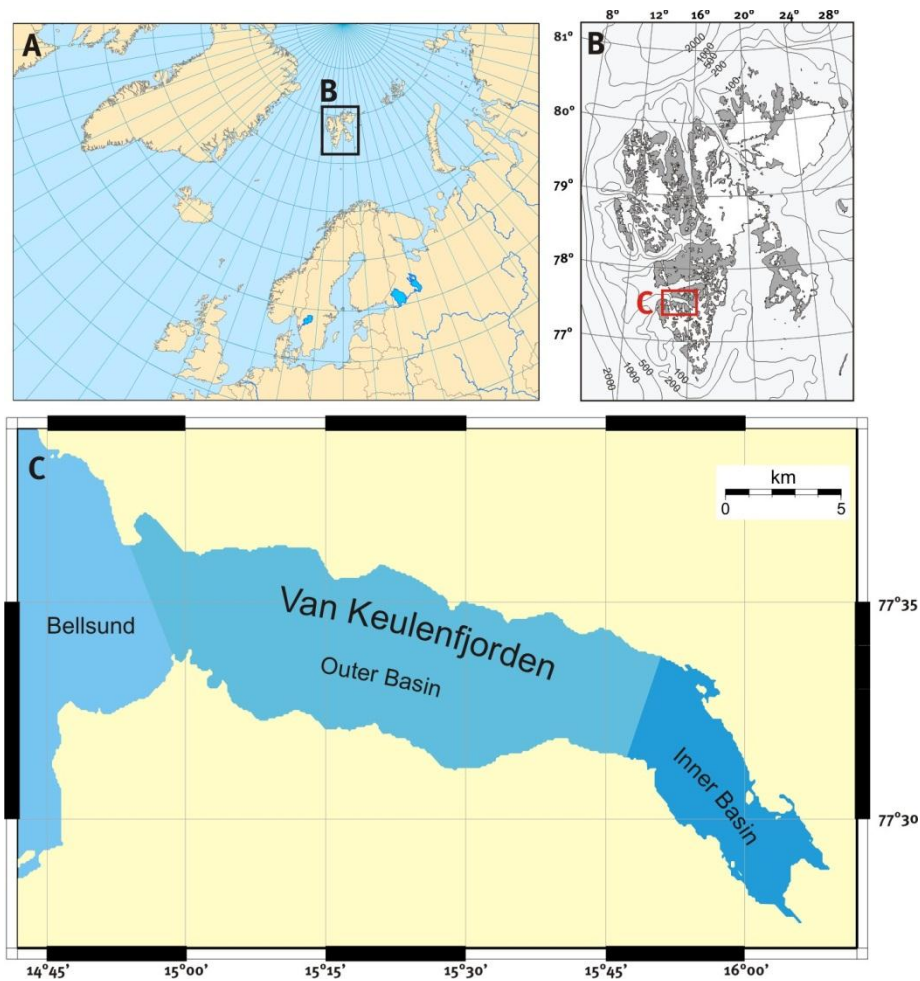


Figure 2.4: Overview maps of the study area and map of Van Keulenfjorden.

Van Keulenfjorden is a ~40 km long and up to ~7.5 km wide E-W trending fjord on the south-western coast of Spitsbergen. It is subdivided into two basins by a large submerged moraine ridge (Ottesen et al., 2008). The catchment area of Van Keulenfjorden (~1270 km²) contains 33 glaciers that account for a total ice volume of ~240 km³ (Hagen et al., 1993).

The five biggest glaciers are Nathorstbreen, Doktorbreen, Liestølbreen, Penckbreen and Zawadskibreen (Hagen et al., 1993) consisting of c. 82,5 % of the glaciated area and accounting for c. 90 % of the total ice volume in the Van Keulenfjorden catchment area. All of these five glaciers are known to be of surge-type (Hagen et al., 1993, Jiskoot et al., 2000, Sund et al., 2009). This influences the sedimentation of the fjord (Elverhøi et al., 1983, Solheim, 1991) and therefore has to be considered when reconstructing the palaeoenvironment and interpreting glacimarine and glacial sediments.

The catchment area has an E-W decline in glaciation. In the east ~80 % is glaciated, while in the west ~50 % is glaciated (Dallmann et al., 1994). All the major glaciers of the catchment area are located in the eastern part. Near the fjord head mountain massifs (Arrheniusfjellet, 880 m; Dishøgdene, 1015 m; and Gloføykja 1115 m) are carved by numerous smaller glaciers, mostly originating in cirques (Dallmann et al., 1990).

Numerous nunataks pierce the ice cover in the whole catchment area. The most prominent of those is in the central NW-SE trending mountain chain including the highest mountains (Beryeliustinden, 1205 m; Tittelberget, 1190 m; and Supanberget, 1100 m). This mountain chain forms the ice shed between Recherchebreen and Penckbreen on the south-western side of Van Keulenfjorden (Dallmann et al., 1990).

2.4.1 Geomorphology

Fjords typically occur in so-called fjord belts along the mid to high latitudes on both hemispheres (fig. 2.5, Howe et al., 2010).

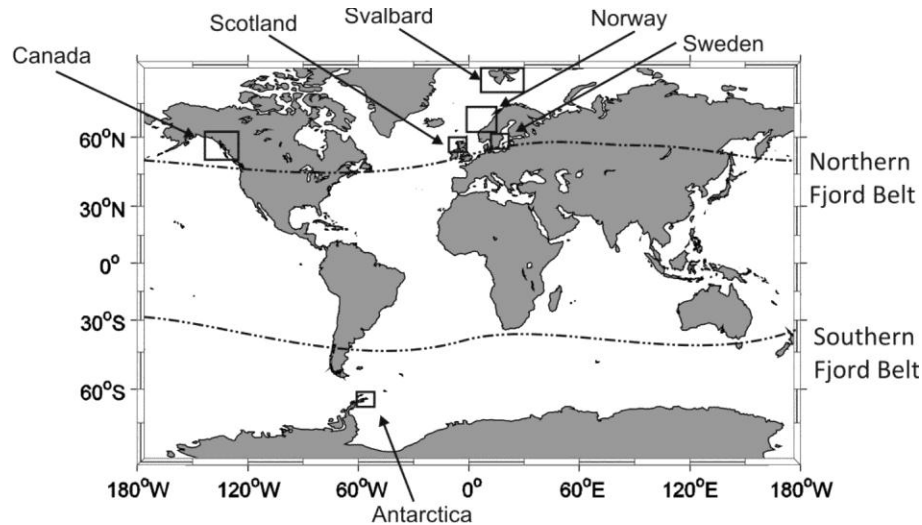


Figure 2.5: Map of fjords occurrence. Displayed are the Northern and the Southern Fjord Belt. From the two belts and higher latitudes fjords do occur. The main areas are labelled (after Syvitski et al., 1987, from Hambrey, 1994).

Fjords are in general defined as steep-sided, deep, high-latitude estuaries, which have been or currently are being excavated or modified by land-based ice (Syvitski et al., 1987, Syvitski and Shaw, 1995, Howe et al., 2010). Fjords are immature, non-steady state systems, evolving on relatively short timescales (Syvitski and Shaw, 1995). The main sediment source for Svalbard regime fjords, such as Van Keulenfjorden, include subglacially derived material, subglacial meltwater runoff (e.g. from Nathorstbreen), icebergs and glacifluvial rivers (e.g. Ulladalen; Hambrey, 1994, Howe et al., 2010).

The Svalbard regime of the fjords described by Hambrey (1994) states dynamic, grounded and slightly cold glaciers terminating in relatively shallow fjords (< 200 m; fig. 2.6). This classification fits well as Van Keulenfjorden is ~125 m deep at its deepest part, the glaciers are non-temperate and the tidewater glaciers in the catchment area are all grounded.

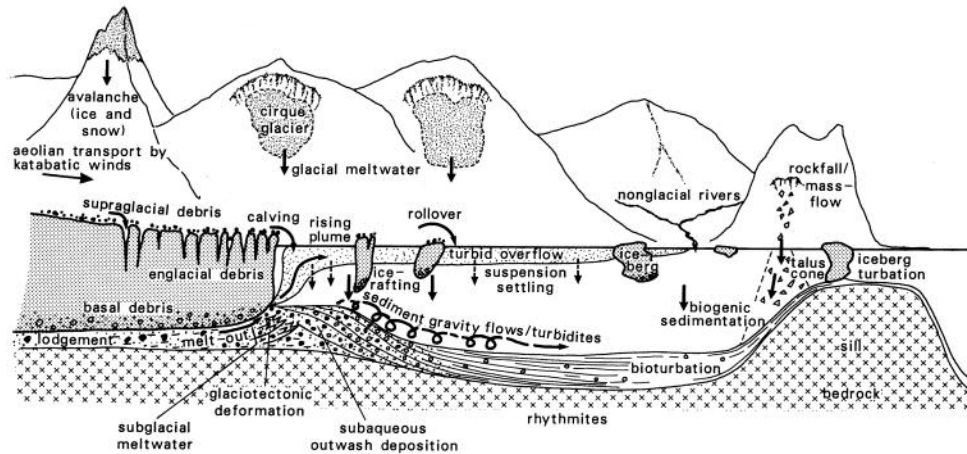


Figure 2.6: Sediment sources and processes operating in a fjord influenced by a grounded tidewater glacier (from Hambrey, 1994).

Sills at the fjord mouth and between the inner and the outer basin affect the fjords' hydrography and therefore also the sedimentary, chemical and biological environment. The inner and outer basins of Van Keulenfjorden are ~4 km and ~7 km wide and ~15 km and ~22 km long, respectively. Their maximum depth is ~70 m and ~125 m, respectively.

2.4.2 Climate

Spitsbergen is affected by the most distal parts of the North Atlantic Drift causing heat flux to the Arctic (Isaksson et al., 2005). Small changes in the drift (e.g. temperature of the seawater or current speed) can cause asymmetrically large climatic changes in Svalbard.

From 1912 until present the mean annual temperature varied between -12.8 and -3.1 °C (fig. 2.7; Hanssen-Bauer, 2002).

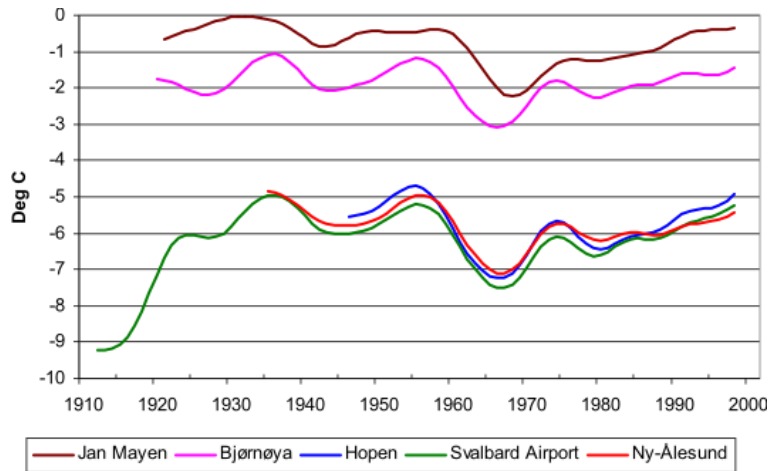


Figure 2.7: Measured annual temperatures at Norwegian research stations in Svalbard (from Førland and Hanssen-Bauer, 2003).

During the last 100 years air temperature is warming, however, trends over the last century are not statistically significant (Hanssen-Bauer, 2002, Førland and Hanssen-Bauer, 2003). The measured annual precipitation at Longyearbyen airport varied between 83 mm and 317 mm (fig. 2.8).

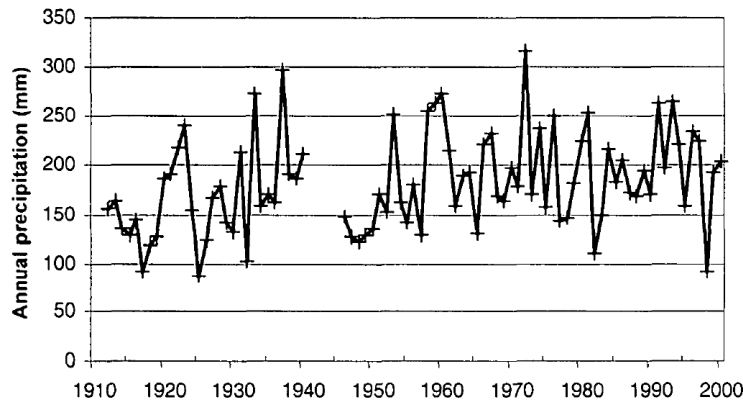


Figure 2.8: Measured annual precipitation at Longyearbyen airport (from Hanssen-Bauer, 2002).

Additionally, an annual precipitation map based on indirect measurements shows the distribution of precipitation over Svalbard (fig. 2.9; Hagen et al., 1993). The map marks an

east-west decline with values as high as 1200 mm a^{-1} in the east and values around 400 mm a^{-1} in the west.

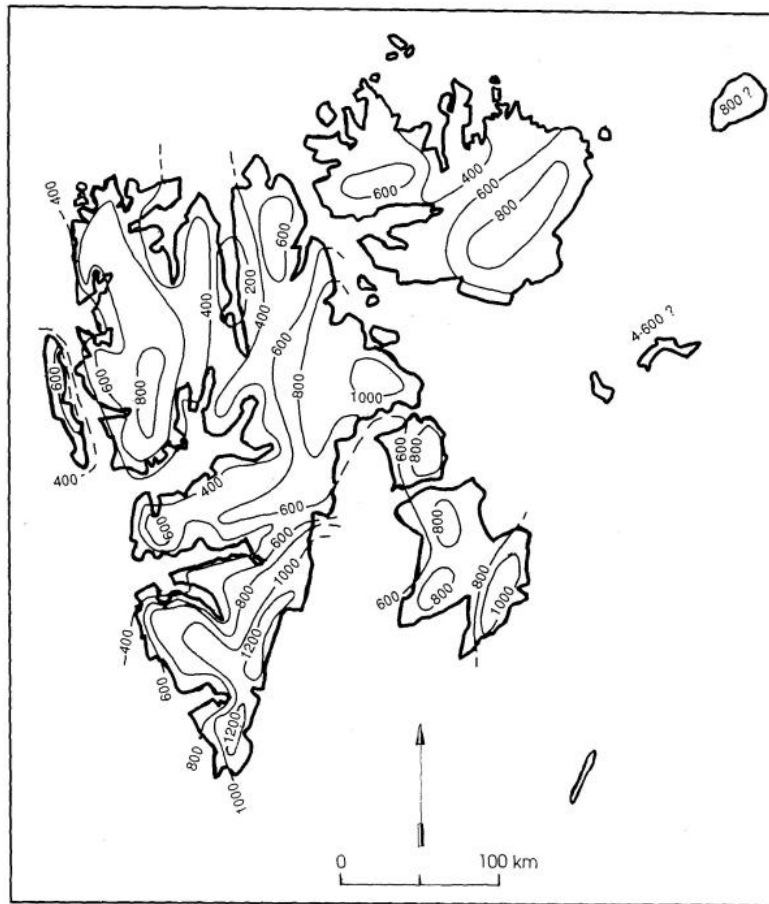


Figure 2.9: Precipitation in Svalbard in mm a^{-1} , based on indirect measurements (from Hagen et al., 1993).

Northern and eastern parts of Spitsbergen are cooler due to cold polar air and drift ice. This creates a temperature gradient of $\sim 2.5 \text{ }^\circ\text{C}$ per degree latitude from north to south during the winter months. In summer this temperature gradient is less (Isaksson et al., 2005).

2.4.3 Oceanography

The west coast of Svalbard is strongly influenced by the northward flowing West Spitsbergen Current (WSC), a rather complex, multipath, barotropic, warm and salty surface current consisting of Atlantic Water (AW) that follows the contours of the western

Svalbard shelf (fig. 2.10; Saloranta and Svendsen, 2001, Cottier and Venables, 2007, Piechura and Walczowski, 2009).

Due to the heat transport of the WSC to the arctic the west coast of Spitsbergen is essentially ice free (Gascard et al., 1995). West of the WSC, the AW is separated from the cold and fresh polar waters of the Greenland Sea by a density front termed the Polar Front (Boyd and Dasaro, 1994). East of the WSC flows the cold arctic Coastal Current (CC), which originates in Storfjorden (fig. 2.10; Rasmussen et al., 2007).

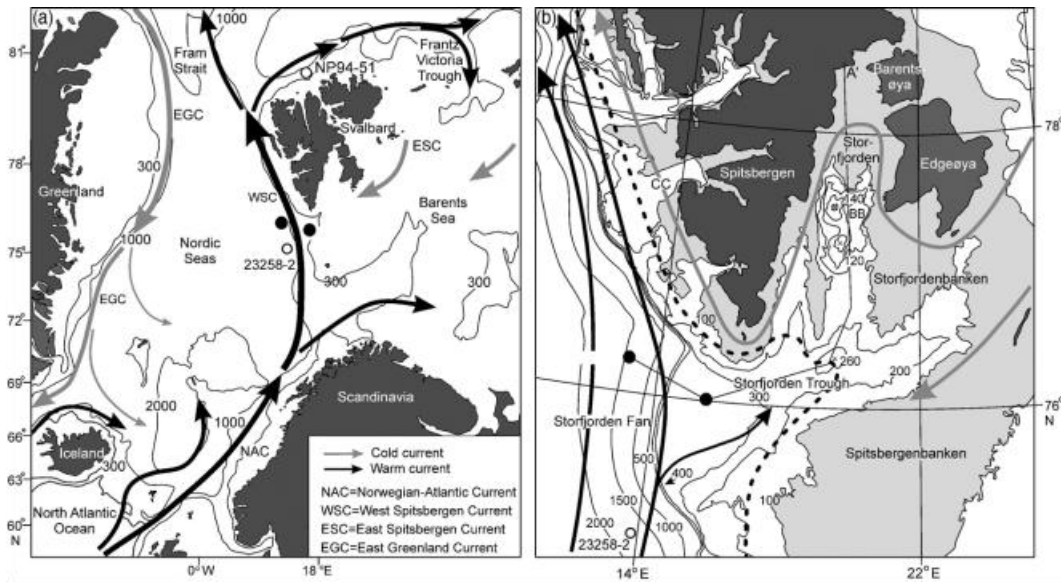


Figure 2.10: a) map of the Nordic seas and the Barents Sea showing major surface currents systems, b) detail map of the South Spitsbergen area showing mean position of the arctic front (from Rasmussen et al., 2007).

Where the WSC and the CC meet, they form the Arctic Front of West Spitsbergen. The Arctic Front is a density front in the upper layer (c. 0 – 50 m). Below 50 m water depth a temperature-salinity front is present, a corresponding density front is missing (fig. 2.11; Saloranta and Svendsen, 2001).

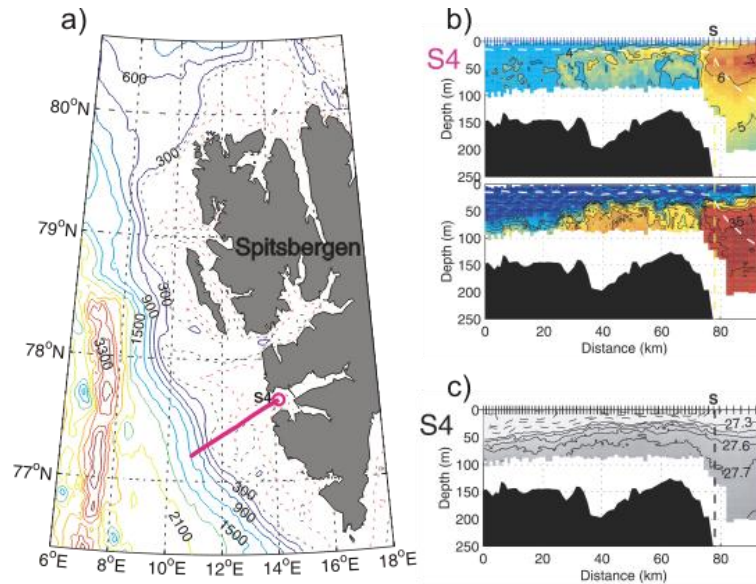


Figure 2.11: a) CTD profile location in the Bellsund trough, the circle denotes the start of the profile, b) temperature (above) and salinity (below) profiles in the Bellsund trough, c) calculated density profile from the profiles of temperature and salinity in b) (from Saloranta and Svendsen, 2001)

The CC is usually mitigating the AW's penetration into the fjords on Spitsbergen's west coast. However, if wind induced southward currents oppose the CC or if there is mixing between the two layers of AW and cold Arctic Water of the CC from the Storfjorden trough, the effect of AW entering the fjords of the west coast of Spitsbergen increases (Saloranta and Svendsen, 2001, Nilsen et al., 2008).

The northward transport of warm and saline AW along the west Norwegian coast and Barents Sea shelf, though varying in strength, was always present since the deglaciation of the Late Weichselian Barents Sea ice sheet (Rasmussen et al., 2007, Slubowska-Woldengen et al., 2008).

The classic physical oceanographic setting for fjord water masses is a three layer arrangement for fjords with sills. This comprises a low salinity, warm surface layer, an intermediate layer at sill depth and a cold, high salinity bottom layer (Farmer and Freeland,

1983). In Svalbard even fjords without sills showed this three layer arrangement (fig. 2.12; Cottier et al., 2005, Nilsen et al., 2008).

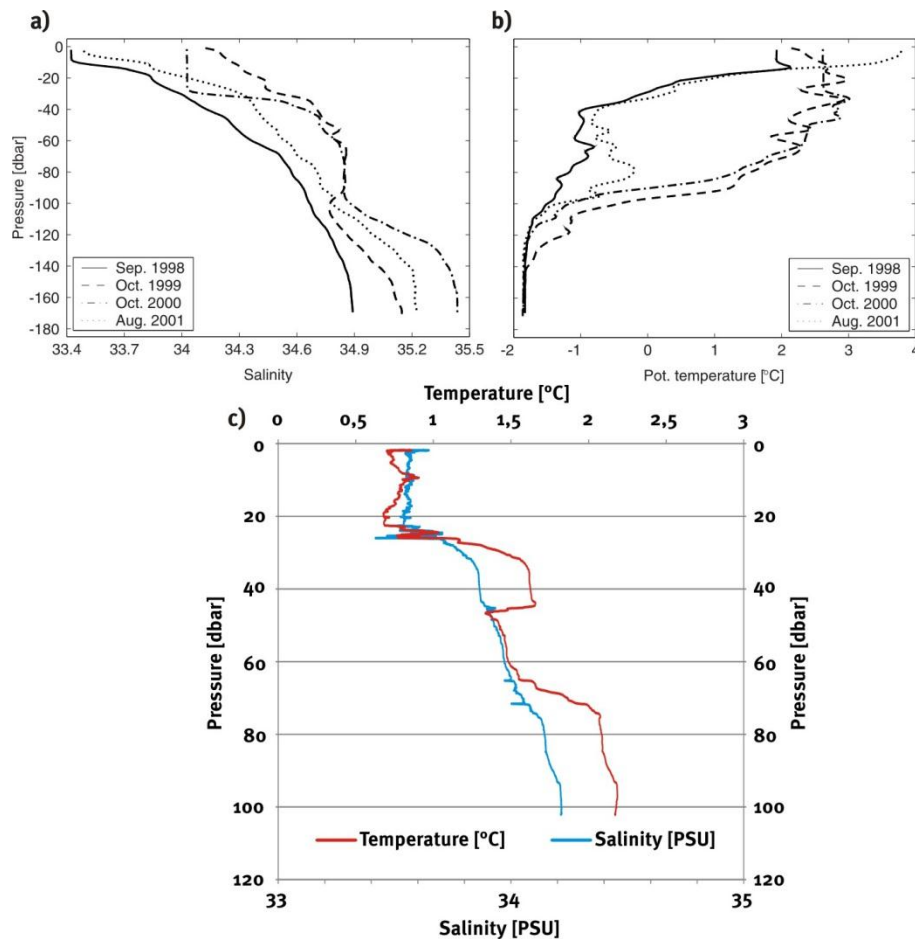


Figure 2.12: a) Salinity sections of CTDs and b) temperature sections of CTDs through the water column in Storjorden in four consecutive years (from Skogseth et al., 2005), c) a CTD recorded on the 4th of October in 2009 in central Van Keulenfjorden. Note the three distinctive layers in the water column in both Storjorden and Van Keulenfjorden. However, the temperature profile differs.

The upper layer is fresher, because of the input of four sources, i) tidal glacier ablation and calving, ii) direct precipitation on the fjord's surface, iii) melting of fast ice and iv) terrestrial, riverine outflow (Weslawski et al., 1995, Cottier et al., 2010). The intermediate layers usually derive from advected water masses external to the fjord. They are often heavily altered by mixing with on-shelf adjacent waters. In Spitsbergen's west coast fjords

the intermediate water layer is most likely to be of water derived from AW (Skogseth et al., 2005, Nilsen et al., 2008). The AW has probably mixed to some extent with shelf waters before entering the fjord, which can be the reason for the cooler and fresher condition (Cottier et al., 2010). The source of deep water in Svalbard fjords is either sea-ice formation and brine releases or AW that has undergone intense cooling during winter (Skogseth et al., 2005, Nilsen et al., 2008). The described stratification within Arctic fjords varies seasonally. The classic layered arrangement, as depicted by fig. 2.12, will mostly be fully developed during summer. Wind mixing and intense cooling breaks down the stratification in winter. Sea-ice formation and brine releases initiate convective overturning thus contributing to further mixing of the layers (Cottier et al., 2010).

2.4.4 Glaciology

About 60% of Svalbard is covered by a variety of glacier types, including ice caps, ice fields, outlet glaciers, piedmont glaciers and cirque glaciers. Ice shelves do not exist at present (Hagen et al., 1993).

The thermal structure of most Svalbard glaciers is polythermal, meaning that the glacier comprise both cold (below pressure melting point) and warm ice (at pressure melting point; Hagen et al., 1993, Benn and Evans, 2010). The glaciers in the catchment area of Van Keulenfjorden have an equilibrium line altitude (ELA) between 310 m.a.s.l. (Liestølbreen) and 480 m.a.s.l. (Steenstrupbreen; Hagen et al., 1993).

Svalbard is one of earth's surge-type glacier clusters (fig. 2.13 and tab. 2.1; Jiskoot et al., 2000). Estimations of how many of the glaciers on Svalbard are surge-type range between 13% (Jiskoot et al., 1998) and 90% (Lefauconnier and Hagen, 1991). This is a typical 'absence of evidence is not evidence of absence' problem, especially when keeping in mind that the quiescent phases of Svalbard surge-type glaciers are particularly long, ranging from ~50 years up to estimated 500 years (Benn and Evans, 2010).

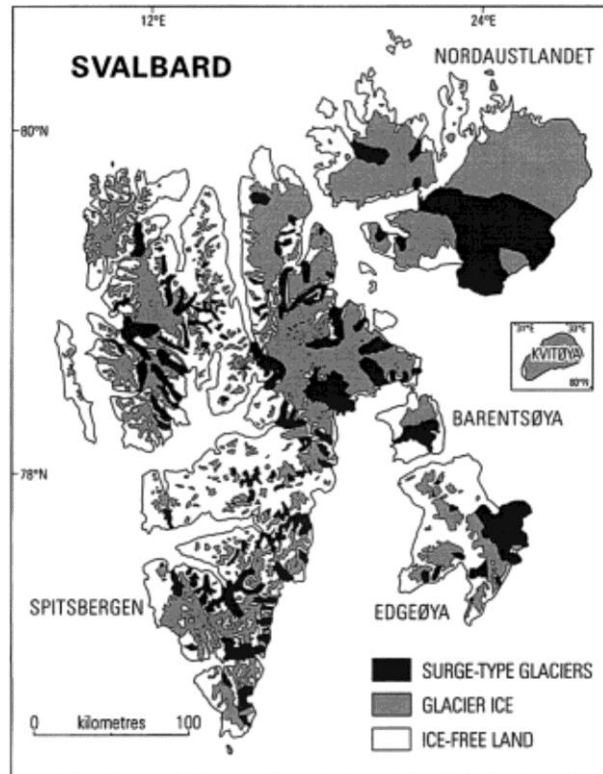


Figure 2.13: Distribution of surge-type glacier over Svalbard (from Jiskoot et al., 2000). Among other areas the Van Keulenfjorden catchment area shows a high occurrence of surge-type glaciers.

Digital Terrain Model (DTM) subtraction was used by Sund (2009) to survey glacier elevation changes in the Van Keulenfjorden catchment area. Negative elevation changes in upper Ljosfonn, a tributary of the Nathorstbreen Glacier System, were observed (fig. 2.14) and inferred to be early signals of a surge. In late 2008 Ljosfonn and subsequently Nathorstbreen began to advance. In October 2010 Nathorstbreen Glacier System's glacier front reached the 1936 AD position, (cf. fig. 2.3) and was in the last phase of surging in February 2011 and most likely still is. This is an advance of 11 km, referred to the mean 2008 glacier front position (Sund et al., 2009, Sund and Eiken, 2010, Sund, 2011).

Table 2.1: Glacier in the Van Keulenfjorden catchment area. L/T expresses whether the glacier has a land based terminus (L) or a tidewater terminus. The source column indicates where the information on surge-type behaviour was taken from. **H** stands for Hagen et al. 1993, **J** stands for Jiskoot et al. 2000 and **S** stands for Sund et al. 2009.

Glacier	L/T	Source	Surge-type	Area [km ²]	Glacier	L/T	Source	Surge-type	Area [km ²]
Aurkollfonna	L		no	4,6	Mjellfonna	L		no	2,1
Berrklettreen	L		no	2,5	Nathorstbreen	T	J, S	yes	368,9
Charpentierbreen	L	H	yes	4,3	Penckbreen	L	J	yes	118,0
Doktorbreen	T	J	yes	295,6	Reidbreen	L		no	7,5
Finsterwalderbreen	L	H	yes	45,5	Richterbreen	L		no	10,6
Hassingbreen	L		no	2,3	Ringbreen	L		no	9,6
Hessbreen	L	H	yes	6,2	Siegerbreen	L	H	yes	1,8
Instebreen	L		no	6,1	Sotryggfonna	L		no	1,5
Langryggbreen	L		no	9,3	Steenstrupbreen	L		no	32,0
Liestølbreen	T	J, S	yes	160,0	Storvolbreen	L		no	3,2
Märjelbreen	L		no	7,5	Sysselembreen	L	J	yes	32,8
Martinbreen	L	H	yes	7,2	Tvillingbreane	L		no	6,6
Midterhukbreen	L		no	1,2	Venezbreen	L		no	4,4
					Zawadskibreen	T	J	yes	110,8

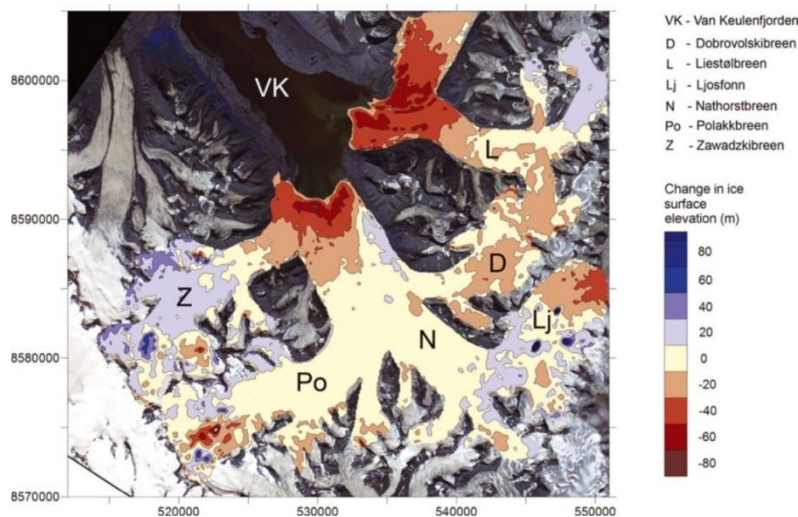


Figure 2.14: Map of elevation changes on glaciers in Van Keulenfjorden's catchment areas calculated by DTM subtraction. The negative changes in upper Ljosfonna were the first signs of the most recent surge of Nathorstbreen Glacier System (from Sund et al., 2009).

2.5 Geology

2.5.1 Tectonic History

Through time Svalbard was plate-tectonically moved with the Eurasian Plate from equatorial latitudes to its current position (fig. 2.15; Worsley, 1986).

The Van Keulenfjorden area contains basement rocks of orogenic events of Proterozoic and Caledonian age, respectively (Dallmann et al., 1990). All Svalbard rocks that are old enough to have experienced the latter or both orogeneses are embraced by the term Hecla Hoek complex (Worsley, 1986). Only small outcrops of these rocks are exposed in the catchment area of Van Keulenfjorden (fig. 2.16).

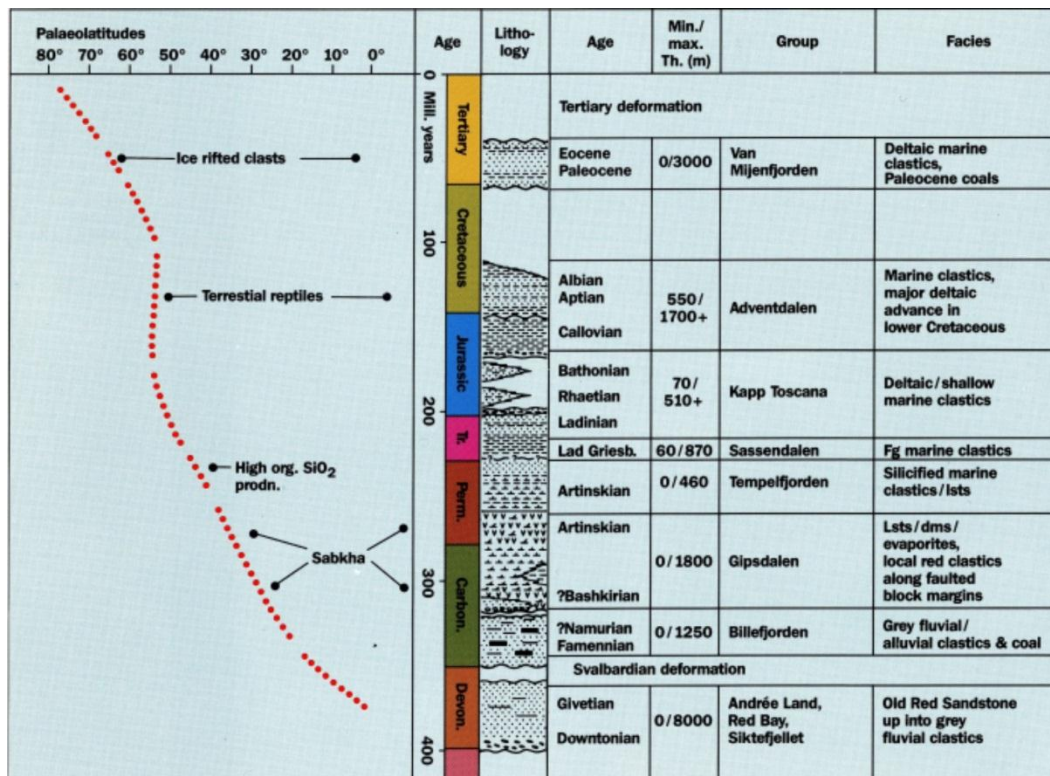
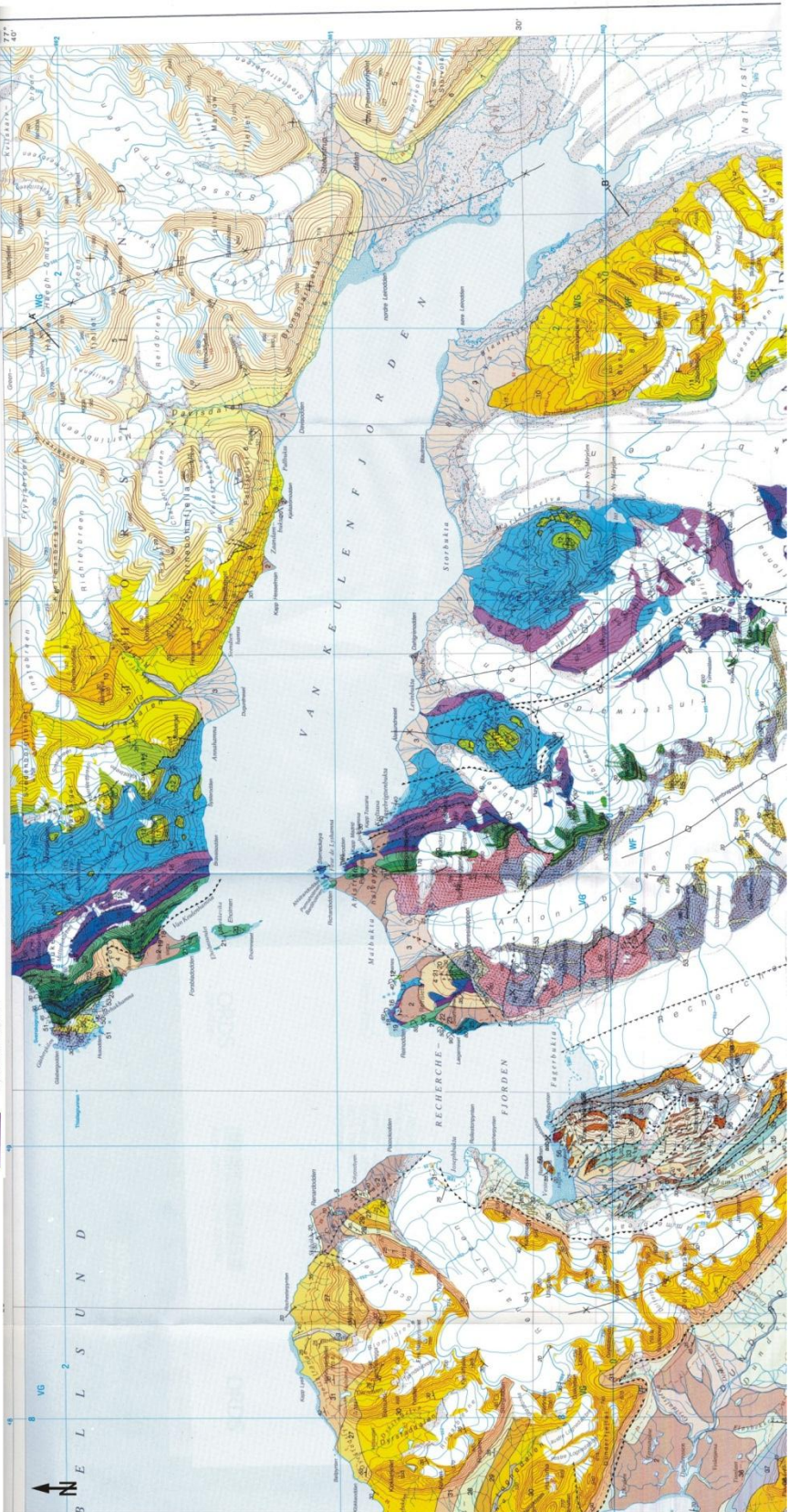
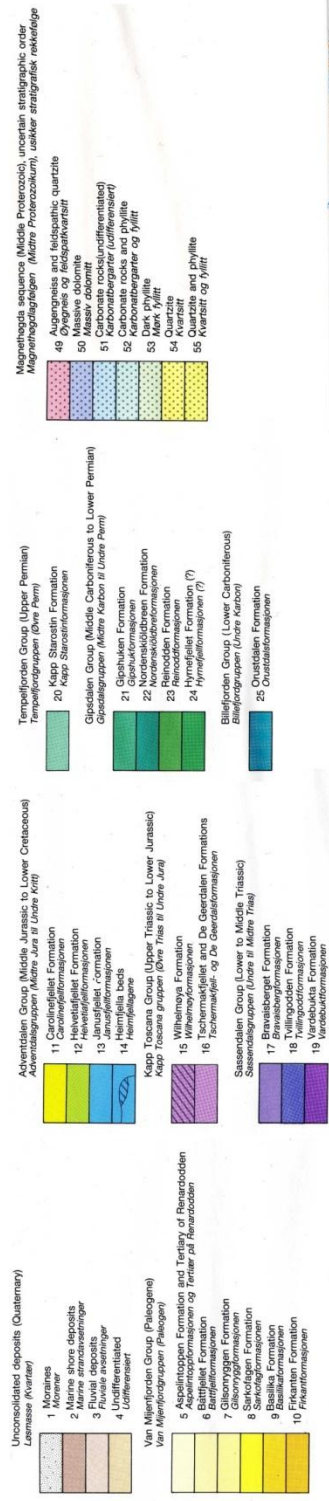


Figure 2.15: Simplified Phanerozoic stratigraphy of Svalbard. To the left is the palaeolatitude history of Svalbard (from Worsley, 1986).

The Palaeozoic and Mesozoic tectonic history of Svalbard is dominated by movements along the mostly N-S trending fault zones, e.g. Billefjorden Fault Zone. Especially subsequent to the Caledonian orogenesis, these block tectonics controlled the sedimentation during the Devonian to Early Permian (Dallmann et al., 1990).

Figure 2.16: Geological map of Van Keulenfjorden, B11G, Temakart nr. 15. The scale is 1:100000 (from Dallmann et al., 1990), see next page.



Around the Jurassic/Cretaceous boundary a period of extension affected Svalbard. It is associated with Dolerite sill and dike intrusions throughout the archipelago. This event is regarded as the first effect of tensional tectonics that later led to the opening of the North Atlantic and the Arctic Oceans. The Palaeocene/Eocene tectonic period was dominated by a compressive force regime. This resulted in the formation of the West Spitsbergen fold and thrust belt (fig. 2.14; Dallmann et al., 1990). The fold and thrust belt's effects were strongest on the units in the western catchment area, where Carboniferous to Eocene strata are heavily folded. A foreland basin – the Central Spitsbergen Tertiary Basin – developed synchronously to the east of the fold and thrust belt (figs. 2.16 and 2.17; Dallmann et al., 1994).

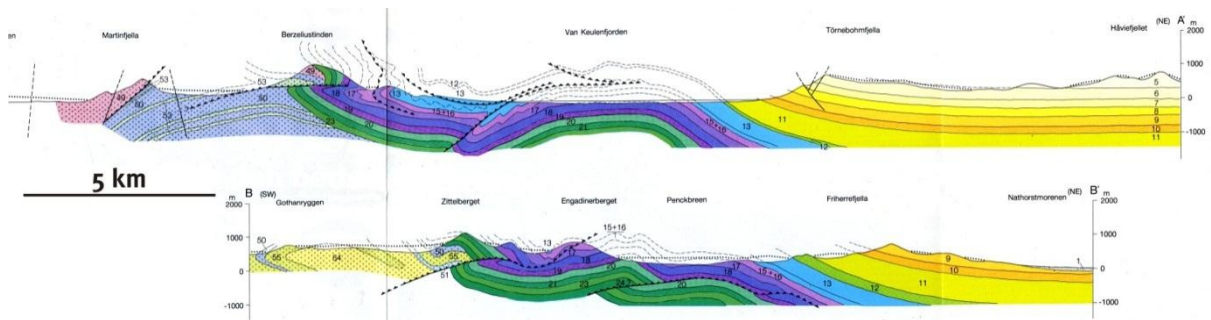


Figure 2.17: Geological profile through the bedrock in Van Keulenfjorden area. The strata are folded and thrust due West (left). For locations and legend see fig. 2.16 (from Dallmann et al., 1990).

2.5.2 Bedrock Geology

Geologically, the Van Keulenfjord area can be divided into two main structural units with NW-SE trending boundaries.

Firstly, Hecla Hoek rocks crop out in small parts of the catchment area of Hessbreen, Finsterwalderbreen and Penckbreen in the south-western part of Van Keulenfjorden (fig. 2.16). It is a basement high with pre-Devonian rocks that underwent the Caledonian tectonometamorphism. The Hecla Hoek complex consists mostly of carbonate rocks, phyllite and quartzite in the lower part, over which, with an unconformity contact, are thick

conglomerates followed by phyllite, carbonate and meta-igneous rocks. To the top lies a roughly 2000 m thick succession of Vendian tilloids (in 2004 the Vendian, from c. 635 to 542 Ma, was renamed to Ediacaran by the International Commission on Stratigraphy, (ICS)). These rocks are low-grade metamorphic and record Caledonian deformation and in some cases of greater ages even Precambrian deformation (Dallmann et al., 1990). The rocks represent the Magnethøgda Sequence. They are of middle Proterozoic age (Dallmann et al., 1990).

Secondly, in the fjord mouth area rocks of the Billefjorden-, Gipsdalen-, Tempelfjorden-, Sassendalen-, Kapp Toscana- and Adventdalen Group are partly tilted steeply in the fold and thrust belt (fig. 2.17). All together, these Late Palaeozoic to Mesozoic groups comprise a sediment package of at least 2800 m thickness. They contain mainly shale, siltstone, sandstone, red conglomerate, dolomite, limestone and chert (Hjelle et al., 1986, Dallmann et al., 1990, Harland et al., 1997). Structurally still belonging to the second unit there is the Van Mijenfjorden Group, mostly Palaeocene/Eocene of age. It fills the majority of the Central Spitsbergen Tertiary Basin. Its exposed thickness exceeds 1900 m, but an additional similar thickness has probably been removed by erosion (Manum and Throndsen, 1986). It is comprised of strata generally gently dipping to ENE with immature textures and compositions ranging from arkosic to lithic arenites and lith-arenites (Dallmann et al., 1990, Harland et al., 1997). Most of the Nunataks in the eastern catchment area consist of these rocks. However, an uncertainty remains about the bedrock of the glaciers in that area (Hjelle et al., 1986, Dallmann et al., 1990, Dallmann et al., 1994).

In addition, quaternary glacifluvial and moraine deposits hem the immediate coast line of most of Van Keulenfjorden (Dallmann et al., 1990).

3 Material and Methods

3.1 Swath Bathymetry

The swath bathymetry data was collected with R/V Jan Mayen in November 2009 using a Kongsberg Maritime Simrad EM 300 Multibeam echo sounder (Forwick, 2009). This is a hull-mounted system with up to 135 beams in the swath. Its range of operation lies between 10 and 5000 m water depth. The nominal operational frequency is 30 kHz with an angular coverage of 150° (Anonymous, 2003). However, on R/V “Jan Mayen”, the maximum angle is reduced to 63° due to an ice-protection window.

After data-acquisition the cleaning and processing of the data was performed using the software Neptune. Tidal artefacts were prevented by recalculating the depth values according to tidal data and simple conversions from Statens Kartverk (Norsk Sjøkartverket). Gridding and visualization were performed with the Interactive Visualization System 3D (IVS 3D) module Fledermaus v. 7.0.

Nevertheless, the multibeam dataset contains artefacts. The most prominent artefact is an acquisition footprint throughout the whole survey caused by the penetration of the central beams into the soft seafloor sediments. This artefact is suppressed by using a shallow biased gridding algorithm in Fledermaus (fig. 3.1). However, the surface becomes rougher when using the shallow biased gridding algorithm. The following figures in this chapter are all gridded either with a shallow biased algorithm, a cell size of 15 m and the next 7 neighbouring cells were weighed or with a weighted moving average algorithm, a cell size of 12 m and the next 3 neighbouring cells were weighed. Cell sizes of 15 m or 12 m, respectively, were chosen, although the resolution of the dataset may be higher at most places (~10 m). Since the deeper places in the fjord have a worse resolution, the greater cell size prevents holes in the surface (fig.3.1).

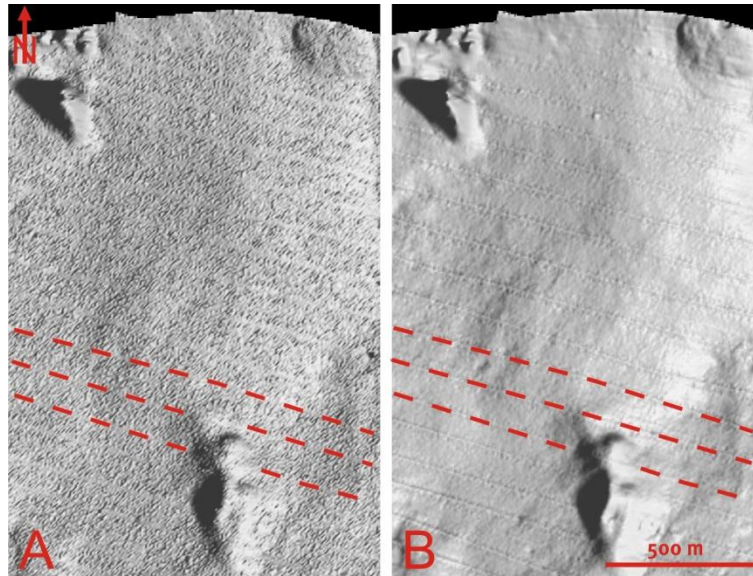


Figure 3.1: Multibeam dataset example, a) the multibeam dataset was gridded with a shallow biased algorithm, a cell of 15 m and 7 weighted neighbouring cells. The random noise is more prominent, but the acquisition footprint artefact (red dashed lines) is weak. b) the multibeam dataset was gridded with a moving weighted average algorithm, a cell size of 12 m and 3 weighted neighbouring cells. The surface has a rather smooth appearance, but the acquisition footprint artefact (red dashed lines) is strong.

3.2 Chirp Sonar

The Chirp profiles were collected in November 2009 (Forwick, 2009). The Chirp system transmits selectable frequency modulated pulses, in essence “sweeping” through a range of frequencies between 400 Hz and 20 kHz. The sweeping creates a large bandwidth. Because the temporal resolution is proportional to the inverse of the bandwidth of the signal the Chirp Sonar achieves high resolution profiles (Hill, 1999). The long pulse length would decrease resolution drastically were it not for a digital compression filter that artificially shortens the pulse (Quinn et al., 1998). With the equipment and the digital support even weak layering in sediment can be detected with a high signal-to-noise ratio (Schock et al., 1989). The profiles were imported into The Kingdom Software v. 8.5 after processing the navigation files (the location control) in GMT (Generic Mapping Tool). The Kingdom Software has a computational module that allows calculations with the data. This module

was used to calculate isopach maps from defined horizons on the 2D seismic lines. Essentially isopach maps which are derived from seismic lines are the two-way-travel-time (TWT) difference between two horizons described by

$$H_A - H_B = \Delta t \quad (1)$$

Where H_A stands for the lower, H_B for the upper horizon and Δt for the TWT difference between the horizons. It was chosen to only interpolate between grid points with data for each horizon to avoid extrapolating too far. To ensure that data points are calculated only where both horizons have values a logic conjunction was used, given by

$$(H_A \cap H_B) = t_{A \text{ of } B} \quad (2)$$

Where again H_A is the lower, H_B the upper horizon and $t_{A \text{ of } B}$ are only the values of horizon H_A , which horizon H_B has a value for at the same horizontal position. In The Kingdom Software the same operation is denoted with

$$\text{and}(H_A, H_B) = H_{A \text{ where } B} \quad (3)$$

Where $H_{A \text{ where } B}$ is the resulting horizon made by this operation in the software. The combination of formula 1 and 3 in The Kingdom Software is then given by

$$(\text{and}(H_A, H_B)) - (\text{and}(H_B, H_A)) = \Delta t_{AB} \quad (4)$$

Where Δt_{AB} is the TWT difference between horizons H_A and H_B , where both horizons have values. Formula 4 was used to calculate the isopach maps presented in chapter 5.

3.3 Sediment Cores

Two box, gravity and piston cores, respectively, were retrieved during a scientific cruise between the 2nd and 8th of July 2007 of R/V Jan Mayen (Forwick, 2007). The locations and further information are shown in table 3.1.

*Table 3.1 Metadata taken from the cruise report (Forwick, 2009). *) value taken from measurements in the lab once the core was opened.*

Station	Date	Time [UTC]	Location [°N]	Location [°E]	Water depth [m]	Recovered depth [m]
JM07-012-BC	07.05.2007	12:51	77°35.27'	014°59.35'	102	0.25*
JM07-014-BC	07.05.2007	16:21	77°33.36'	015°35.56'	83	0.26*
JM07-012-GC	07.05.2007	12:16	77°35.12'	014°59.95'	100	2.70*
JM07-014-GC	07.05.2007	16:51	77°33.28'	015°35.83'	82	2.70*
JM07-012-PC	07.05.2007	10:16	77°35.07'	015°00.73'	101	3.82*
JM07-014-PC	07.05.2007	15:19	77°33.33'	015°35.29'	82	5.38*

The box corer was used to retrieve undisturbed samples of the seafloor (50 cm x 50 cm). It was subsampled by pushing a plastic liner of 11 cm outer diameter by hand into the sample. The tube was cleaned, labelled and sealed off with caps on both ends before storing it in a 4 °C cooling chamber.

The gravity corer aboard R/V Jan Mayen contains a 6 m long steel barrel attached to a lead bomb of ~1.6 t weight. A plastic liner was pushed into the barrel and fixed with a core catcher and core cutter. After retrieval, the plastic liner was pulled out of the steel barrel, cleaned, and cut into ~1 m sections. All sections were sealed with caps, labelled and stored in a 4 °C cooling chamber.

A piston corer is made for deeper penetration of soft sediment than the gravity corer. When the corer penetrates the sediment gravity is forcing the corer into the sediment. In addition to gravity, a piston produces suction in the metal barrel (~12 m long and attached to a lead bomb of ~1.6 t weight on R/V Jan Mayen) that gives the corer an extra force enabling the deeper penetration. After retrieval the samples were treated following the same procedure as for samples of the gravity corer.

3.4 Laboratory Work on the Sediment Cores

3.4.1 Multi-Sensor Core Logger

Prior to opening the cores were logged with a multi-sensor core logger (MSCL; by GEOTEK Ltd.). This device uses several non-destructive methods, namely γ -ray attenuation, magnetic susceptibility, p-wave velocity, p-wave amplitude and the diameter of the core, to determine physical properties of the core (see below for further explanations). For the measurements the core section is put on the sample guide rail and is transported forwards at pre-defined increments by a core pusher. A laser relay and a positioning sensor are coupled with the motor of the core pusher to form the position control system of the MSCL. The analysis devices are queued up behind the photoelectric relay at known positions to correlate the points of measurements (fig. 3.2; Anonymous, 1998). The measuring increment was set to 1 cm.

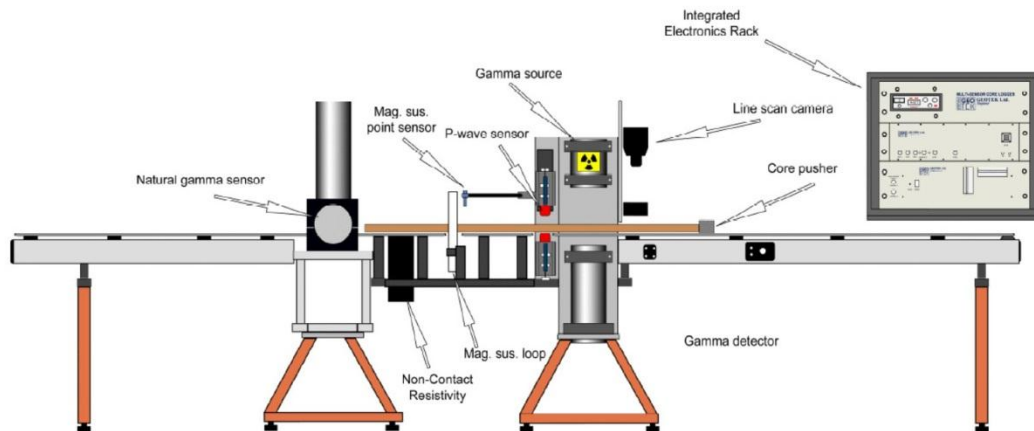


Figure 3.2: Sketch of the Multi-Sensor Core Logger from the user manual. Some of the depicted measure devices were not used, i.e. natural gamma sensor, non-contact resistivity, magnetic susceptibility point sensor and line scan camera, because the devices were either not available or not applicable for whole cores.

3.4.1.1 γ -Ray Attenuation

Radioactive ^{137}Cs in a thick lead mantle is emitting a narrow beam of γ -rays with energy at 662 keV. The photons pass through the core and are detected on the other side of the core. At this level of γ -ray energy the primary mechanism of attenuation is by Compton scattering, essentially causing a partial energy loss of the γ -rays (wavelength increase) whenever hitting an electron. This means that the amount of γ -rays detected is controlled by the number of electrons in the beam's way, which is dependent on the core diameter and the electron density of the core material. The diameter of the core is measured and the density of electrons and the density of a material are closely linked and therefore the bulk density of the core can be calculated from the γ -ray attenuation measurements (Anonymous, 1998).

3.4.1.2 P-Wave Velocity System

The p-wave velocity system measures three values at the same time, i) the time the generated p-wave pulse needs to travel through the liner plus sediment (travel time), ii) the thickness of the liner (travel distance), and iii) the amplitude difference between the produced p-wave and the detected p-wave.

The system is equipped with p-wave transducers, which produce and record a short pulse of an ultrasonic p-wave making use of the normal and the inverse piezo-effect. The pulse propagates through the core and is detected by the receiving transducer. Pulse timing circuitry is used to measure the travel time with a resolution of 50 ns. The travel distance is measured within the same device with an accuracy of 0.1 mm. Experiments have shown that results within a ± 3 ms (1σ) window are achievable. The p-wave amplitude is used to detect decoupling between the transducers and the liner and the sediment and the liner. If any of the four couplings (transducer-liner, liner-sediment, sediment-liner, liner-transducer) is faulty the p-wave amplitude decreases significantly. The p-wave amplitude is expressed in percentage of perfect coupling. If the values for the p-wave amplitude are small the validity of the produced values for p-wave velocity is not given.

The diameter is measured as the distance between the active faces of the two p-wave transducers. In practice it is measured with reference to a known thickness (Anonymous, 1998).

3.4.1.3 Magnetic Susceptibility Loop Sensor

The magnetic susceptibility loop sensor measures the bulk magnetic susceptibility of the core. The magnetic susceptibility is basically the potential of a material to be magnetized by an applied magnetic field. For maximum resolution the loop diameter should be minimally bigger than the core diameter. In this analysis the loop diameter is 12.5 cm and the core diameter is ~11 cm (~11.5 cm where the caps are sealing the ends of each core section).

In the loop sensor an oscillator circuit produces a low intensity alternating magnetic field (565 Hz). Any material in the close vicinity to the sensor will cause a change in the oscillator frequency. The electronics of the sensor convert this pulsed frequency information into magnetic susceptibility values (Anonymous, 1998).

3.4.1.4 Temperature Measurement

The cores were stored in the lab (not the cooling room) at least one day prior to MSCL analysis, because some physical properties (e.g. p-wave velocity, magnetic susceptibility) are temperature dependent. For example, the p-wave velocity can change with $\sim 3 \text{ m s}^{-1} \text{ } ^\circ\text{C}^{-1}$ (Weber et al., 1997, Anonymous, 1998). A thermometer records the current room temperature for each measurement and it is assumed that the core temperature is identical to the room temperature. The temperature range during the measurement was less than 1 $^\circ\text{C}$. This generates an inaccuracy error of $< 2 \text{ } \%$ (Anonymous, 1998).

3.4.2 Opening of the Cores

After measuring the physical properties with the MSCL, the cores liners were cut using a circular saw. Subsequently, the core material was split with an osmotic knife that was dragged from the bottom to the top of each segment. After the cores were split the section

halves were labelled and packed in cling film and then put into a plastic tube which was sealed to prevent it from drying out. One split core was labelled for the archive, the other for labwork.

3.4.3 X-Ray Photography

X-ray photos of half-core sections were taken. It is physically very difficult to bundle or reflect x-rays. Therefore the x-ray source, the sample and the detector (film) form one axis. The x-ray photography is based on the attenuation principle and gives shadow pictures. The attenuation is dependent on the nuclei's atomic number and the number of nuclei in the ray path. Dropstones or macrofossils usually have a bright (highly attenuated) signal because of their high density, compared to the surrounding mud.

A Philips™ Macrotank with a Be source, 5 mA current and 80 kV acceleration voltage was used. The exposure time varied between 1:40 min and 2:30 min, depending on the density results from the MSCL results. AGFA D7 film was used for all pictures. The radiographs were used to log internal structures, dropstones, bioturbation and fossils in the cores.

3.4.4 XRF-Scanner

The analytical method of x-ray fluorescence (XRF) scanning is non-destructive. The Avaatech XRF Core Scanner is equipped with a high resolution camera and a Rh target x-ray tube. The detector is energy dispersive. The range of elements that can be analysed by this device reaches from Mg ($Z = 12$) to U ($Z = 92$) (Richter et al., 2006; www.avaatech.com).

XRF spectrometry is based on ionization of atoms by x-rays or γ -rays. When an electron is ejected from one of the inner orbits the electronic structure of the atom is rendered unstable and an electron from an outer orbit falls into its place. In falling, the electron emits a specific amount of energy in form of photons depending on the energy differences between the involved electrons' orbits. The emission is element specific and is used for analysis (Beckhoff et al., 2006).

Prior to analyses, the sediment surface was flattened to perform the camera scan, after which the surface was covered with a 44 μm ultralene film. During measuring the sediment sample has to be covered to avoid contamination to the measuring chamber pressing on the surface.

3.4.5 Sedimentological Logs

A systematic description of the surfaces of the cores was carried out. This included observations of fossils, bioturbation, sediment colour (after the Munsell Soil Colour Chart), lamination, structures, layers of coarser grains and general comments, if needed (e.g. the occurrence of black mottles, vanishing after some time of oxygen exposure).

3.4.6 Wet Sieving

The cores were sampled approximately every 10 cm, while the sampling thickness was between 0,5 and 1 cm . Samples were freeze-dried to record the water content and to loosen up the intergranular bonds. Every sample was then sieved with a 2 mm ($\phi = -1$) and a 63 μm ($\phi = 4$) sieve. The residual sample ($\phi > 4$) was collected in 2-liter glasses and dried at 40 °C. Each of the fractions dry weight was recorded.

3.4.7 Dry Sieving

The grainsize fraction of $-1 \leq \phi < 4$ was dried and subsequently dry-sieved using sieves with mesh sizes of 1 mm ($\phi = 0$), 0.5 mm ($\phi = 1$), 0.25 mm ($\phi = 2$) and 125 μm ($\phi = 3$), respectively, to get a higher resolution on the grainsize distribution in the sand fraction.

3.4.8 Sedigraph

Grainsize distribution of the $\phi < 4$ fraction was analysed using the SediGraph 5100 analysis system from Micromeritics™. The sedigraph makes use of Stoke's Law, which correlates the particle diameter with the sedimentation velocity in a viscous liquid, i.e. water. In the analysis cell of the sedigraph, the transmitted x-ray intensity through a suspended sample is

measured over time intervals. The results are reported in equivalent spherical diameter and for the density of 2.675 g cm^{-3} , since shape and density affect the sedimentation velocity.

Prior to the measurement each sample is mixed with distilled water and with a drop of sodium hexametaphosphate (Calgon) solution to break the cohesive bonds of flocculated particles.

3.4.9 Shear Strength Analysis

A fall cone test was used for shear strength analysis. A cone with a known weight and a known apex angle penetrates the sediment as deep as the shear strength of the sediment allows it. The cone is magnetically held up and the tip just touches the sediment surface. When the magnet is released the cone is driven into the sediment by gravity. The penetration depth can be converted into shear strength given in kPa (kilo Pascal) using empirically related charts for each cone. A cone of 60 g with a 60° apex angle and a 100 g cone with a 30° apex angle were used (Hansbo, 1957).

3.4.10 Radiocarbon Dating

3.4.10.1 Basic Principles

The radiocarbon method is based on the decay of one atomic species (^{14}C) into another (^{14}N). The source of ^{14}C is in the higher atmosphere, where cosmic ray neutrons interact with ^{14}N -atoms from the atmosphere under loss of a proton (^{13}C) and neutron capture to form ^{14}C . These ^{14}C -atoms behave chemically identical to the other two stable isotopes and connect with two oxygen atoms to form $^{14}\text{CO}_2$.

The CO_2 is photosynthesised into plant material or will be dissolved in ocean water. Eventually the dissolved CO_2 potentially becomes part of a CaCO_3 skeletal element of a marine calcareous organism, thus finding its way into the biogenic circle of carbon. The amount of ^{14}C that is stored in the global carbon reservoir remains approximately constant through time. Effectively a dynamic equilibrium is reached between the ^{14}C -producing atmosphere and the ^{14}C -storing ocean. Once an organism dies or once the calcareous shell

is built it becomes isolated from the permanent exchange of C-atoms. The continuing decay of ^{14}C is no longer matched by the constant balanced input.

Under normal circumstances the limit of measurement of ^{14}C activity is around 8 half-lives, being roughly 45 ka for the radiocarbon method (Bowman, 1990).

3.4.10.2 Accelerator Mass Spectrometry (AMS)

Accelerator mass spectrometry (AMS) analysis was performed at the Poznan Radiocarbon Laboratory (www.radiocarbon.pl). Though chemically identical the carbon isotopes differ in weight. This property is used to mechanically separate the ^{14}C from its lighter fellow isotopes. The discrimination between ^{14}C and ^{14}N is achieved by the AMS making use of the differences of the ion's size (stripper, fig. 3.3).

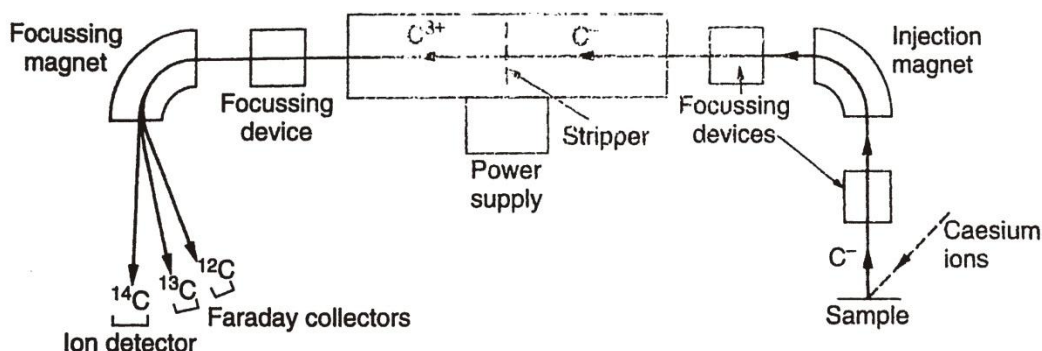


Figure 3.3: Schematic diagram of a tandem accelerator for the detection and measurement of the ratio of ^{14}C -atoms in a carbon sample (Bowman 1990).

3.4.10.3 Marine Reservoir Effects

The fresh ^{14}C supply for ocean waters takes place at the ocean-atmosphere boundary. At the sea surface the oceans have a modern ^{14}C age. However, when water masses sink ^{14}C decays without exchange with the atmosphere. Intermediate or deep water masses can therefore be seen as closed systems with regard to the ^{14}C decay. Thus, the ocean water will have an apparent age, which is called the marine reservoir age. This aging effect can vary

from a few tens of years to more than 1000 years (Ruddiman, 2001). The marine reservoir age varies in space and time, just as much as ocean currents are variable in space and time as well. This poses a difficulty, because the present-day reservoir age of the water may not represent an appropriate correction for the fossil of the radiocarbon dating analysis (Bowman, 1990).

The Calib 6.0html software uses the average marine reservoir age of 400 years. Each marine sample has a locally specific reservoir age. The local deviation of the average value of 400 years is expressed by the ΔR value (<http://calib.qub.ac.uk/calib/manual/>). In this study all marine radiocarbon dates were treated as suggested by Bondevik and Gulliksen with $\Delta R = 105 \pm 24$ for the Svalbard region (Mangerud et al., 2006).

In this study I have chosen to present all radiocarbon dates in cal. years BP (calendar years before present). This includes the dates from literature that are given in ^{14}C years BP (radiocarbon years before present). “Present” means 1950 AD. This is due to the extremely increased production of ^{14}C in association with atomic bomb drops in the USA and in Japan in 1945 and further tests thereafter. All radiocarbon dates from literature and those of this study were calibrated. The used calibration datasets were intcal09.14c and marine09.14c (Hughen et al., 2009, Reimer et al., 2009).

4 Swath Bathymetry

This chapter introduces the multibeam dataset that was acquired in November 2009 in Van Keulenfjorden. The large-scale morphology is presented before going into more detail on the smaller-scale morphologic features. All smaller-scale morphologic features were also covered with chirp-sonar profiles. In chapter 5 the features are presented again and interpretations based on the morphology and on the internal structures will be given there.

4.1 Large Scale Morphology and Bedrock Related Ridges

Both the sill separating the inner and outer basins and the sill at the mouth of Van Keulenfjorden are ~30 m deep. The outer basin is up to 110 m deep and is characterised by shallower areas, mostly controlled by NW-SE oriented ridges (figs. 4.1a and 4.1b). Some ridges are broad with diffuse limits due to a relatively thick sediment cover, i.e. the ca. 5.5 km broad shallower area on the northern side in the central part of the outer basin. Other ridges are relatively small and are sharply outlined, e.g. two ~300 m long elevations in the far north-western corner of the outer fjord basin (figs. 4.1a and 4.1b). The ridges are interpreted as bedrock related, because they strike in the same direction as the Mesozoic and Cenozoic bedrock from the West Spitsbergen fold and thrust belt (fig. 2.16; Dallmann et al., 1990), varying from NNW in the West to NW in the east (figs. 4.1a and 4.1b). The ridges delineate three sub-basins.

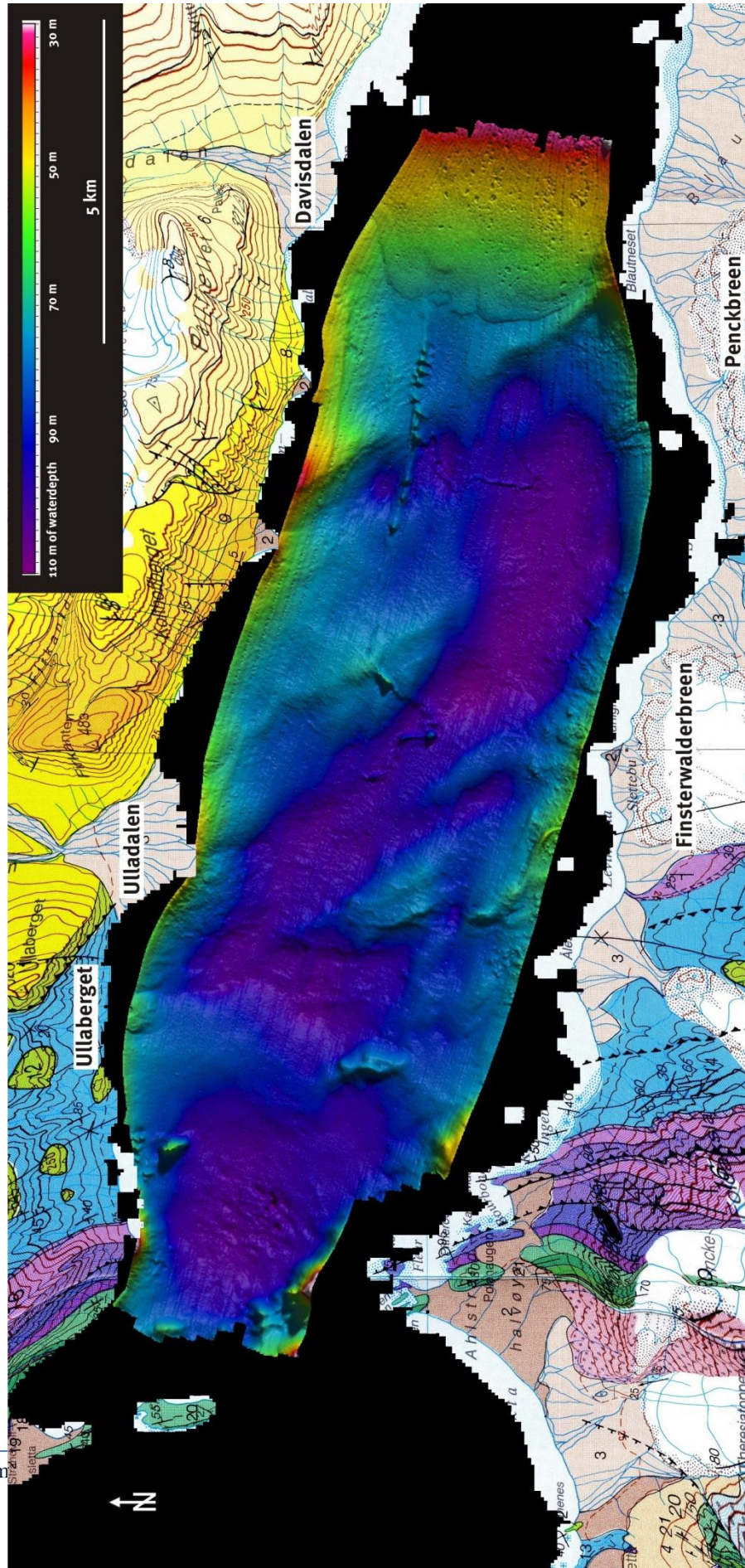


Figure 4.1a: Overview of the swath bathymetry data in Van Keulenfjorden placed within the topography, which is draped by the geologic map by Dallmann et al. (1990).

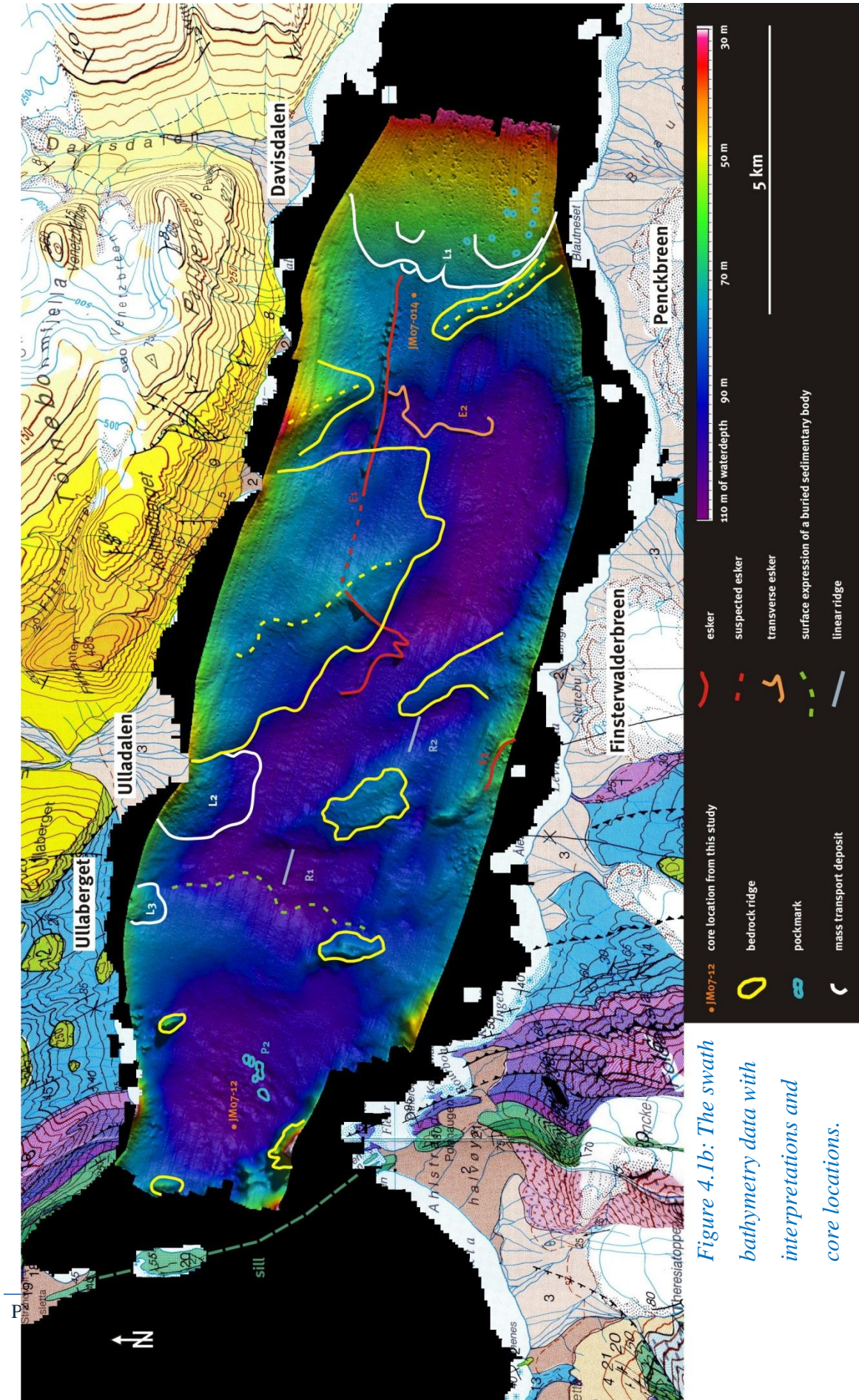


Figure 4.1b: The swath bathymetry data with interpretations and core locations.

4.2 Short Linear Ridges

Two small ridges, R1 and R2, are located in the central part of the outer fjord basin. They occur at 99 and 93 m water depth, respectively. The ridges are linear and oriented parallel to the fjord axis. The ridges are respectively 700 and 750 m long, 260 m and 280 m wide and 2 to 1.5 m high (fig. 4.2 and tab. 4.1).

Table 4.1: Geometric data on the ridges observed on the multibeam dataset.

Name	Length [m]	Width [m]	Height [m]	Water depth [m]	Form
R1	700	260	2	100	linear
R2	750	280	1.5	95	linear

These two ridges are interpreted to be subglacial features. The terminology for this particular feature is not precise. Glacial lineation ranges in scale from striation on rock surfaces to mega-scale glacial lineation. The processes involved also range from strictly erosive (Benn and Evans, 2010) to strictly depositional (Smith and Murray, 2009) as two end-members.

The ridges lack the ratio of length to width and the overall size to be called mega-scale glacial lineation. Both ridges are within the scale-window of drumlins (Korkalainen et al., 2007, Benn and Evans, 2010). However, the plan view shape and the absence of any other similar features are not entirely typical for drumlins as they are most often drop shaped and occur in assemblages, in so-called drumlin fields (Benn and Evans, 2010). The features in question have a positive morphology so the process is inferred to be mostly depositional. The descriptive term linear ridge will be used for this feature.

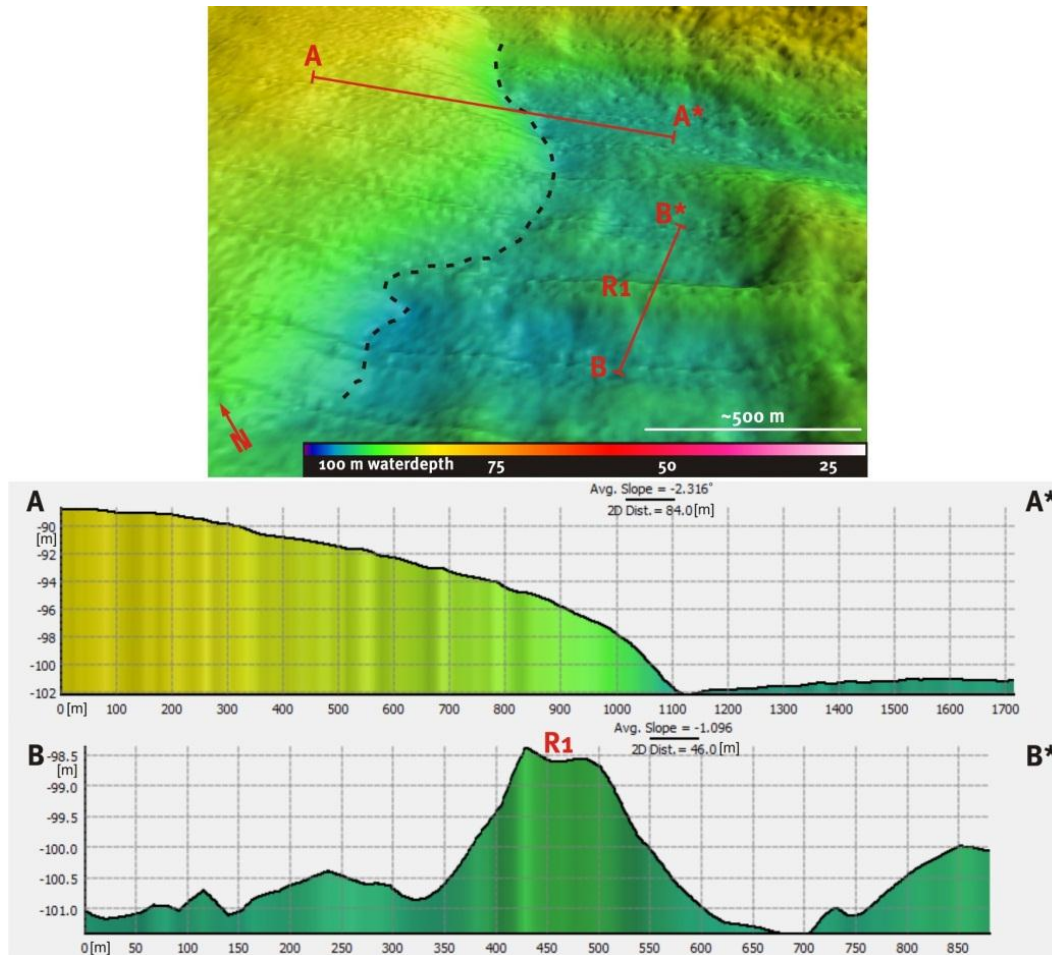


Figure 4.2: Above: Close-up angular view on the surface expression of a sedimentary body and the linear ridge. Below: Profile A-A* across the sedimentary body and profile B-B* across the linear ridge.

4.3 Eskers

Three ridges occur in the eastern part of the outer basin. Their shapes vary between straight to zigzagged, and continuous to beaded (figs. 4.1a, 4.1b, 4.3 and 4.4). The most prominent ridge, E1, is sub-parallel to the fjord axis, ~7.5 km long and 100 to 150 m wide (tab. 4.2). In the east this ridge is linear. There, it is covered with eleven mounds that are up to 12 m high. Towards the west it becomes sinuous and occasionally zigzagged.

Table 4.2: Geometric data of the eskers identified on the multibeam dataset.

Name	Length [km]	Width [km]	Height [m]	Water depth [m]	Orientation relative to fjord axis	Form
E1	7,5	150	1,5 - 14	77 - 96	sub-parallel	linear, sinuous, zigzagged
E2	2	130	1 - 2	92	transverse	sinuous
E3	1,3	110	1 - 7	60	sub-parallel	sinuous

Ridge E2 branches off from ridge E1. It is oriented transverse to the fjord axis and is more continuous and has a higher sinuosity. It is ~2 km long, 80 m wide and ~2 m high. Close to its southern end the ridge turns ~160° around towards east and can be followed for another ~400 m (figs. 4.1a, 4.1b and 4.3).

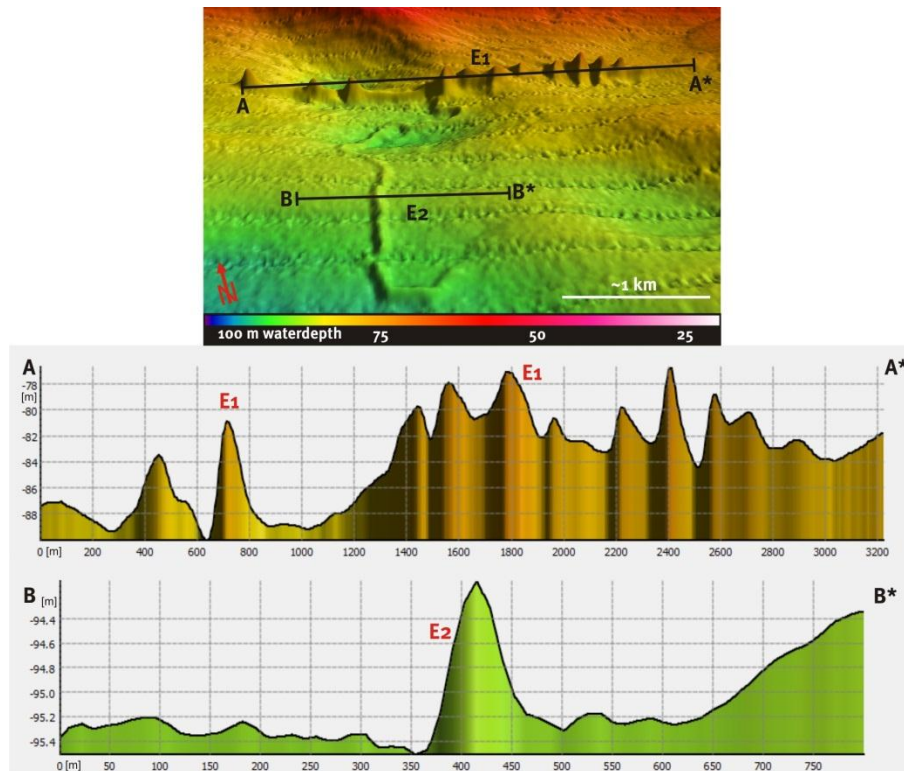


Figure 4.3: Above: Close-up angular view on the two eskers E1 (in the back) and E2 (in the front). Below: Profile A-A* along E1 and profile B-B* across E2.

Ridge E3 is ~1.2 km long and enters the fjord from the south in the vicinity of the glacifluvial delta in front of Finsterwalderbreen (fig. 4.4). The part closest to shore is oriented N-S, turning in the direction of the fjord axis (WNW) and then to NWN again.

All three ridges are interpreted to be eskers. Though eskers are usually parallel or sub-parallel to ice-flow direction there are documented cases of transverse eskers as E2 (Warren and Ashley, 1994, Benn and Evans, 2010).

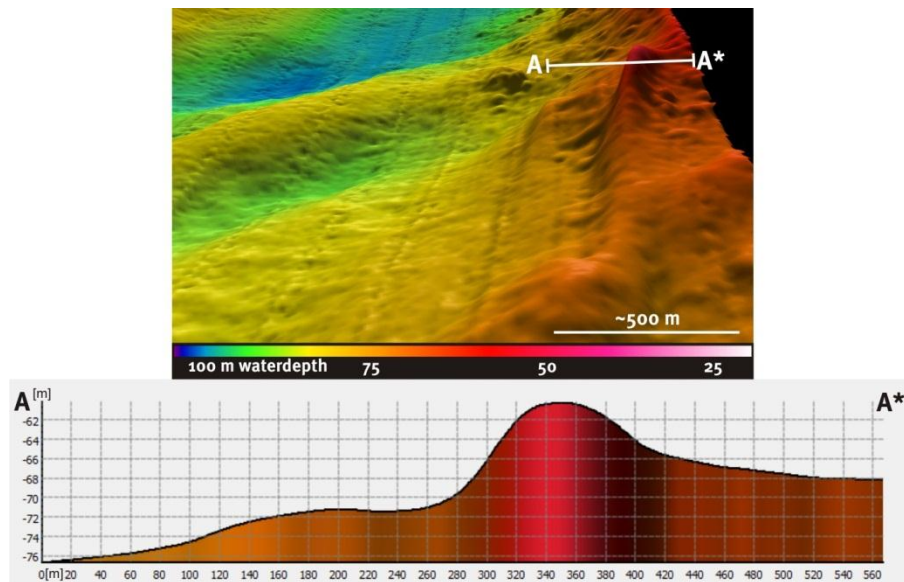


Figure 4.4: Above: Close-up angular view on the esker E3. Below: Profile A-A across E3.*

4.4 Mass-Transport Deposits

Three mass-transport deposits are identified. A ~4.5 km wide and >5 km long lobe with a generally constant surface dip of $\sim 0.75^\circ$, L1, occurs in the eastern part of the outer basin (figs. 4.1a, 4.1b and 4.5). Pockmarks are spread over most of its surface. This deposit was interpreted as a debris flow lobe in front of the Little Ice Age morainal bank (Ottesen et al., 2008, Forwick et al., 2009).

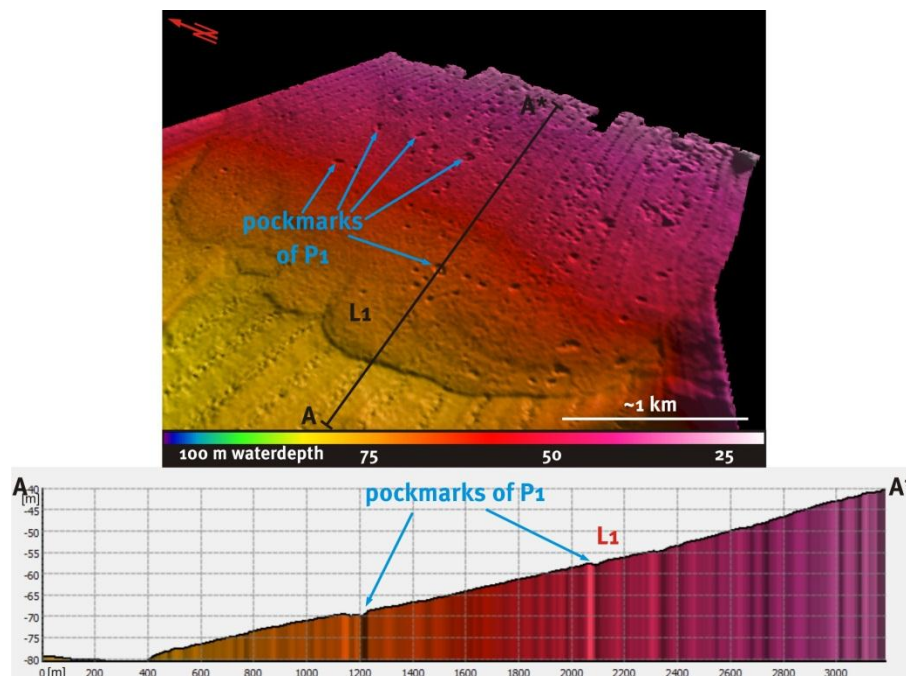


Figure 4.5: Above: Close-up angular view on the debris flow lobe, L1, in the east of the study area. Below: Profile A-A* along L1.

On the northern side of the outer basin, a lobe is located in front of the glacifluvial delta at the mouth of Ulladalen (L2, figs. 4.1b and 4.6). It is roughly 1.5 km wide, >1.2 km long and has an uneven surface. The dip of the lobe is decreasing downslope giving the slope a concave character. The thickness of the lobe is difficult to estimate, because numerous small deposits are amalgamated with the regular fjord sedimentation, however, the lobe accounts for at least extra ~5 m sediment (cf. chapter 5).

Table 4.3: Geometric data on the sedimentary lobes identified on the multibeam dataset.

Name	Length [km]	Width [km]	Water depth [m]	Description
L1	> 3	3,5	<35 - 80	pockmarks, several lobes
L2	>1,2	2,2	<55 - 95	hummocky surface
L3	>0,6	0,66	<68 - 86	two lobes, smooth surface

The third lobe (L3) is located ~2 km west of L2, south of Ullaberget. It is >650 m long, ~700 m wide and at least 6 m thick. The surface is smooth (tab. 4.3 and fig. 4.7). The strong convex appearance points towards cohesive transport processes. Two depositional events were identified (outlined with black dots on fig. 4.7).

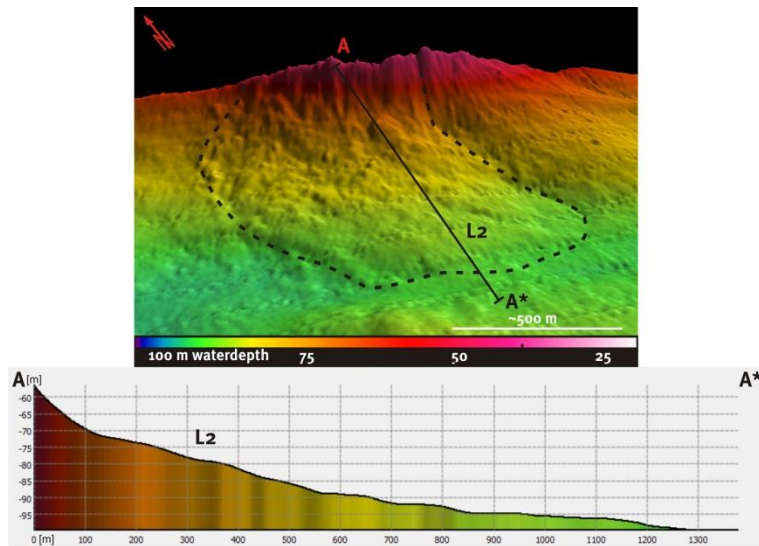


Figure 4.6: Above: Close-up angular view on the mass-transport deposit lobe L2. Below: Profile A-A* along L2. Note the concave slope form.

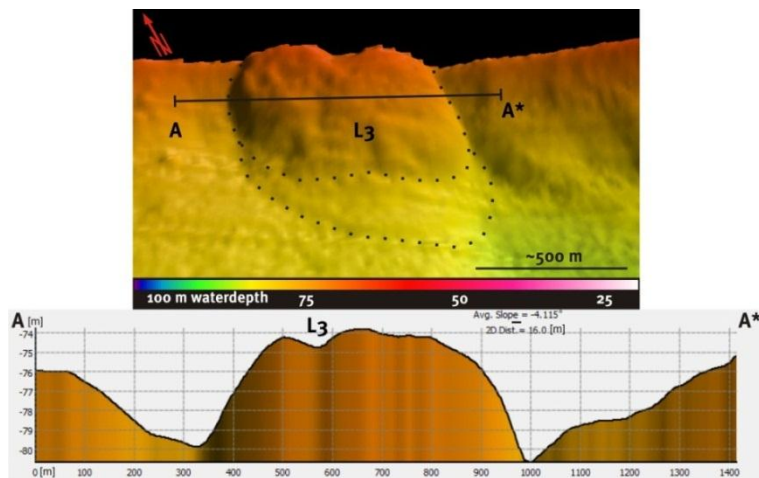


Figure 4.7: Above: Close-up angular view on the debris flow lobe L3. Below: Profile A-A* along L3.

4.5 Pockmarks

Two clusters of circular, conical depressions occur in the fjord basin. Over 100 sharply outlined depressions occur in the first cluster, P1, which is located on top of the debris flow lobe, L1. Their diameters are ~50 m and they are ~1 m deep (fig. 4.5). These features will be discussed with help of chirp sonar profiles in chapter 5.

The second cluster, P2, is located close to the sill at the fjord mouth. There, the depressions have diameters of 200 m to 300 m and depths up to ~6.5 m. Six depressions are well visible, whereas several less distinctive circular depressions occur in the vicinity. In general the P2-features are not sharp-crested (tab. 4.4 and fig. 4.8).

Due to their geometry these features are interpreted to be pockmarks.

Table 4.4: Geometric data on the two pockmark clusters identified on the multibeam dataset.

Name	Diameter [m]	Water depth [m]	Amount	Description
P1	~50	<40 - 75	>100	sharp crested
P2	~150	95 - 105	6 (15)	unsharp outlines

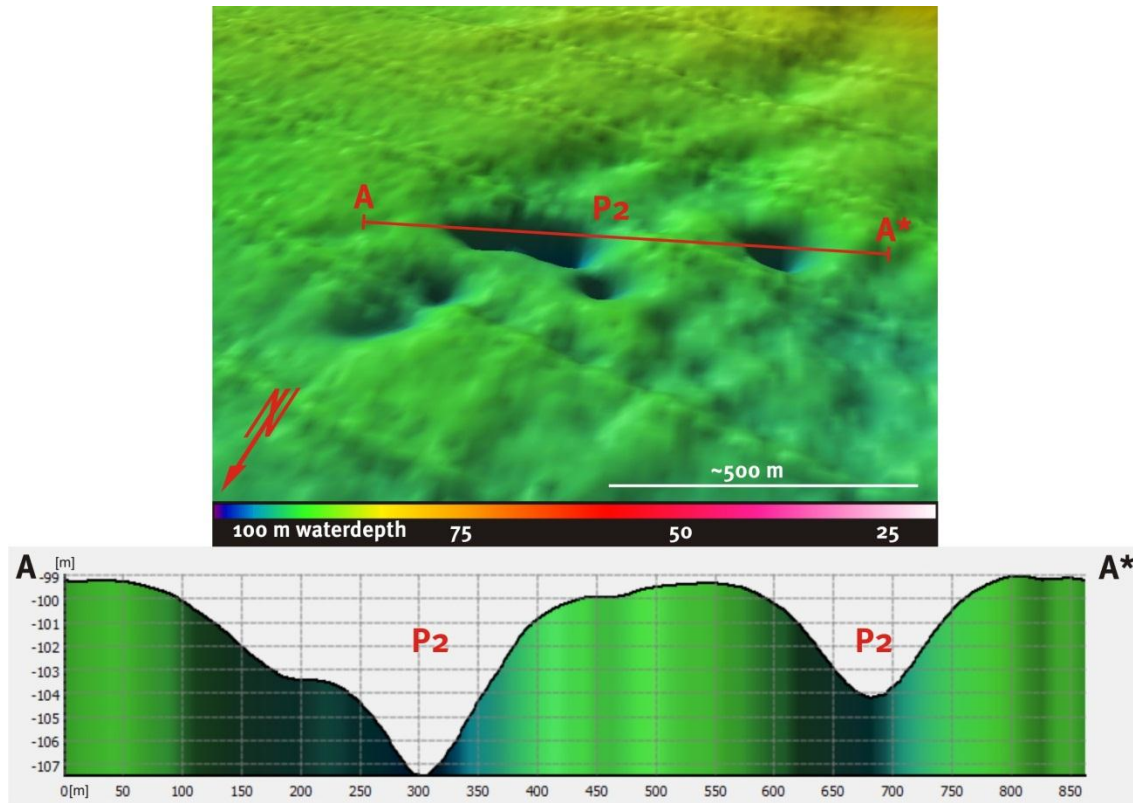


Figure 4.8: Above: Close-up angular view on the surface expression of the pockmarks of the P2 cluster. Below: Profile A-A across two of the depressions.

5 Chirp Sonar

Thirty three chirp sonar profiles were collected simultaneously with the multibeam data. This resulted in a close-meshed chirp sonar survey (fig. 5.1). The chirp profiles will be used to describe seismostratigraphic units and to deduce sedimentary processes.

5.1 Seismostratigraphy and Sedimentary Architecture

A regional seismostratigraphy is established for Van Keulenfjorden based on acoustic attributes, signature and units geometry. Five horizons are defined (figs. 5.2 and fig. 5.3). The horizons follow generally strong reflections (R1 to R4 and the seafloor) that can be followed throughout almost the entire basin and they define four units termed Vk1, Vk2, Vk3 and Vk4. However, at some places the reflections are attenuated or get too close to one another making it difficult or impossible to define the horizon.

From a sparker profile, taken in 1997, and from results presented from Bratlie (1994), a unit below Vk1 is defined as Vk0 (fig. 5.4). A summary of the unit and their seismostratigraphic properties is given in table 5.1.

In the western part of the fjord there is an area with distinctively thinner strata above horizon R1. The internal reflections are very weak at the top and phase out completely below (fig. 5.5). The thinning is strongest in the sub-basin on the proximal side of the sill. From that area away to both east and west the post-R1 succession is thickening.

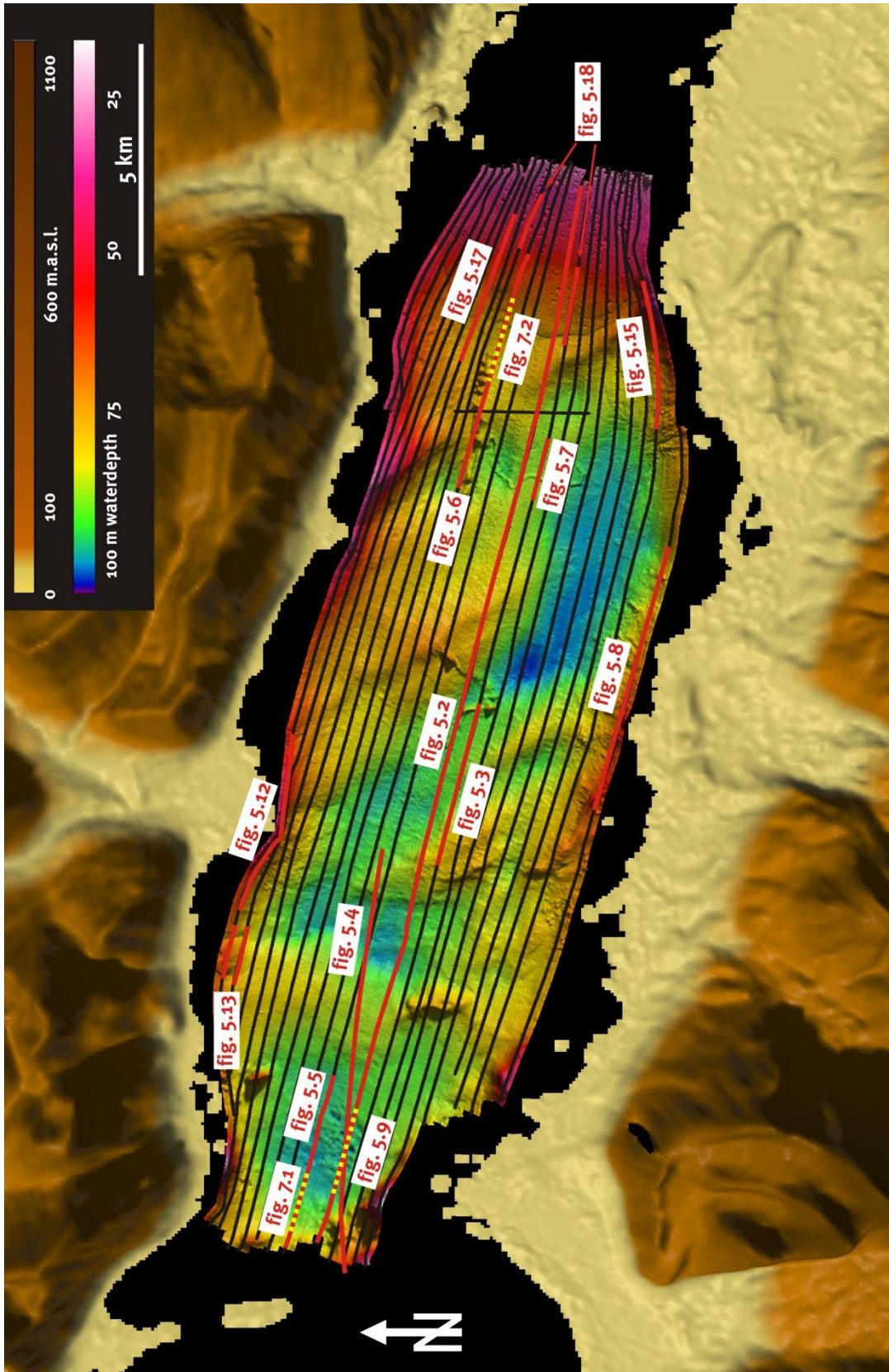


Figure 5.1: Locations of the chirp sonar profiles (black lines). Sections shown in this chapter are highlighted in red.

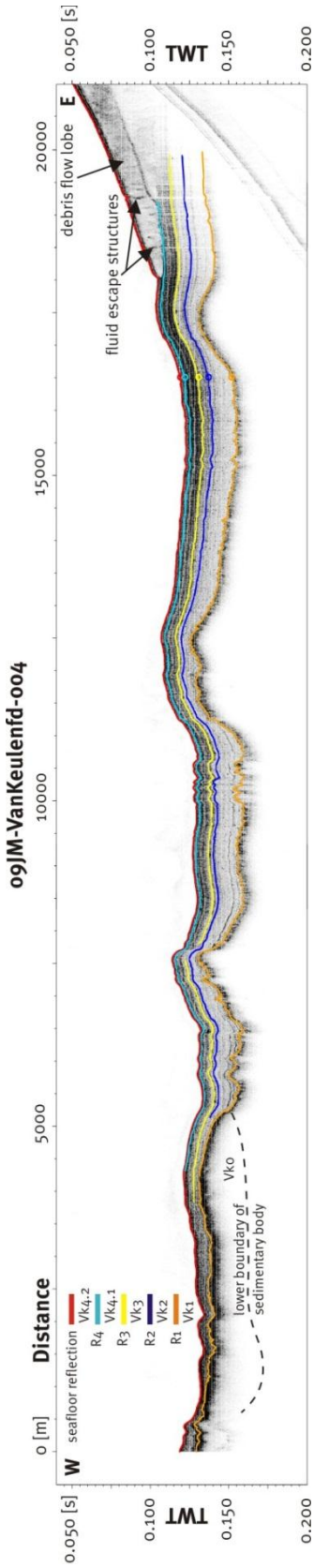


Figure 5.2: Chirp profile 09JM-VanKeulenfd-004, parallel to the fjord axis (for location see figure 5.1). The locations of horizons R1 to R4 and the seafloor are shown. The approximated outline of a sedimentary body in the western part of the fjord was inferred from a sparker profile collected in 1997 (fig.5.4).

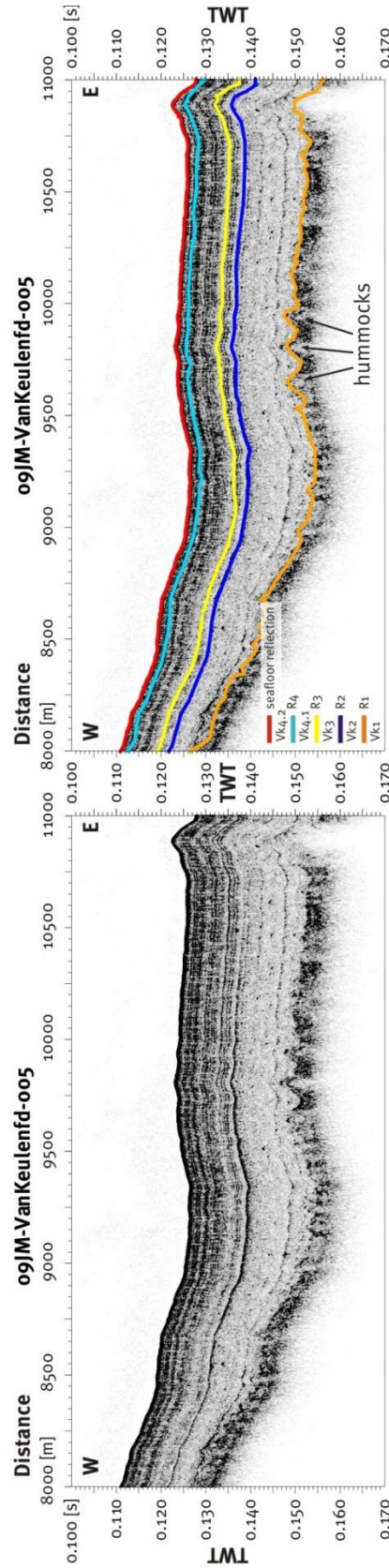


Figure 5.3: Section of Chirp profile 09JM-VanKeulenfd-005 from central parts of the fjord without and with horizons showing the typical profile composition (for location see fig. 5.1).

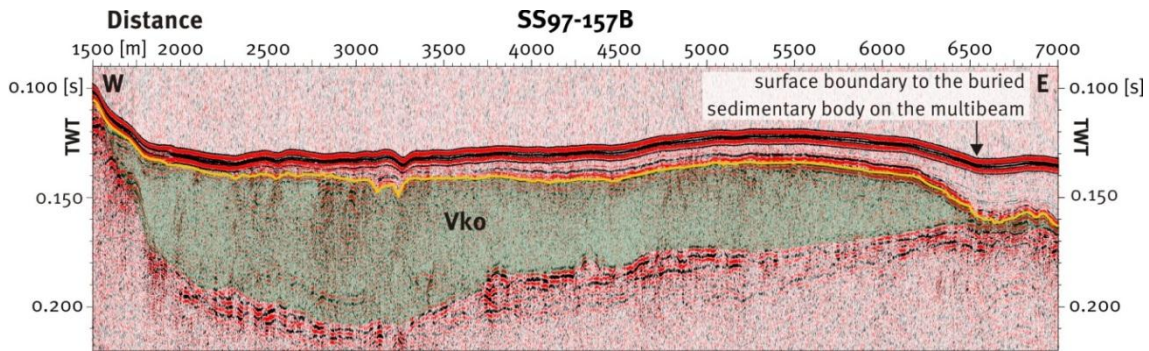


Figure 5.2: Sparker profile acquired in 1997. Deeper penetration into the fjords sediments reveals a seismic unit (Vk0, green opaque area) situated on the inside of the sill below the horizon described by the dark yellow line. The arrow indicates the location of the surface boundary of Vk0 that is visible on the multibeam dataset (cf. figs. 4.1a and 4.1b).

Table 5.1: Overview of the characteristics of the seismostratigraphic units in Van Keulenfjorden. *) the maximum value in brackets accounts for the debris flow lobe L1.

Unit Name	Thickness	Reflection Configuration	Reflection Continuity	Reflection Magnitude	Reflection Abundance	Lower Boundary	Upper Boundary
	range [ms TWT]						
Vk4.2	0 - 9 (40)*	parallel, even	continuous	high	high	concordant	modern seafloor
Vk4.1	0 - 15	parallel, even	continuous	high	high	gradual, concordant	concordant
Vk3	0 - 12	parallel, even	continuous	low	high	gradual, concordant	gradual, concordant
Vk2	0 - 20	parallel, even	weakly continuous	very low	very low	marked, onlap to concordant	marked to gradual, concordant
Vk1	no lower boundary on chirp	parallel, even	discontinuous	high	low	marked, concordant	marked, concordant
Vk0	-	transparent	-	low	low	marked, discordant	marked, concordant

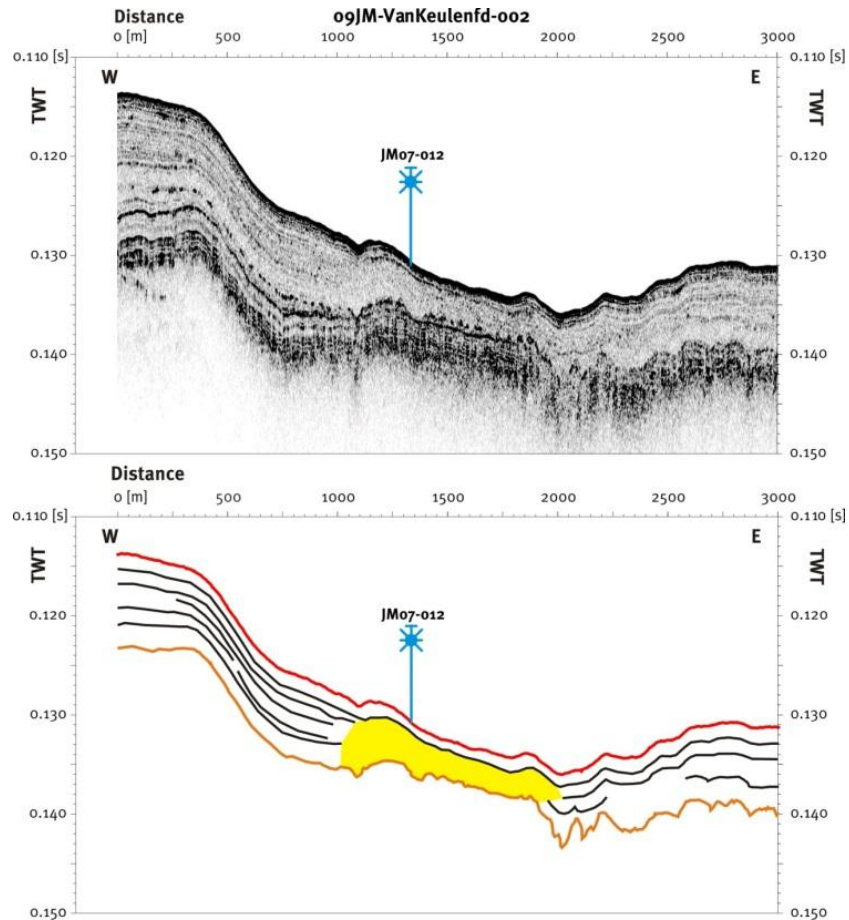


Figure 5.3: Above: Clean chirp profile 09JM-VanKeulend-002. Below: Horizon interpretations of the same section as shown above. The red line denotes the seafloor reflection, the orange line denotes horizon R1. The yellow area indicates the volume of strong thinning and transparent to chaotic signature.

5.1.1 Unit Vk0

Vk0 is the lowermost seismostratigraphic unit in the fjord above the Mesozoic and Cenozoic bedrock (fig. 5.4 ; Bratlie, 1994). In most of the fjord it is a thin layer. It is assumed to be present in the entire fjord area, but it thins out beyond sparker seismic resolution in some places. In the east the unit thickens significantly to more than 50 ms TWT. The internal signature is transparent and chaotic with one faint reflector in its lowest part. The upper boundary is sharp. To the west Vk0 wedges out onto the sill.

5.1.2 Unit Vk1

Vk1 is the lower most seismostratigraphic unit recorded by the chirp data. Its upper boundary is defined by horizon R1. The lower boundary is not identified on chirp profiles. On the sparker line the boundary is marked with a strong reflection. R1 is often the deepest chirp-recorded reflection in the study area. Where there are internal reflections in unit Vk1, the acoustic signature is characterised by discontinuous internal stratification. In a few places a maximum of three internal reflections beneath R1 can be identified. In other places Vk1 shows chaotic to transparent acoustic signature (figs. 5.3 and 5.6). Vk1 occurs in the entire fjord and overlays the Vk0 in the west (fig. 5.4)

The topography of the upper boundary is often hummocky, but can also be smooth. Numerous small-scale hummocks with a wavelength of ~ 30 to 40 m and a vertical extent of ~ 2 ms TWT occur frequently. In addition there are some larger positive features that also can be identified on the present seafloor, e.g. the beaded esker E1 (fig. 5.6). Most of the landforms discussed in the previous chapter (chapter 4) originate from Vk1 or deeper, while the units above act as a drape (tab. 5.2).

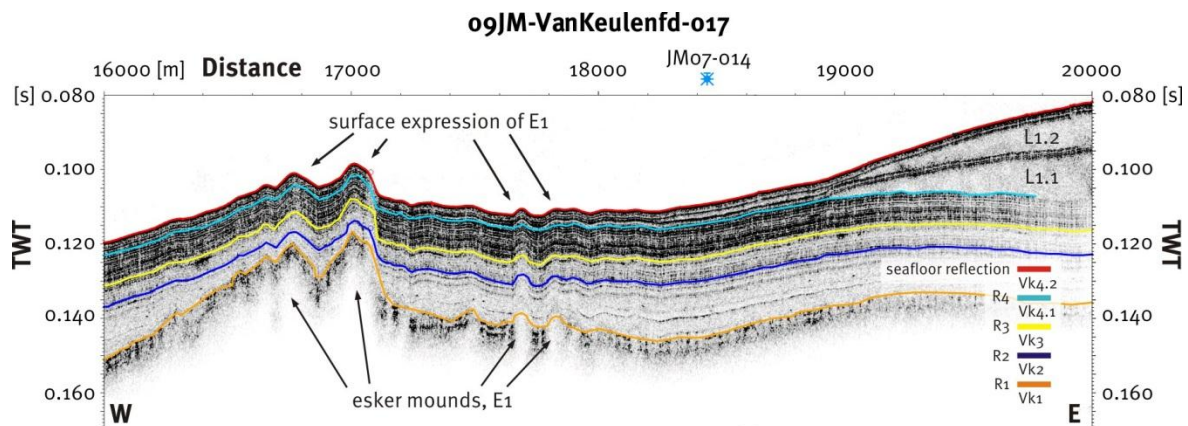


Figure 5.4: Chirp profile 09JM-VanKeulenfd-017. Note that horizon R4 divides Vk4 into the pre-L1 sub-unit Vk4.1 and the syn- and post-L1 sub-unit Vk4.2. The mounds of E1 originate in or below unit Vk1. The light blue sign indicates the projected location of core site JM07-014 onto the profile. For location see fig. 5.1. The same feature's surface is shown in fig. 4.3.

Table 5.2: Geometric properties of some of the described features derived from chirp sonar profiles.

Name	Internal Signature	Unit of origin	Height surface [ms TWT]	Height at lowest visible datum [ms TWT]
Esker E1	no internal reflections	Vk1, or deeper	9	15
Esker E2	no internal reflections	Vk1, or deeper	3	9
Esker E3	no internal reflections	Vk1, or deeper	6	10
Lobes L1.1 and L1.2	transparent	Vk4.2	-	-
Lobe L2	chaotic, transparent	Vk3, Vk4.1 and Vk4.2	-	-
Lobe L3	transparent	Vk3	12	28
Pockmarks P1	chaotic, masked	in L1.2 (Vk4.2)	2	-
Pockmarks P2	normal basin sedimentation	Vk1, or deeper	10	12

All three eskers (E1, E2 and E3) on the multibeam dataset originate from unit Vk1 or deeper and the surface expression of the eskers have a strongly attenuated relative elevation change due to the draping sediments on top (figs. 5.6, 5.7 and 5.8). The original landforms of the eskers are steeper (tab. 5.2). The internal signature of these eskers cannot be determined, because of low penetration of the chirp data.

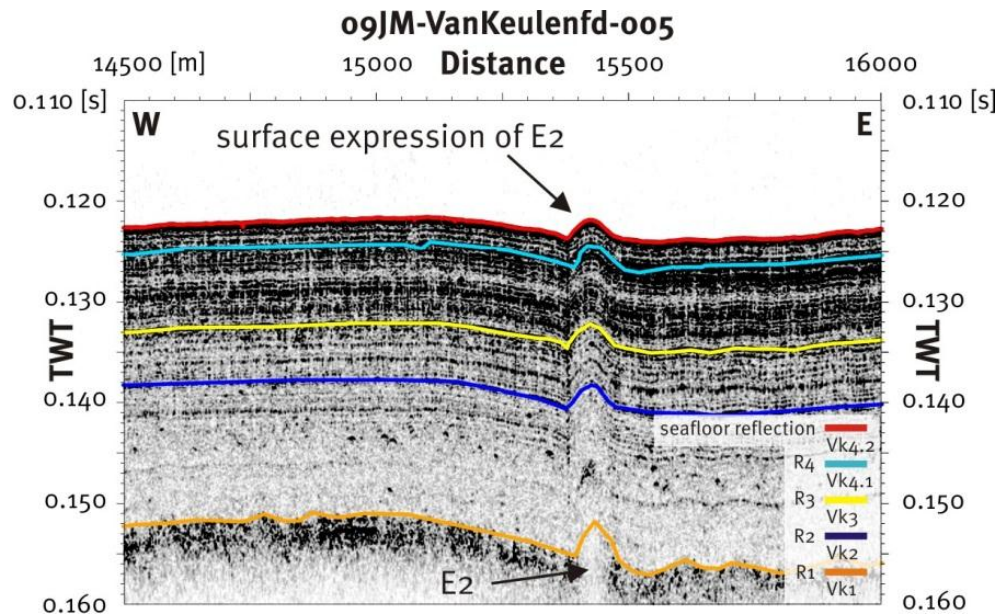


Figure 5.5: Chirp profile 09JM-VanKeulenfd-005 crossing esker E2. For location see fig. 5.1. The same feature's surface is shown in fig. 4.3.

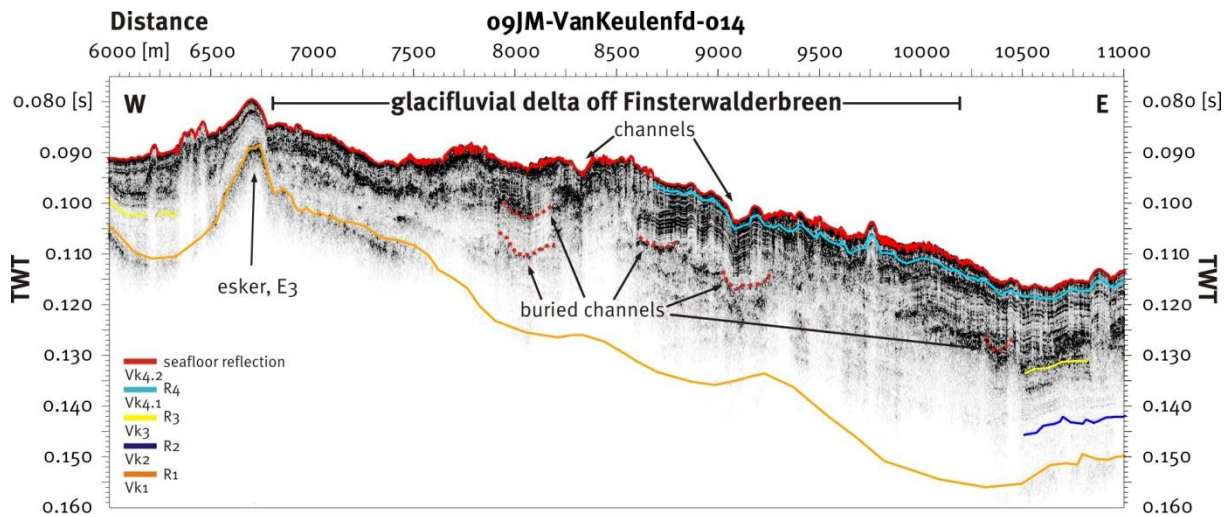


Figure 5.6: Chirp profile line 09JM-VanKeulenfd-014 in front of Finsterwalderbreen. The chaotic and disturbed architecture of the sediments is suggested to result from interfering processes (suspension fall-out, gravity-flows) on the glacialfluvial delta in front of Finsterwalderbreen. Esker E3 is visible in the western part of the profile (see also fig. 4.4). Red dotted lines indicate bases of buried channels. For location see fig. 5.1.

The pockmark morphology on the seafloor is inherited from seismic horizon R1. The sediments above R1 show no sign of disturbance (fig. 5.9). This suggests that the last active phase of the pockmarks predates the sedimentation of Vk2. This fact also explains the smooth appearance of the P2 pockmarks on the swath bathymetry dataset (fig. 4.8).

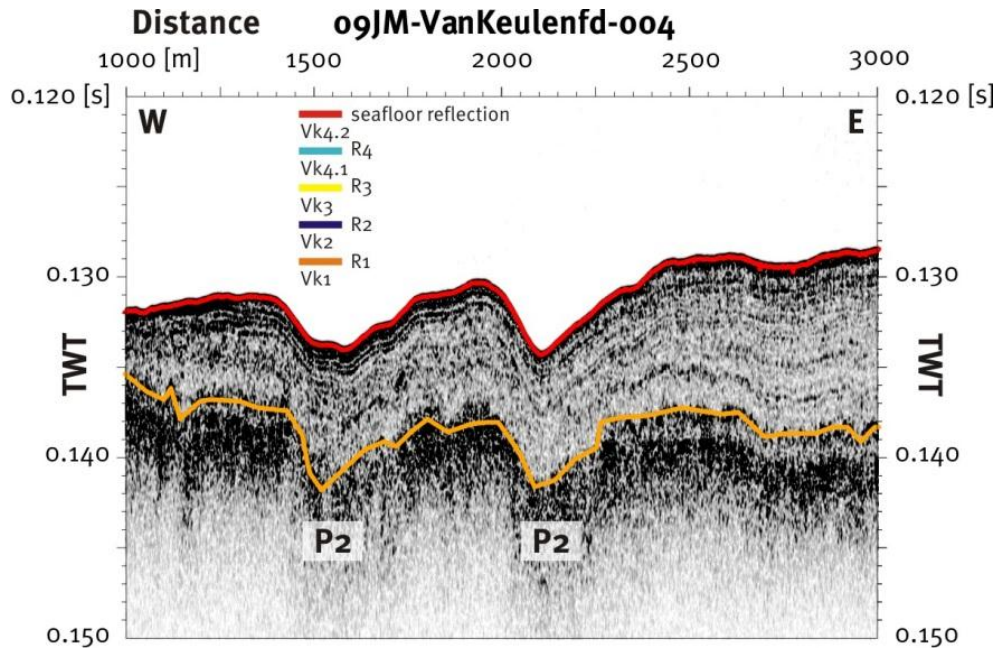


Figure 5.7: Chirp profile 09JM-VanKeulenfd-004 across two pockmarks of the pockmark field P2 (for location see figs. 4.1a, 4.1b and 5.1). The internal stratification of the sediments in the depressions shows no prominent sign of disturbance. The same feature's surface is shown in fig. 4.8.

5.1.3 Unit Vk2

Unit VK2 is defined by the horizons R1 (base) and R2 (top; figs. 5.2 and 5.3). The unit occurs in the whole outer fjord basin. In most places the unit has a transparent acoustic signature with very few and weakly stratified parts. The isopach map (fig. 5.10) reveals that the unit is thinning above the bedrock ridges. The upper boundary of unit Vk2 is marked by a transitional but distinctive change in internal acoustic signature from transparent to less transparent and more acoustically stratified above.

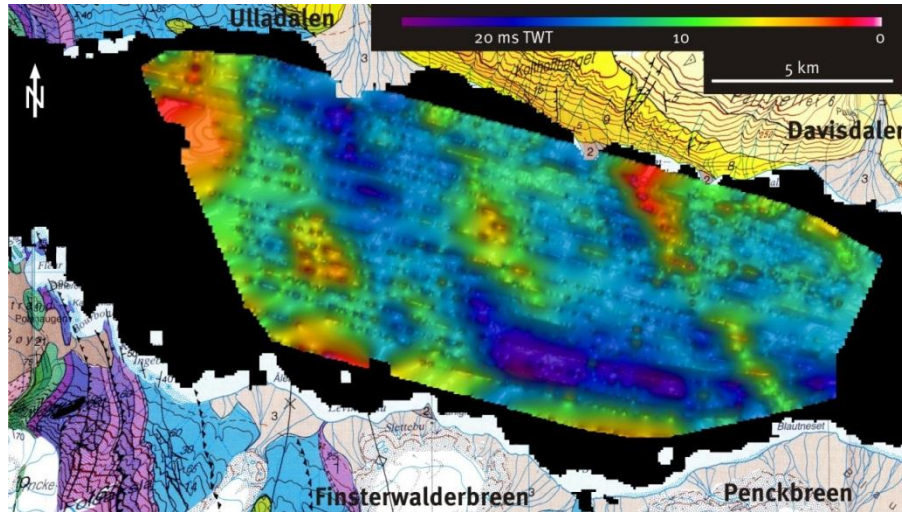


Figure 5.8: Isopach map of unit Vk2.

5.1.4 Unit Vk3

Unit Vk3 is defined by the horizons R2 (base) and R3 (top). The internal reflection characteristics show weak, continuous stratification. It occurs in the whole study area and thins from the east towards the west (see isopach map, fig. 5.11). Compared to unit Vk2 the isopach map shows a more homogenous sedimentation rate throughout the basin. However, sediment supply from rivers draining through Ulladalen, as well as from Finsterwalderbreen and Penckbreen result in locally thicker accumulations. It should be noted that Davisdalen to the NE shows no increased sediment input during the same time interval between R2 and R3. The lower boundary of unit Vk3 is marked by the transition from transparent to weakly stratified signature. The upper boundary of Vk3 is a gradual change in magnitude of the stratifications indicated by R3.

The internal structure of the lobe in front of Ulladalen in the NW is more complex. There sediment from the main basin is interrupted by several small sedimentary bodies with transparent, semi-transparent and chaotic internal signature (fig. 5.12). In addition, the modern channel and several buried channels occur on the cross-delta slope profile, the biggest of which are indicated on fig. 5.12. The additional sediment input from Ulladalen seems to have been highest above horizon R2. The interference of the deltaic sedimentation continues up to the seafloor.

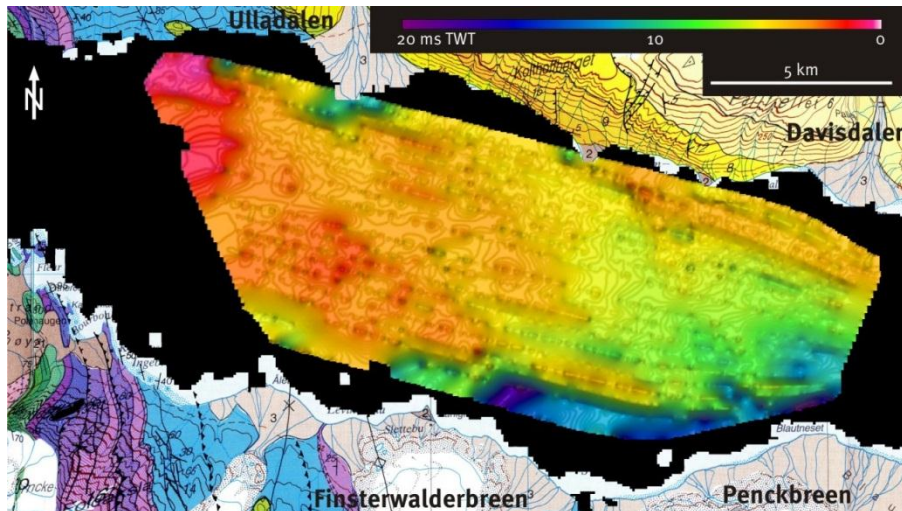


Figure 5.9: Isopach map of unit Vk3.

The debris flow lobe, L3, in front of Ullaberget in the north western area of the basin has a typical and distinctive lobe shaped outline on the swath bathymetry dataset. The lobe's internal signature is transparent. There are ~10 ms TWT of sediment covering the lobe (fig 5.13). The multibeam dataset reveals two lobes stacked on top of each other. The chirp profiles do not show this due to unfortunate seismic line location.

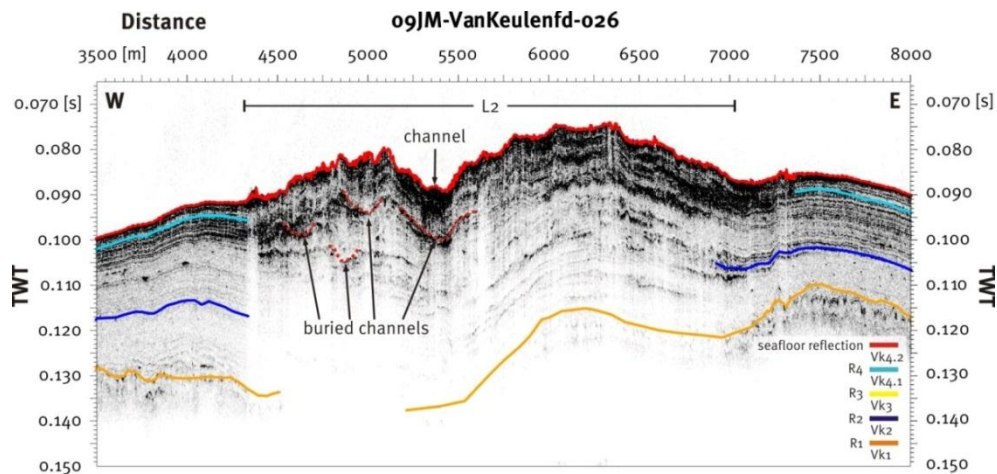


Figure 5.10: Chirp profile 09JM-VanKeulenfd-026 crossing lobe L2 showing intense sediment deformation off the river draining through Ulladalen. Red dotted lines indicate channel-shaped palaeo-surfaces. The same feature's surface is shown in fig. 4.6. For location see fig. 5.1.

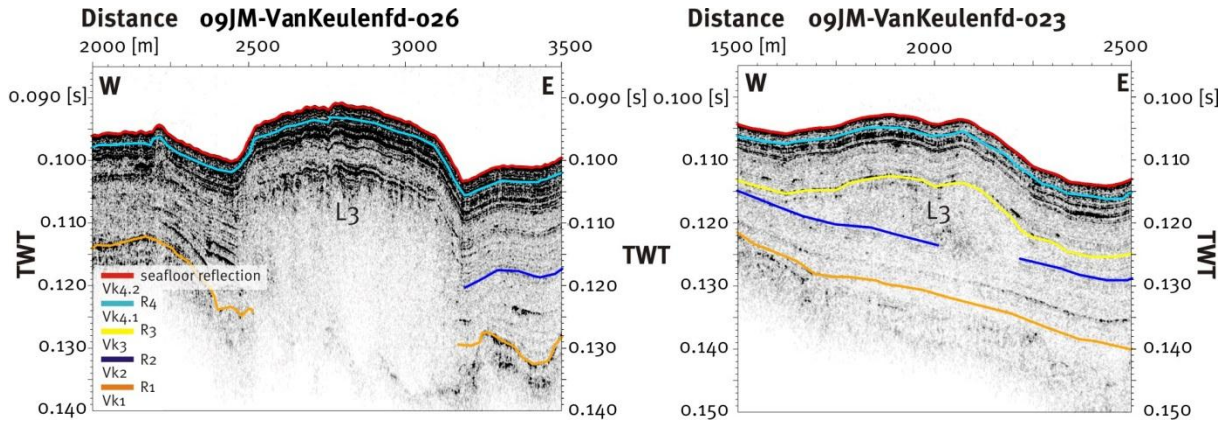


Figure 5.11: Chirp profiles 09JM-VanKeulenfd-026 and 09JM-VanKeulenfd-023 across lobe L3. Chirp sonar line 09JM-VanKeulenfd-026 is more proximal than line 09JM-VanKeulenfd-023. The same feature's surface is shown in fig. 4.7. For location see fig. 5.1.

5.1.5 Unit Vk4

Unit Vk4 is the uppermost unit in the Van Keulenfjorden sediment succession. It is defined by the horizon R3 (base) and the present seafloor reflection, and it is existent in the whole fjord area. Like unit Vk2 and Vk3 it shows an east to west thinning trend. The internal acoustic signature is dominated by continuous, high magnitude reflections, which show little variation. The sediment thickness is regular with deviations only near the fjord sides, where mass-transport deposits interfere with the basin sedimentation. Unit Vk4 is subdivided into two sub-units called Vk4.1 and Vk4.2.

5.1.5.1 Sub-Unit Vk4.1

Unit Vk4.1, the lower of the two Vk4 sub-units, is defined by horizon R3 below and R4 above. The horizon R4 was chosen in order to differentiate between the part of unit Vk4 that accumulated prior to and subsequent to the deposition of debris flow lobe L1.

Unit Vk4.1 shows a regular sedimentation pattern with increased sedimentation along the fjord sides originating from Ulladalen in the NW, Davisdalen in the NE, Finsterwalderbreen to the south and especially Penckbreen in the southeast. Thicker accumulations off Finsterwalderbreen and Penckbreen can be related to mass-transport

activity (figs. 5.8, 5.14 and 5.15). The basin sedimentation, which is mostly controlled by suspension fall-out and ice rafting from the tidewater glaciers at the fjord head, is disturbed by interfingering glaci-fluvial sediments. Small-scale debris flows and proximal and spatially limited suspension fall-out are added from the glaci-fluvial deltas (figs. 5.8 and 5.15).

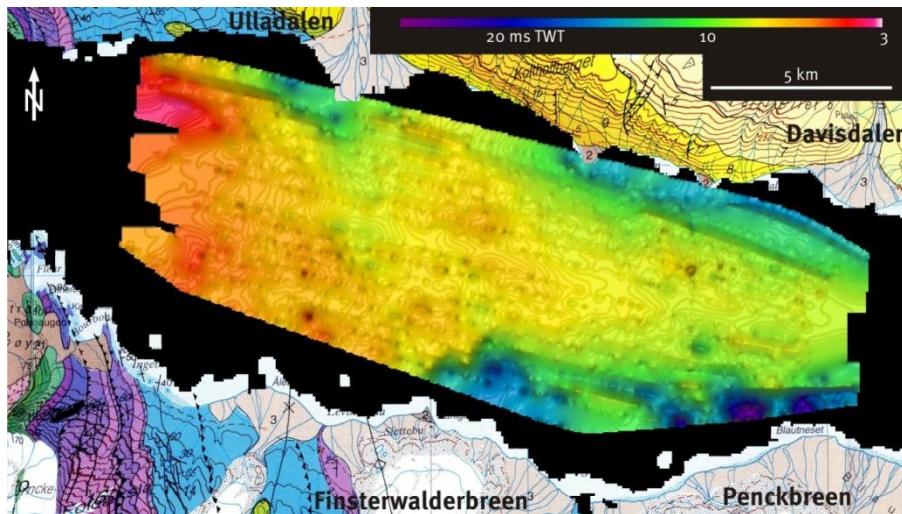


Figure 5.12: Isopach map of unit Vk4.1.

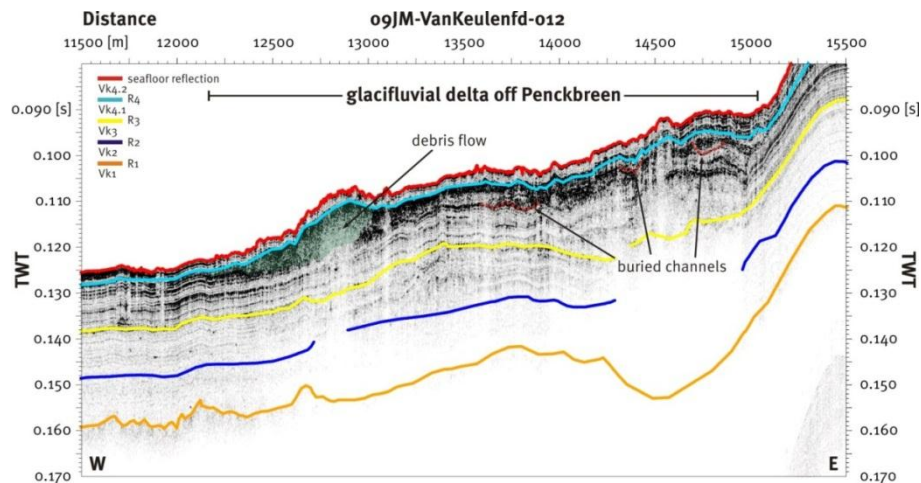


Figure 5.13: Chirp profile line 09JM-VanKeulenfd-012 in front of Penckbreen. The transparent to chaotic internal signature and complex architecture of the sediments is due to mass-transport input from the south. Red dotted line indicates channel-shaped buried surfaces. The green transparent overlay indicates a debris flow deposit.

5.1.5.2 Sub-Unit Vk4.2

Unit Vk4.2 is defined by horizon R4 below and the present seafloor reflection above. Of all units it shows the most even distribution of sediment, with a thinning trend towards the west. Slightly increased sedimentation is shown from Ulladalen and Davisdalen (fig. 5.15). However, the most prominent features are the debris flow lobes L1.1 and L1.2 in the eastern part of the outer basin (figs. 5.2, 5.6, and 5.16).

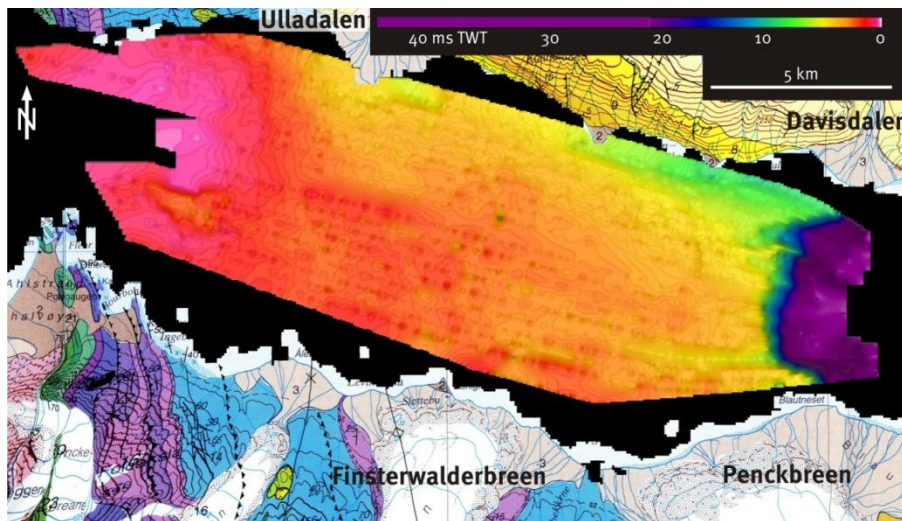


Figure 5.14: Isopach map of unit Vk4.2.

The chirp profiles reveal that the lobe identified on the swath bathymetry data is underlain by another lobe and that both lobes are separated by acoustically stratified sediments (fig. 5.17; Bratlie, 1994, Ottesen et al., 2008). The strata of the basin sedimentation at the lower boundary of the debris flow are truncated. The process of deposition of the debris flow was therefore partly erosive (fig. 5.18).

Pockmark field P1 is situated on the debris flow lobes L1.1 and L1.2 and is displayed on the figures 5.2 and 5.17. It is difficult to determine the origin of the fluid escape structures, because of the masking effect of the features. Nevertheless it looks like the only part affected by fluid escape structures is the upper lobe, L1.2.

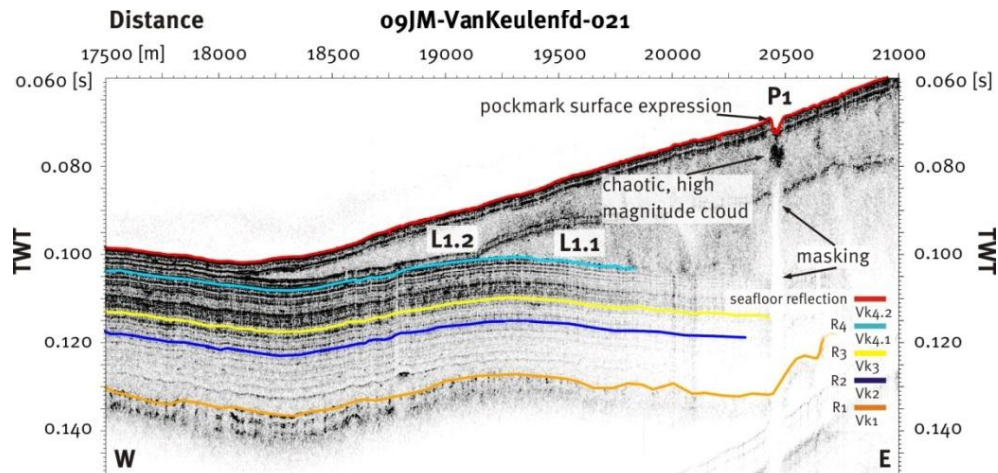


Figure 5.15: Chirp profile 09JM-VanKeulend-021 showing the two debris flow lobes, L1.1 and L1.2. The same feature's surface is shown in fig. 4.5. For location see fig. 5.1.

The general pattern of the pockmarks of P1 is a ~100 m wide and ~5 ms TWT deep surface depression. Underneath there is usually a chaotic, high magnitude reflection cloud associated with strong masking effects below (figs. 5.17 and 5.18). These pockmarks are not a common feature on debris flow lobes. So there are no examples of other debris flow associated pockmarks from Spitsbergen fjords to relate to (cf. Plassen et al., 2004).

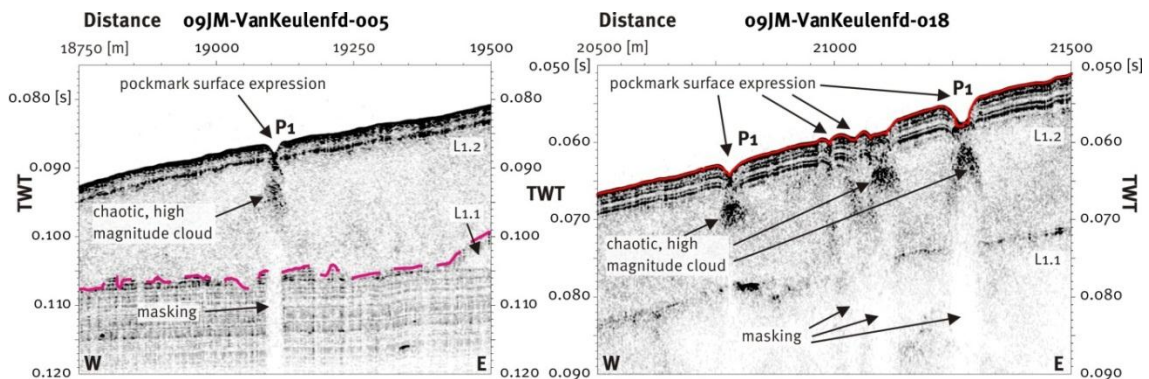


Figure 5.16: Chirp profiles 09JM-VanKeulend-005 and 09JM-VanKeulend-018 showing examples of the pockmarks in pockmark field P1. The lower, erosive, boundary of the lobe L1.2 is indicated by the dashed pink line. The same feature's surface is shown in fig. 4.5. For location see fig. 5.1.

6 Lithostratigraphy

This chapter presents the collected sediment cores. Lithostratigraphic units will be introduced and complement to the geophysical data presented in the previous two chapters. The cores will be described in form of lithological core logs, grainsize distribution logs, physical property logs and XRF-scanner data logs.

The sediment cores are divided into lithostratigraphic units that are defined by marked or transitional changes in one or more of the following parameters: grainsize, colour, internal structures or physical and chemical properties. The core locations and further information are shown in table 3.1 and figure 6.1. The lithological facies abbreviations stated on each core log are presented in table 6.1. The lithofacies code used for glacial sediments is modified from Evans and Benn (2004). The legend used in the logs is presented in figure 6.2.

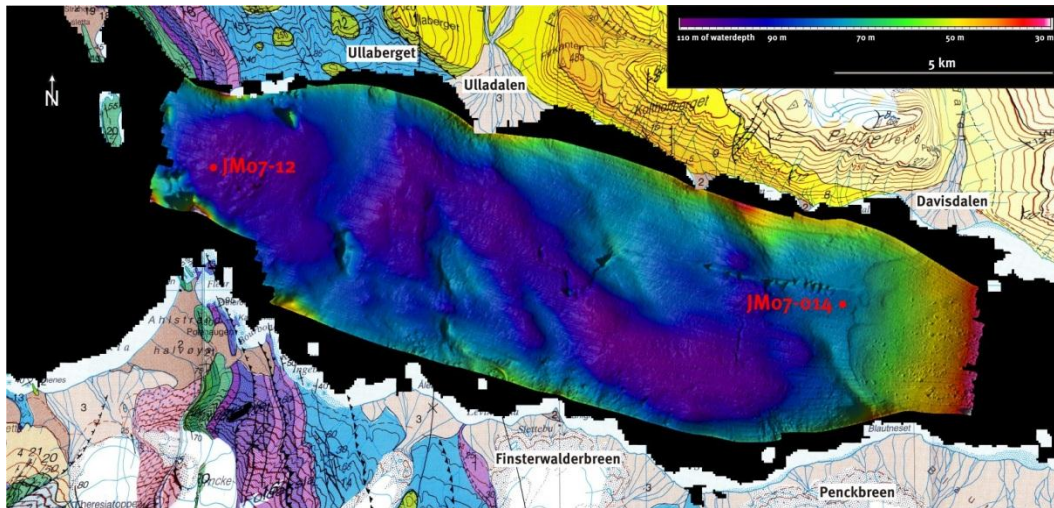


Figure 6.1: Core locations indicated by the red dots.

Several of the distinctive excursions of the graphs of physical properties occur at the core section boundaries. If there is reason to believe that a marked change in a graph is artificial then the marked change is chosen to be neglected in the description and interpretation.

Table 6.1: Overview of the lithofacies codes used in this study (adapted from Evans and Benn, 2004).

Lithofacies Code	
f---	Fine
c---	Coarse
F	Fine-grained, clayey-silty
-m	Massive
-l	fine lamination
--p	with intraclasts or lenses
---(d)	with dropstones (IRD)

Legend			
	Clay	2.5Y 3/2	Colour code after the Munsell Soil Colour Charts
	Silt	(10YR 3/1)	Colour code of a single layer after MSCC
	Sand with gravel	☉	Fossil
	Gravelly lamination	∞	Bioturbation
	Fine lamination	■	Sulphide spots
	Dropstones	6920 ± 70	Age in cal. yrs. BP and one standard deviation
	Gravelly or pebbly layer	12BC-1	Unit name, composed with location (two digits), core type (two letters) and unit number
		Fmp (d)	Lithofacies code adapted after Benn and Evans (2010)

Figure 6.2: Legend for all core logs.

6.1 Core Site JM07-012

The core site JM07-012 is located close to the fjord mouth, ~2 km east of the Island Eholmen (fig. 6.1 and tab. 3.1).

6.1.1 Box Core JM07-012-BC

Core JM07-012-BC is 25 cm long and contains the lithological unit 12BC-1 (Fig. 6.3).

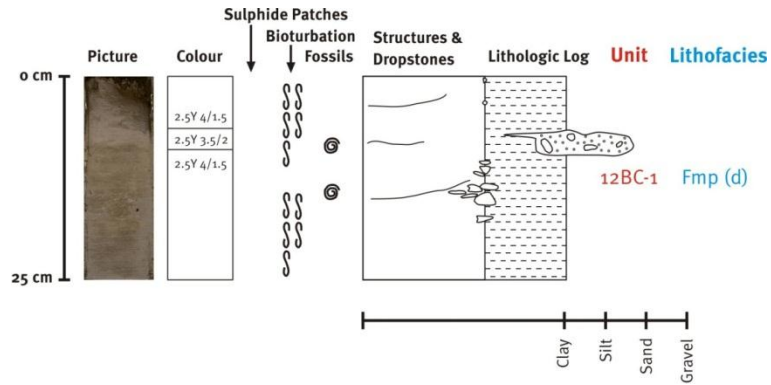


Figure 6.3: Colour image, colour codes and lithological log of box core JM07-012-BC. Note that the physical properties are not displayed, and a grainsize analysis was not performed, because the same sediments are found in the top of core JM07-012-GC.

6.1.1.1 Unit 12BC-1 (25 – 0 cm)

Core JM07-012-BC is composed of mud with gravel and pebble clasts (lithofacies Fmp (d); fig. 6.1, tab. 6.1 and tab. 6.2). A sandy lens occurs at ~8 cm depth. The sediment colour is dark grey (Munsell Soil Colour Codes (MSCC) 2.5Y 4/1.5 to 2.5Y 3.5/2). Shells and intense bioturbation occur (fig. 6.4). The differentiation between clay and silt cannot be made, because no sample of the box core was analysed by the sedigraph.

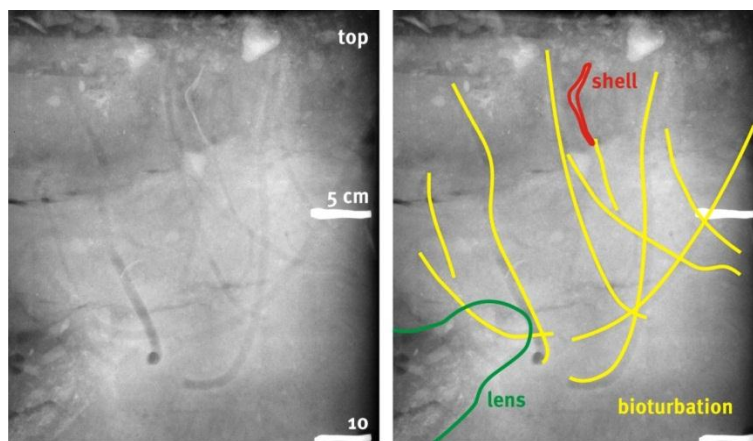


Figure 6.4: Radiograph (left) and interpretation (right) of core JM07-012-BC between 0 and 10 cm depth. Note that such well-preserved bioturbation is not found in other core.

Table 6.2: Minimum and maximum values of the measured physical properties of all lithological unit.

Unit	Bulk Density		Magnetic Susceptibility (mass-specific)		Magnetic Susceptibility (volume-specific)		P-Wave Velocity		Shear-Strength		Fractional Porosity		Water Content (Freeze Drying)	
	[g cm ⁻³]		[m ³ kg ⁻¹]		[10 ⁻⁵ SI]		[m s ⁻¹]		[kPa]		[volume %]		[weight %]	
	min.	max.	min.	max.	min.	max.	min.	max.	min.	max.	min.	max.	min.	max.
12BC-1	1,577	1,738	2,528	5,799	4,180	9,951	1473,6	1514,9	-	-	58,69	68,05	-	-
12GC-3	1,240	2,210	3,849	25,015	6,358	15,851	1434,6	1559,0	6,25	49,70	31,35	67,65	21,08	33,48
12GC-2	1,693	2,019	7,857	10,807	14,581	18,747	1498,8	1513,7	25,51	34,34	42,43	61,32	29,38	31,95
12GC-1	1,010	2,172	3,714	10,128	3,750	18,070	1444,2	1660,8	8,80	34,53	33,52	60,02	13,85	31,97
12PC-3	1,612	1,964	9,418	14,554	14,204	26,421	1358,9	1546,3	19,74	33,72	45,57	66,00	22,61	31,72
12PC-2	1,438	2,208	5,338	9,934	10,441	18,301	1326,7	1694,0	8,14	39,08	31,43	69,59	14,93	36,27
12PC-1	1,623	2,042	3,128	7,751	3,491	14,491	1527,9	1559,0	13,65	24,69	41,11	65,37	23,63	26,25
14BC-1	1,524	1,760	3,156	6,863	5,084	11,698	1398,3	1514,0	-	-	57,42	71,14	-	-
14GC-2	1,607	1,789	4,160	5,800	6,334	10,335	1477,2	1510,3	-	-	55,76	66,33	55,76	66,33
14GC-1	1,674	1,871	3,798	8,036	2,379	12,115	1488,2	1533,1	-	-	50,97	62,40	28,68	34,42
14PC-2	1,153	1,731	3,439	6,990	2,792	9,040	1338,2	1535,7	2,780	35,81	59,12	78,20	28,25	35,26
14PC-1	1,530	2,019	2,670	21,214	3,068	39,262	1459,3	1600,1	20,27	37,28	42,40	70,75	22,36	27,89

6.1.2 Gravity Core JM07-012-GC

Core JM07-012-GC is divided into three units, 12GC-1 to 12GC-3 (figs. 6.5, 6.6 and 6.7). The linear sedimentation rate model depicted on fig. 6.5 is described by tab.6.3.

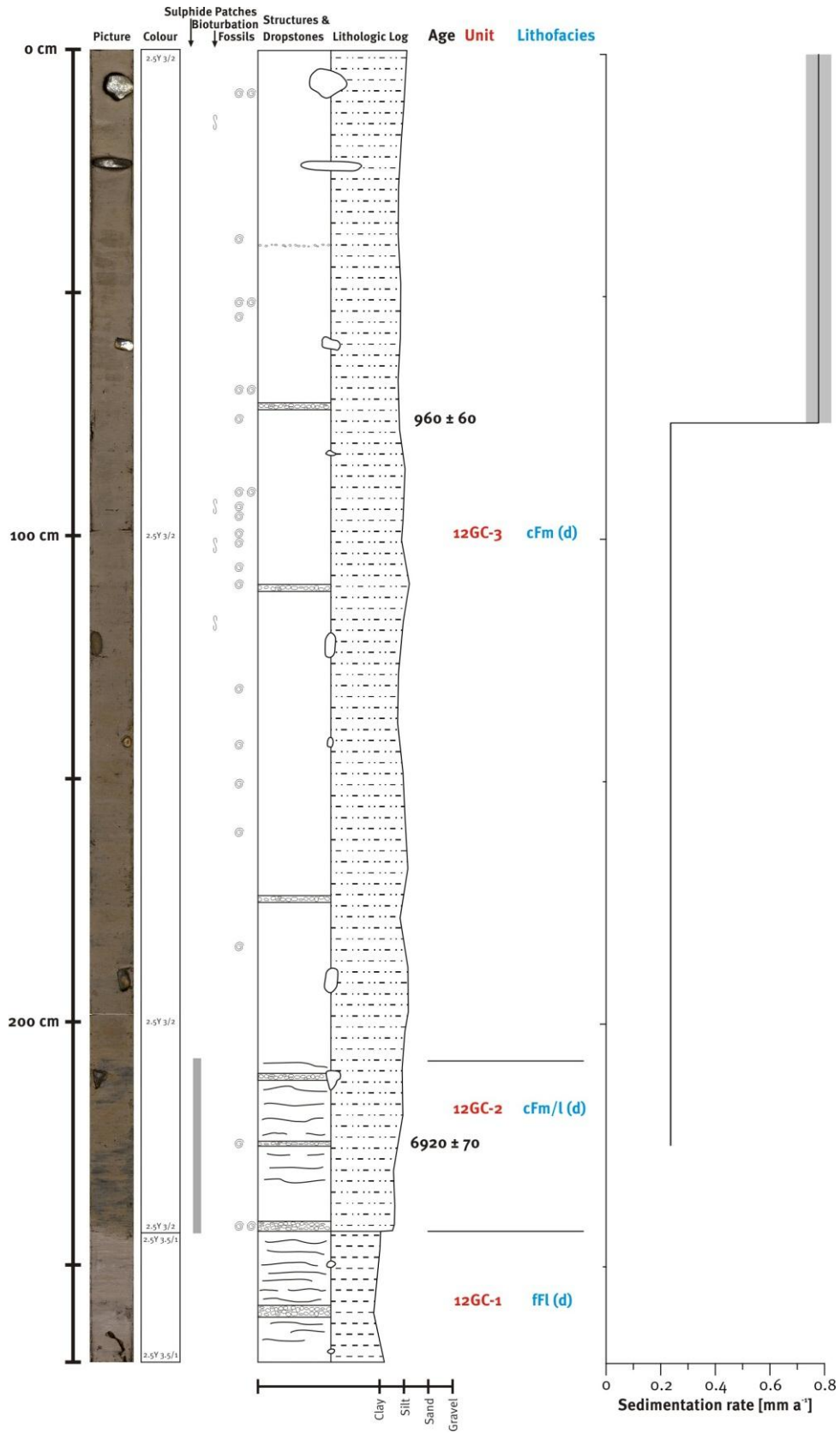
Table 6.3: Linear sedimentation rate model of core JM07-012-GC based on the radiocarbon dates with standard deviation values according to the standard deviations of the radiocarbon dates.

JM07-012-GC	
depth [cm]	sedimentation rate [mm a ⁻¹]
0 - 76	0.79 ± 0.050
76 - 225	0.25 ± 0.004

6.1.2.1 Unit 12GC-1 (270 – 244 cm)

Laminated silty clay with gravel and pebble clasts comprise unit 12GC-1 (lithofacies code fFl(d)) between 270 and 244 cm. The colour is dark to very dark grey (MSCC 2.5Y 3.5/1). For a summary of the physical properties see tab. 6.2. Neither macrofossils nor bioturbation were found in this unit. The real thickness of this unit is unknown, since it is the lowermost unit and only an upper, sharp boundary has been recovered (fig. 6.7). Shear-strength and magnetic susceptibility increase upwards (fig. 6.7 and tab. 6.2).

Figure 6.5: Colour image, colour codes and lithological log of core JM07-012-GC with a linear sedimentation rate model based on the radiocarbon dates. The grey shadow around the sedimentation rate graphs accounts for the uncertainty in sedimentation rates based on the standard deviation of the radiocarbon dates. In the lower part the error bars are so small that they are barely visible (see next page).



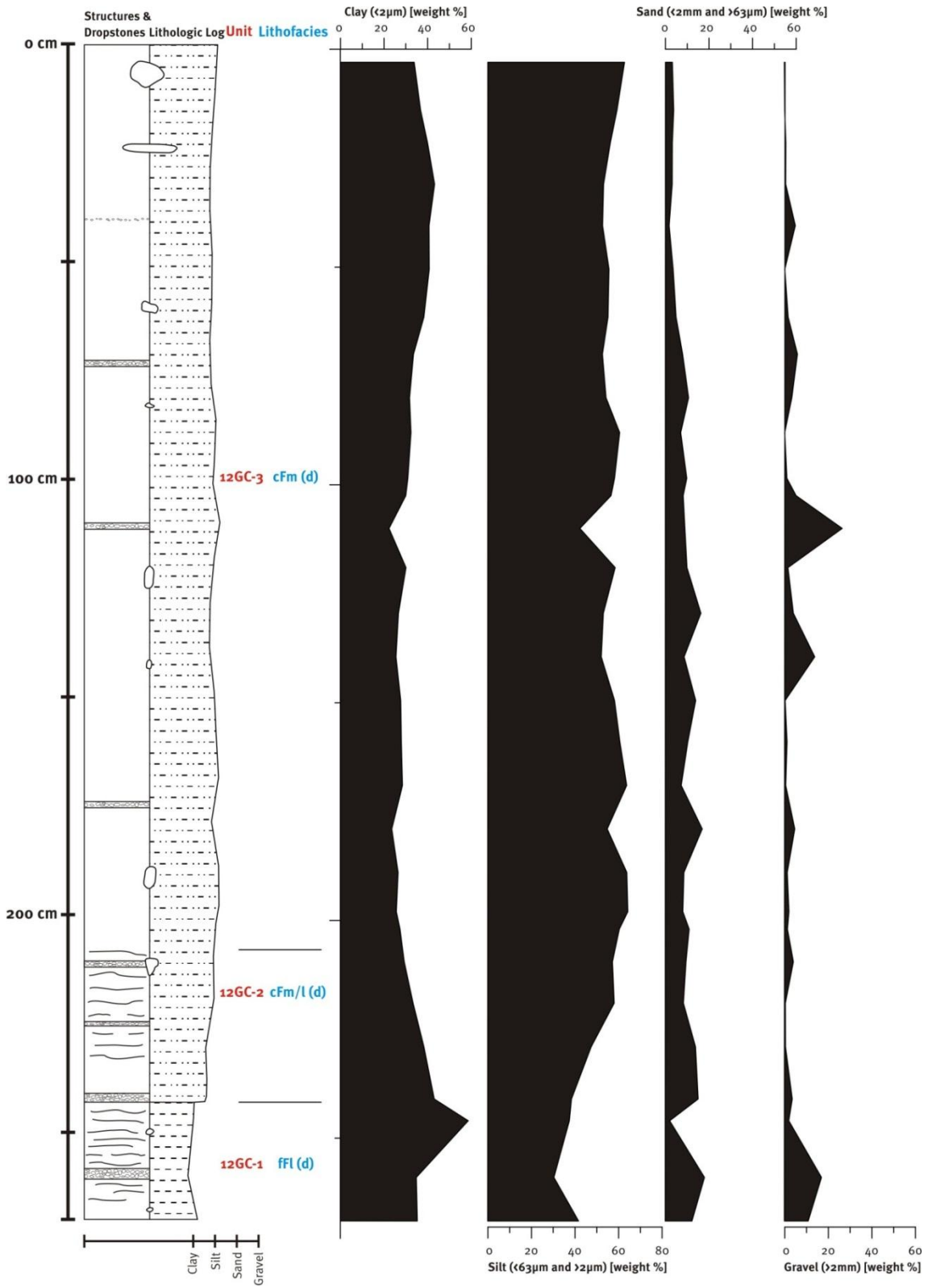


Figure 6.6: Lithological log and grain size distribution log of core JM07-012-GC.

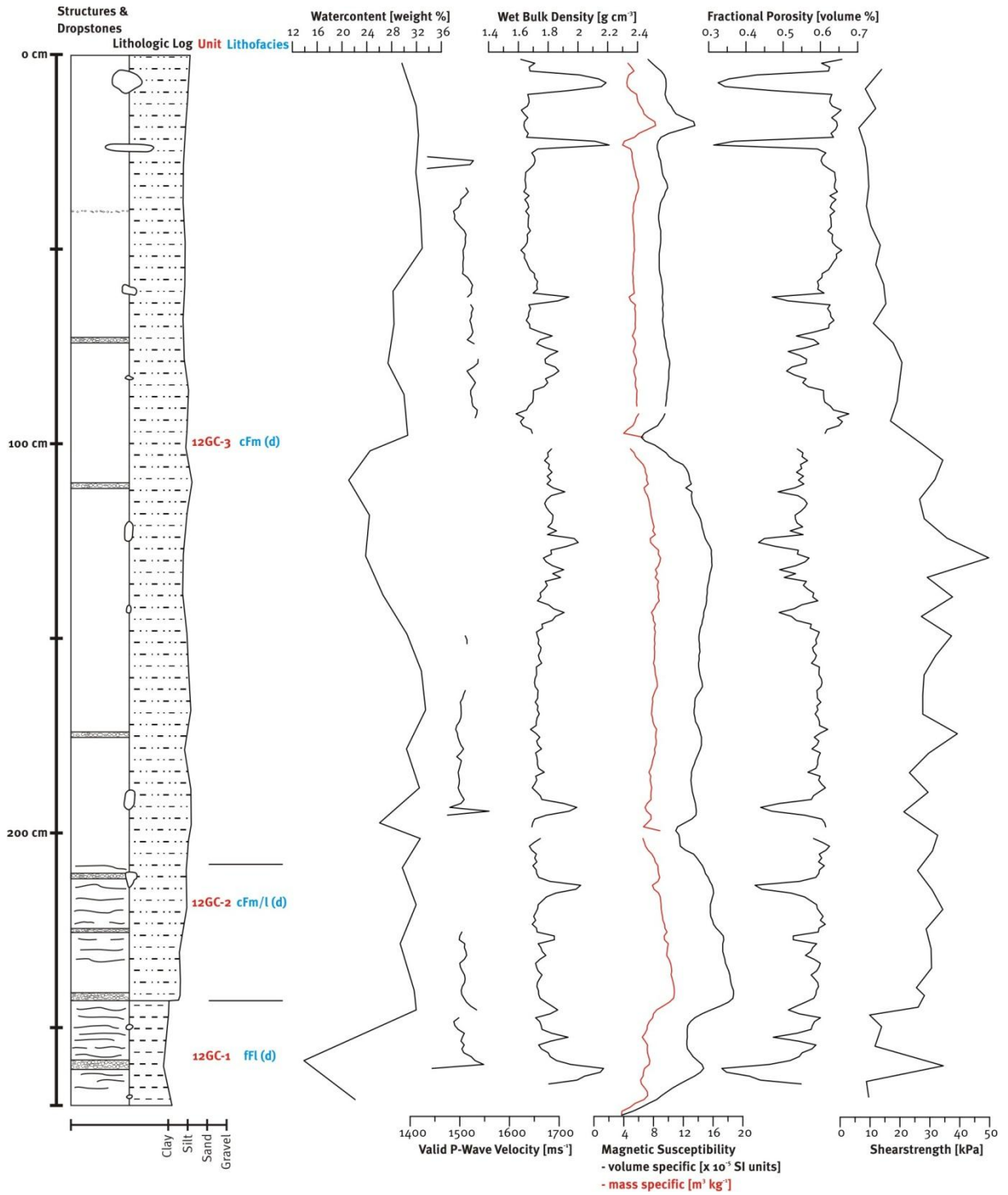


Figure 6.7: Lithological log and physical properties of core JM07-012-GC.

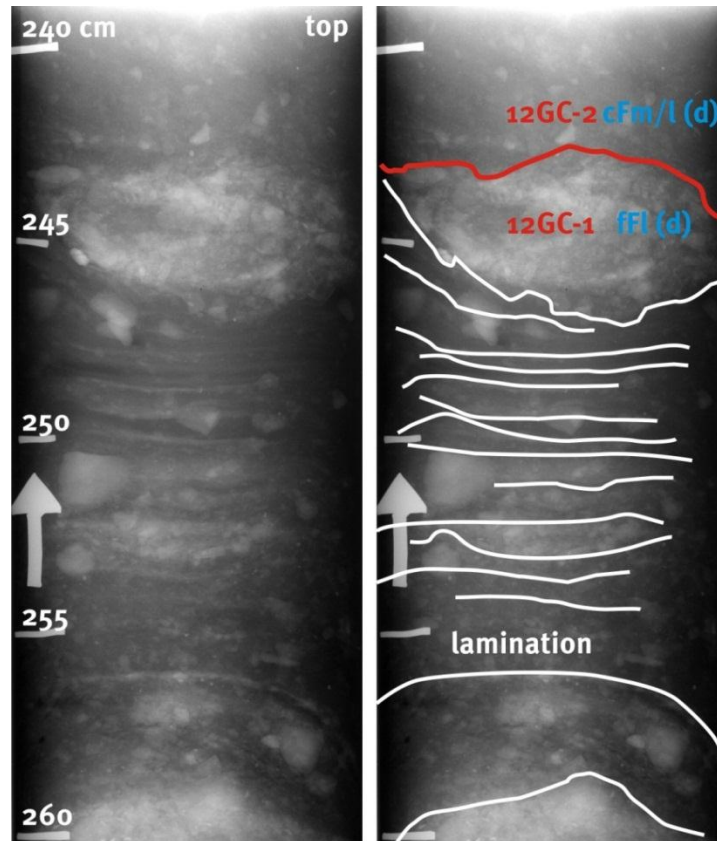


Figure 6.8: Radiograph (left) and interpretation (right) of the interval between 240 and 260 cm in core JM07-012-GC. Note the absence of lamination above the unit boundary.

6.1.2.2 Unit 12GC-2 (244 – 208 cm)

Unit 12GC-2 contains very weakly laminated mostly massive clayey silt with evenly distributed gravel and pebble clasts (lithofacies code cFm/l (d)). The colour of the sediment is a very dark greyish brown (MSCC 2.5Y 3/2). Black patches of sulphides derived from organic matter occur on fresh sediment surfaces. They oxidise and disappear after a few tens of minutes of air exposure. On radiographs layers of coarse grained material are visible (fig. 6.9). Shells, echinoid spicules and corals occur. At a depth of 225 cm a bivalve of the species *Nuculana minut*, was radiocarbon dated to 6920 ± 70 cal. yrs. BP (6540 ± 40 ^{14}C yrs. BP). The upper boundary is transitional and defined by lack of black sulphide spots and lack of lamination above. The lower boundary is a marked change in colour, shear-strength, grainsize and chemical composition (figs. 6.5, 6.6, and 6.7 and tab. 6.3).

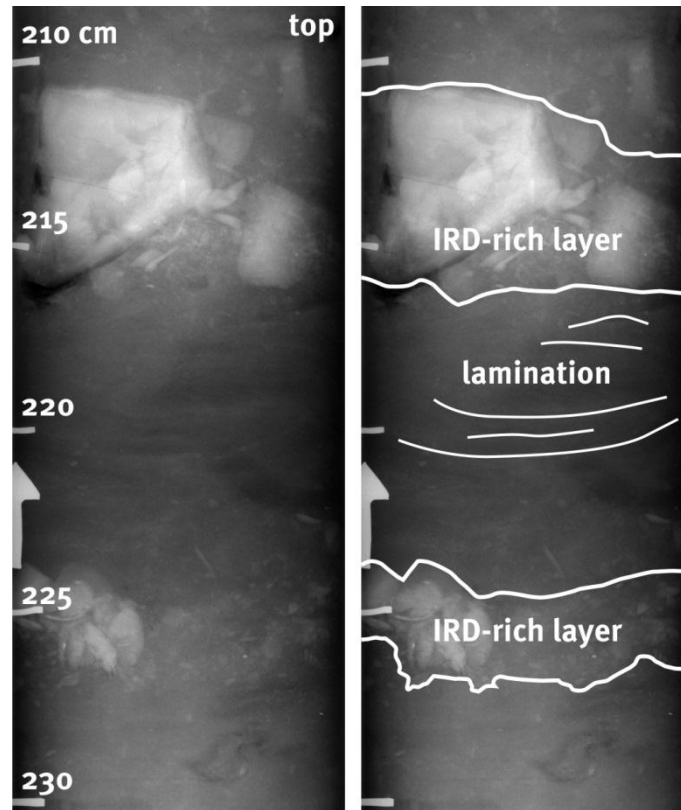


Figure 6.9: Radiograph (left) and interpretations (right) of core JM07-012-GC between 230 and 208 cm depth. The IRD is concentrated in two layers.

6.1.2.3 Unit 12GC-3 (208 – 0 cm)

The lithofacies code for this unit is cFm (d). Massive clayey silt is the dominant sediment type. Gravel and pebble clasts are common and evenly distributed. The colour of the sediment is a very dark greyish brown (MSCC 2.5Y 3/2). Macrofossils (bivalves, polychaeta and snails) are common and bioturbation occurs. There is bioturbation with elongated burrow shape and with swiss cheese-like appearance (figs. 6.10 and 6.11). At the depth of 76 cm a snail of the family *Turritelidae* was radiocarbon dated to 960 ± 45 cal. yrs. BP (1520 ± 30 ^{14}C yrs. BP).

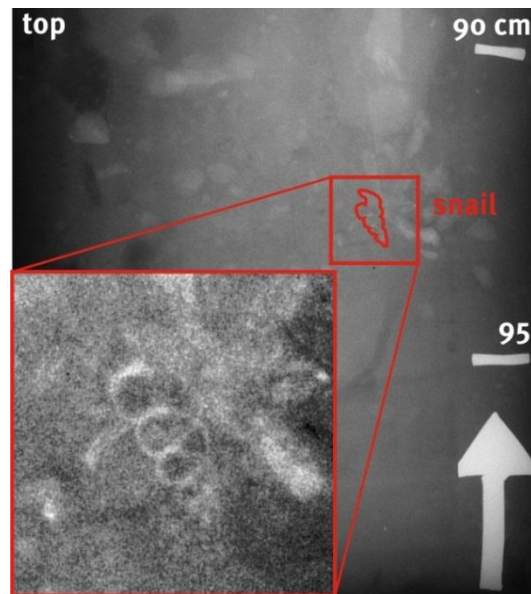


Figure 6.10: Radiograph of core JM07-012-GC between 99 and 89 cm depth. An example of a snail (not radiocarbon dated) is shown in the inset.

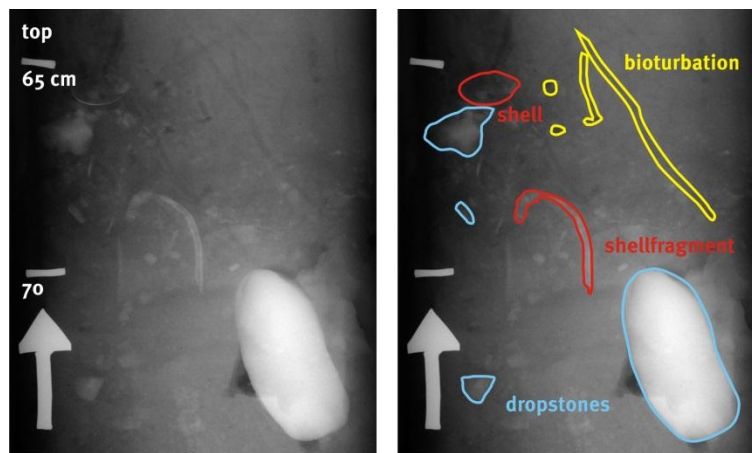


Figure 6.11: Radiograph (left) and interpretation (right) of core JM07-012-GC between 63 and 74 cm depth. Selected dropstones shell (fragments) and bioturbation are indicated.

6.1.2.4 XRF-Data of Core JM07-012-GC

The element composition, shown in form of Ca/Fe and Ca/Si ratios, changes markedly at the unit boundary from 12GC-1 to 12GC-2. Ca/Fe and Ca/Si ratios are generally lower in unit 12GC-1 and are more variable (fig. 6.12). Major excursions of the proxies are often

coincident with large dropstones or gravelly to pebbly layers. The Si/all ratio is calculated by dividing the counts for Si by the sum of all counts at that depth. It decreases significantly at the unit boundary between 12GC-1 and 12GC-2, but increases to the average level above and below the unit boundary.

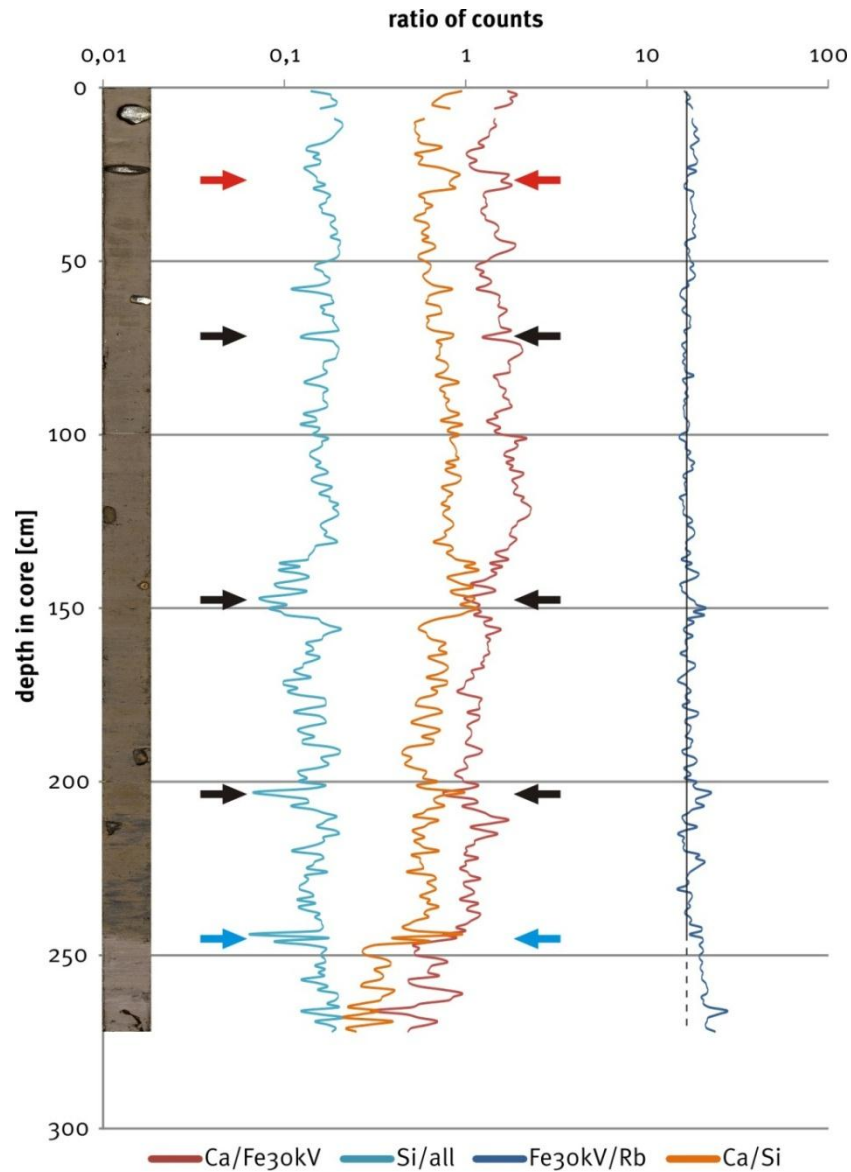


Figure 6.12: XRF-Scanner element ratios of core JM07-012-GC. Black arrows point at opposing excursions of the Ca/Fe and Ca/Si proxies, red arrow points at a non-opposing excursion. The blue arrows indicate the unit boundary between 12GC-1 and 12GC-2.

6.1.3 Piston Core JM07-012-PC

Core JM07-012-PC contains a 382 cm thick sediment sequence. However, it should be noted that the upper ~2 m are missing (Forwick, 2007).

6.1.3.1 Unit 12PC-1 (382 – 339 cm)

The lithofacies code for this unit is fFm (d). Massive silty clay is the dominant sediment in the unit. Gravel and pebbly clasts are common and evenly distributed. The colour of the sediment is dark grey (MSCC 2.5Y 4/1). Macrofossils were not found. The upper boundary is transitional and it is defined by lamination in the unit above (figs. 6.13, 6.14, 6.15 and 6.16).

6.1.3.2 Unit 12PC-2 (339 – 28 cm)

The unit is composed of strong to weakly laminated silty clay with relatively high amounts of gravel and pebble clasts (lithofacies code fFl (d)). The colour of the sediment is dark greyish brown to very dark grey (MSCC 2.5Y 3.5/1 to 2.5Y 4/2). Macrofossils were not found in the unit. The upper boundary is sharp and is defined by a marked change in colour, shear-strength, grainsize distribution and magnetic susceptibility. The lower boundary is a transition from massive sediment below to laminated sediments above (fig. 6.16).

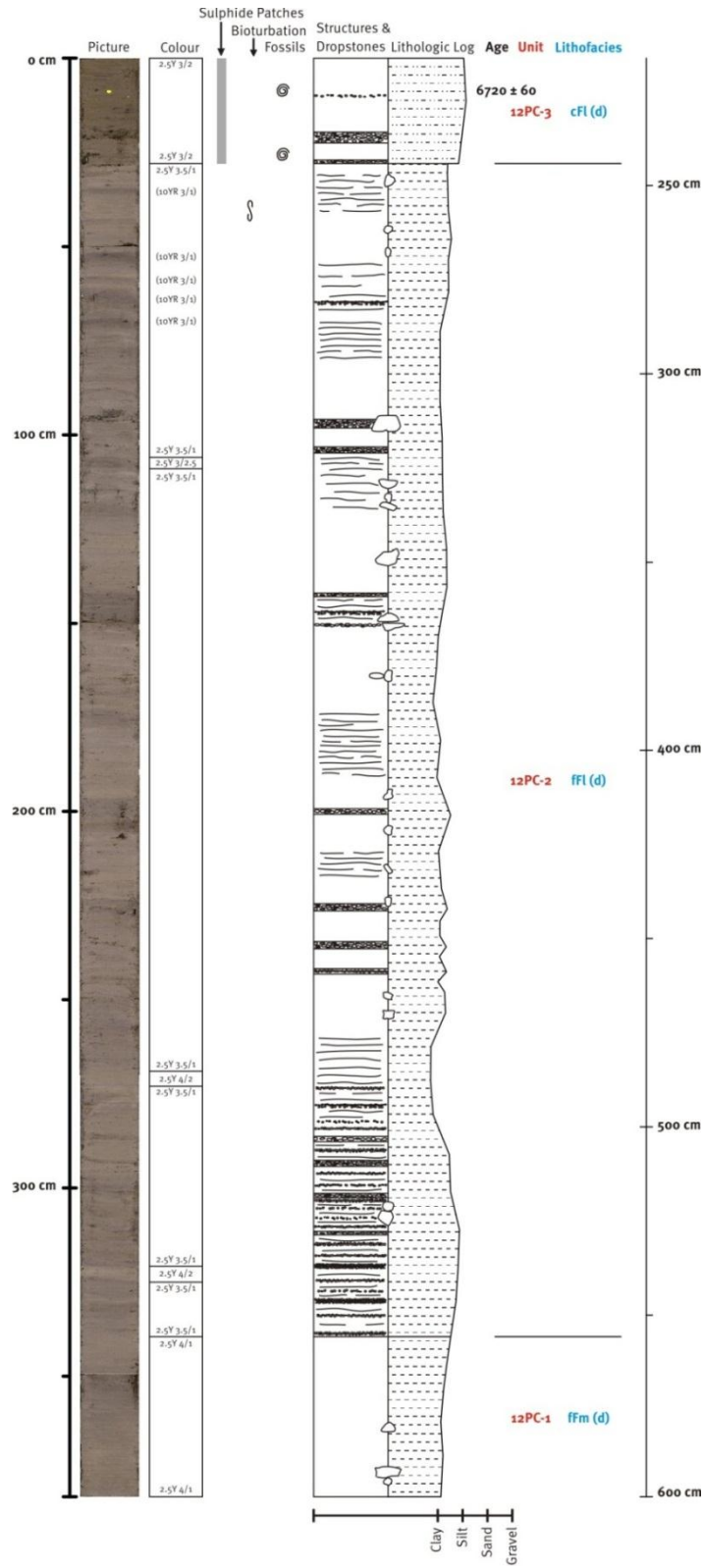


Figure 6.13: Colour image, sediment colours and lithological log of core JM07-012-PC.

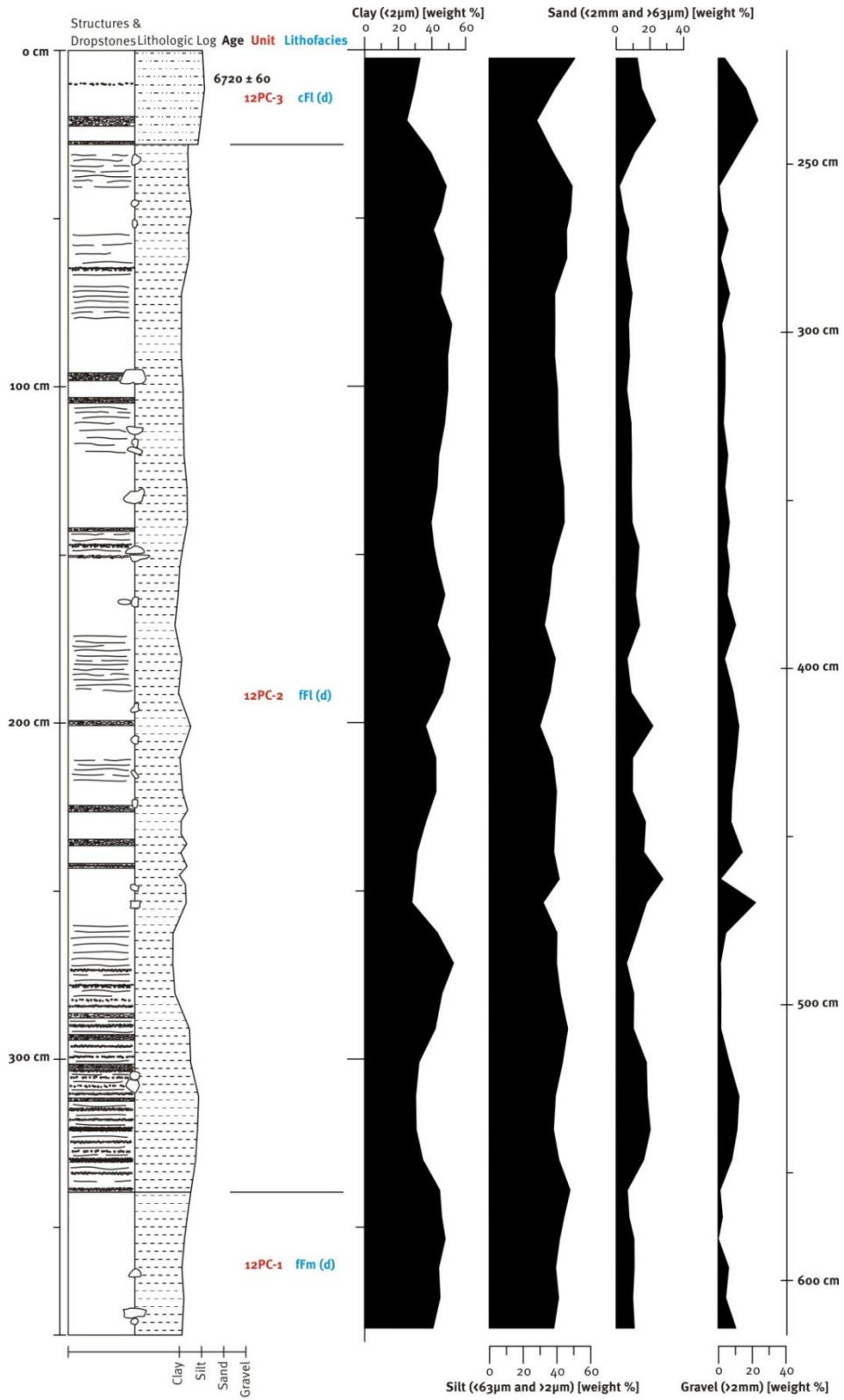


Figure 6.14: Lithological log and grain size distribution log of core JM07-012-PC.

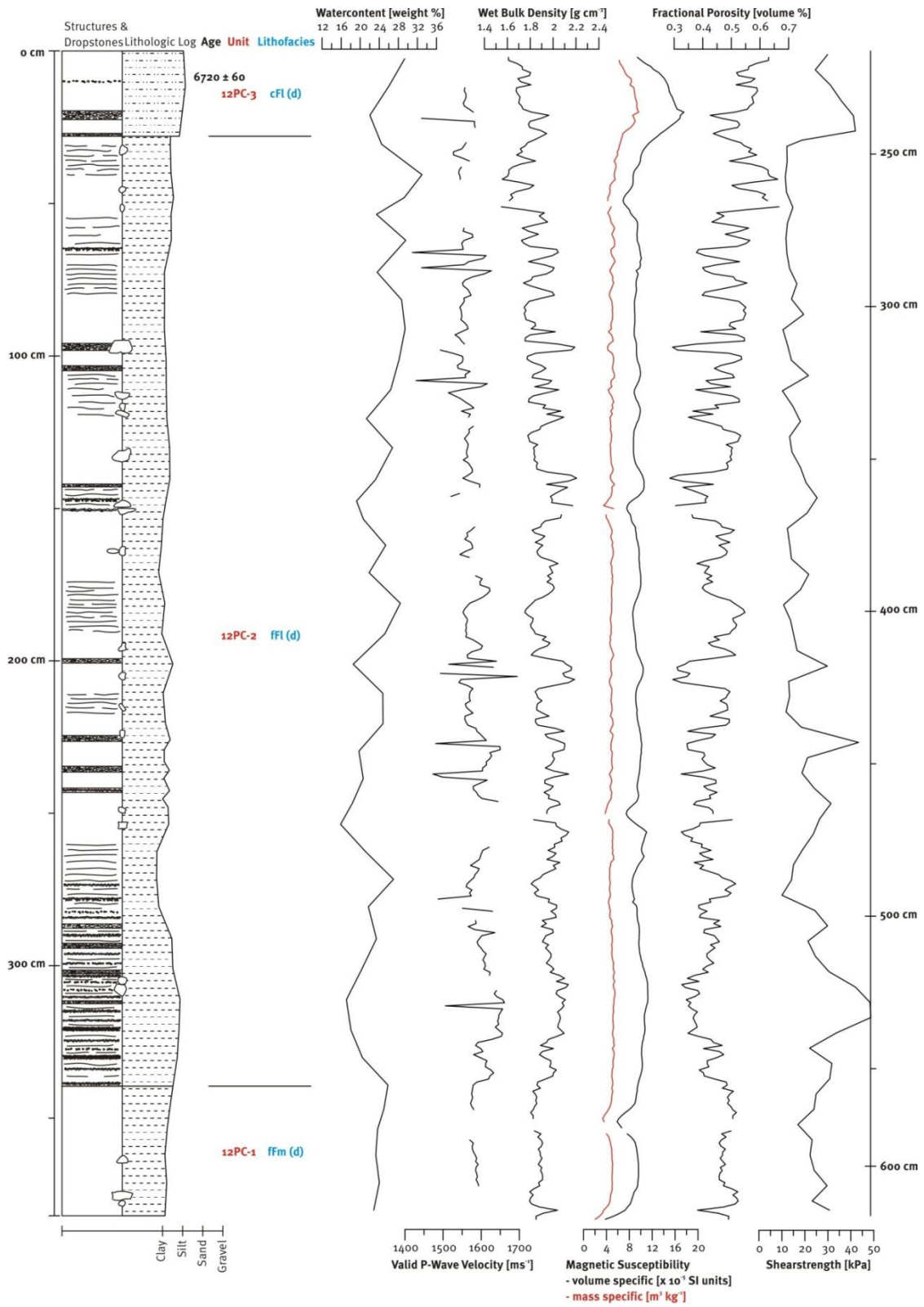


Figure 6.15: Lithological log and physical properties log of core JM07-012-PC.

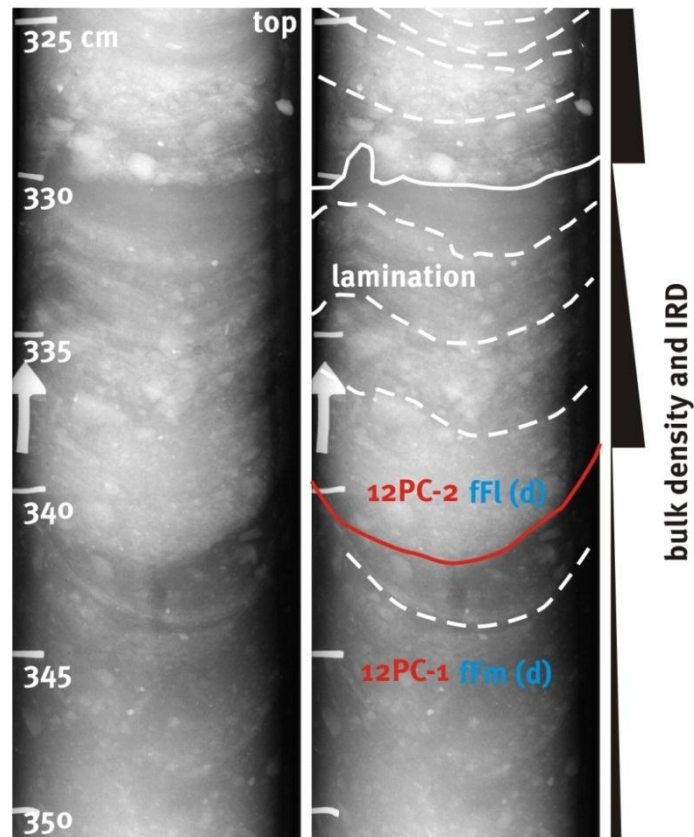


Figure 6.16: Radiograph (left) and interpretations (right) of core JM07-012-PC between 325 cm and 350 cm depth. A schematic bulk density and IRD gradation graph points out the layering of the sediment. Lamination is indicated with white dashed lines.

6.1.3.3 Unit 12PC-3 (28 – 0 cm)

The lithofacies code for this unit is cFl (d), indicating that weakly laminated clayey silt is the dominant sediment in the unit. Gravel and pebble clasts are common. The colour of the sediment is very dark greyish brown (MSCC 2.5Y 3/2). Macrofossils occur rarely (one brachiopod and a very small fragment of either a coral or a bryozoan). At a depth of 8 cm the brachiopod of the species *Hemithris psittacea* was radiocarbon dated to 6720 ± 60 cal. yrs. BP (6380 ± 40 ^{14}C yrs. BP). The lower boundary is sharp and is defined by a marked change in colour, shear-strength, grainsize distribution and magnetic susceptibility.

6.1.3.4 XRF-Data of Core JM07-012-PC

The element composition, shown by the Ca/Fe and Ca/Si ratios, changes markedly at the boundary between unit 12PC-2 and unit 12PC-3. Ca/Fe and Ca/Si ratios are generally lower in unit 12PC-1 and 12PC-2 and are more variable (fig. 6.17). Major excursions of the proxies are recorded only in units 12PC-1 and 12PC-2. The frequency of the excursions of Ca/Fe and Ca/Si between ~125 cm and ~210 cm depth seems rhythmical. However, these cyclic variations were not observed in core logs, physical properties or radiographs. The Fe/Rb ratio in unit 12PC-3 is generally lower than in units 12PC-1 and 12PC-2 and shows little variation.

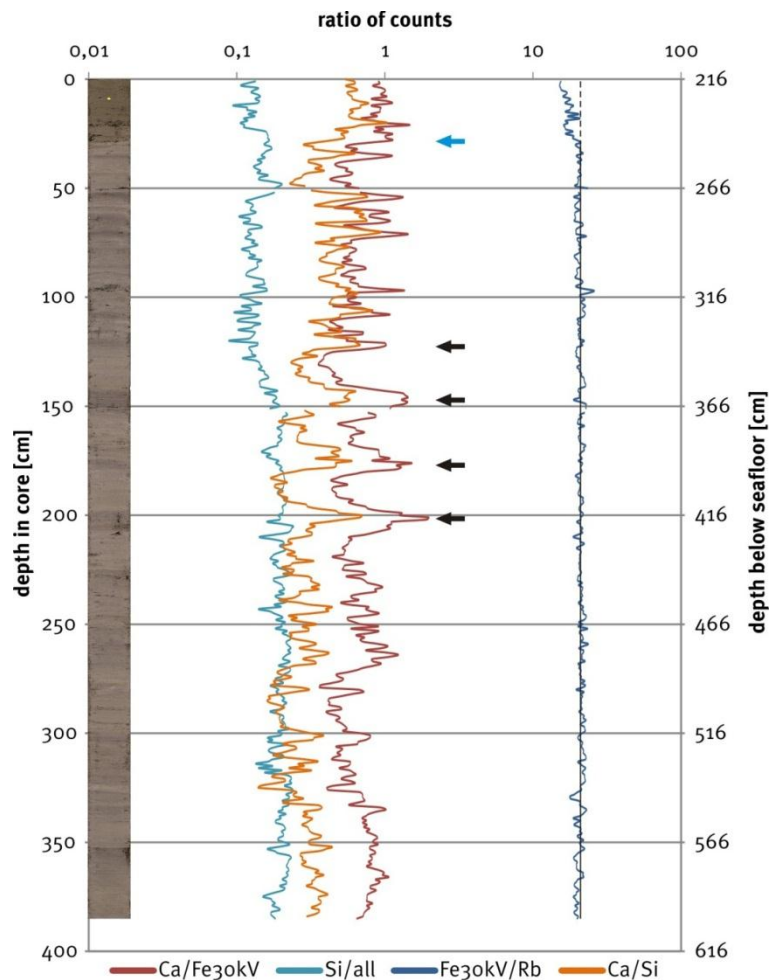


Figure 6.17: XRF-Scanner element ratios of core JM07-012-PC. Black arrows point at peaks of Ca/Fe and Ca/Si. Blue arrow points at the boundary between 12PC-2 and -3.

6.1.3.5 Correlation between Cores JM07-012-GC and JM07-012-PC

In the gravity core (JM07-012-GC) the most distinctive change is described from unit 12GC-1 to 12GC-2. The sediment changes colour from 2.5Y 3.5/1 to 2.5Y 3/2 on the MSCC, the dominant grain size changes from clay to silt. In addition sulphide spots as well as macrofossils become abundant in the upper unit.

This change, described for the boundary between 12GC-1 and 12GC-2, is very similar to what is observed and described for the unit boundary between 12PC-2 and 12PC-3. Here also the colour shifts from 2.5Y 3.5/1 to 2.5Y 3/2 on the MSCC, the dominant grain size changes from clay to silt and sulphide spots and macrofossils become abundant in the upper unit (fig. 6.5).

All this suggests that the unit boundary between 12GC-1 and 12GC-2 and the unit boundary between 12PC-2 and 12PC-3 are essentially the same. An additional depth value of 216 cm must be added to the JM07-012-PC data to get the real depth.

6.1.4 Deductions from the Core Data of Core Site JM07-012

In the three cores JM07-012-BC, -GC and -PC exclusively glacial marine sediments were found. All units are interpreted to be comprised of suspension fall-out and IRD. 12PC-1 and 12PC-2 (i.e. 12GC-1) have low shear-strengths which may indicate rapid sedimentation. This indicates a glacier proximal environment. The units above are accordingly interpreted to reflect a glacier distal sedimentary environment with low sedimentation rates and lower relative IRD input.

6.2 Core Site JM07-014

The core site JM07-014 is located in the eastern parts of the outer Van Keulenfjorden basin. It is located directly in front (west) of the debris flow deposit, L1 (fig. 4.1b).

6.2.1 Box Core JM07-014-BC

Core JM07-014-BC is 26 cm long and contains the lithological unit 14BC-1 (Fig. 6.18).

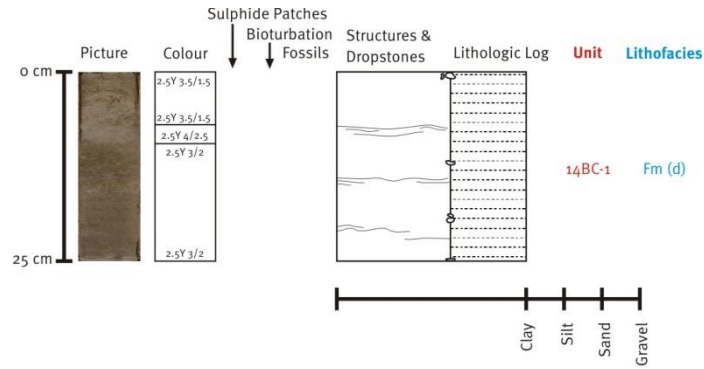


Figure 6.18: Colour image, colour codes, lithological log of box core JM07-014-BC.

6.2.1.1 Unit 14BC-1 (26 – 0 cm)

The lithofacies code for this unit is Fm (d). It is composed of massive mud with scattered gravel and pebble clasts. The differentiation between clay and silt cannot be made, because no sample of the box core was analysed by the sedigraph. The colour of the sediment is very dark greyish brown to olive brown (MSCC 2.5Y 3/2 to 2.5Y 4/2.5). Macrofossils were not found.

6.2.2 Gravity Core JM07-014-GC

The 270 cm long gravity core JM07-014-GC is divided into the units 14GC-1 and -2 (figs. 6.19, 6.20 and 6.21).

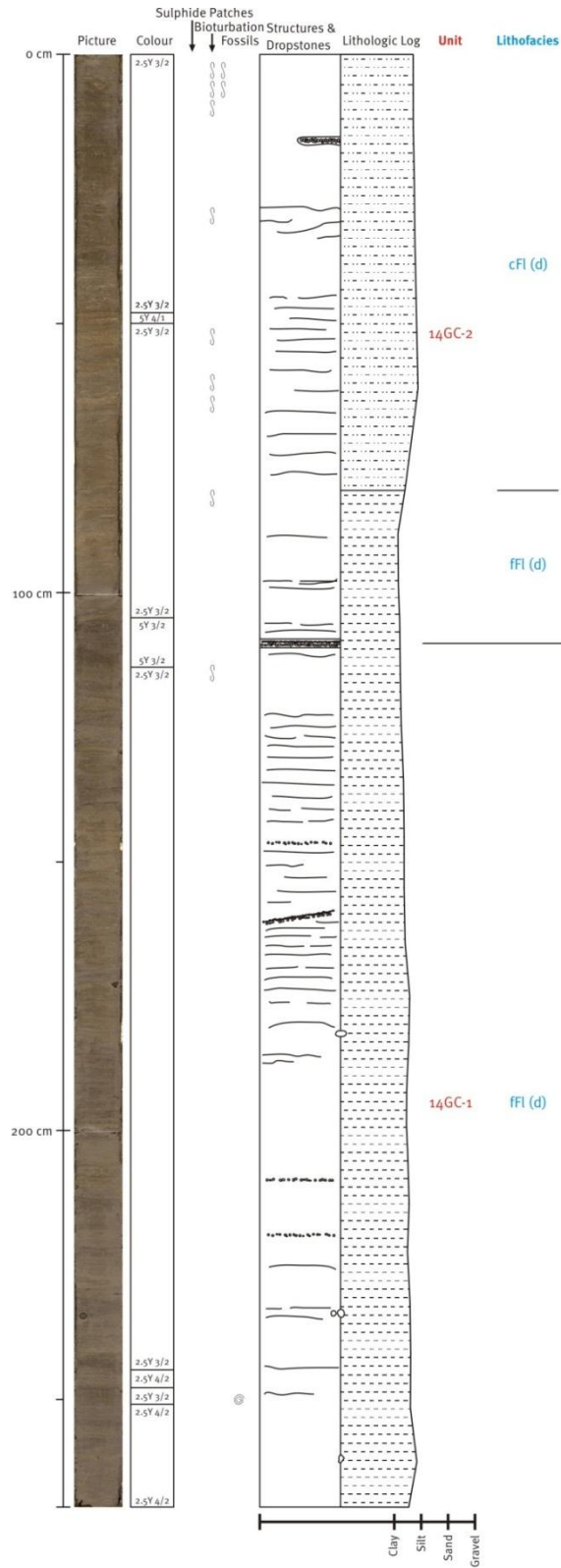


Figure 6.19: Colour image, colour codes and lithological log of core JM07-014-GC.

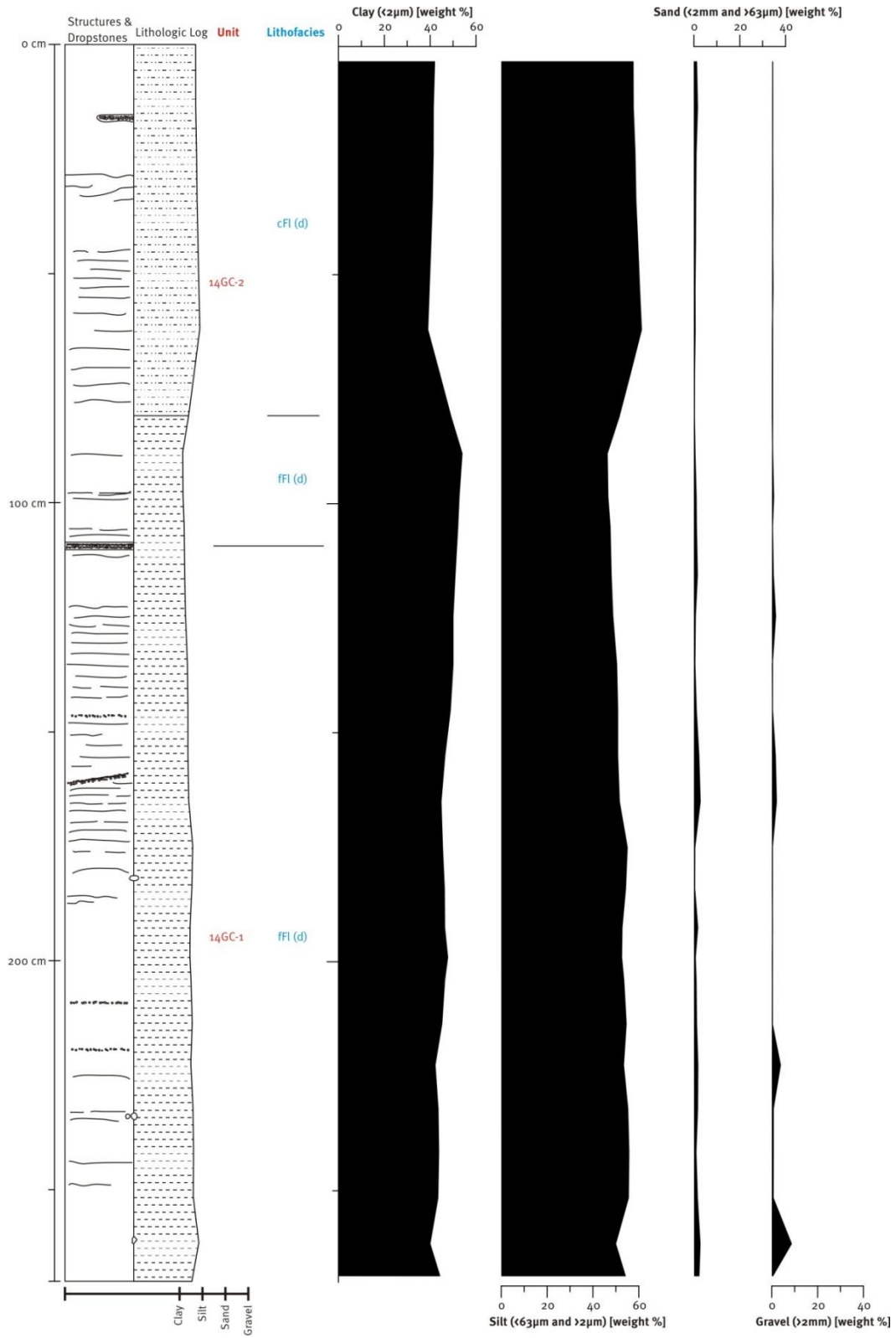


Figure 6.20: Lithological log and grain size distribution log of core JM07-012-PC.

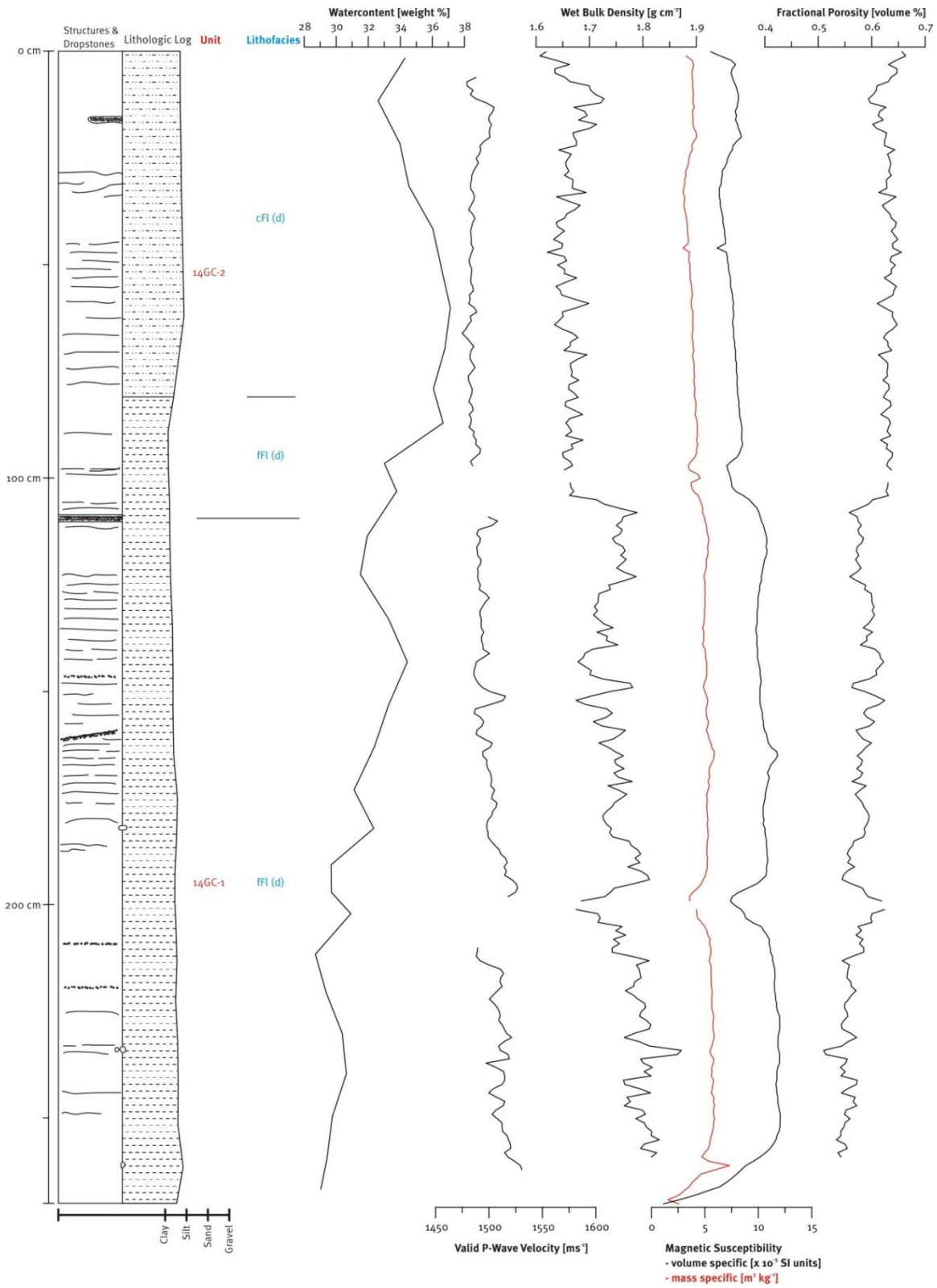


Figure 6.21: Lithological log and physical properties log of core JM07-012-PC.

6.2.2.1 Unit 14GC-1 (270 – 109 cm)

Unit 14GC-1 contains strongly to weakly laminated silty clay with scattered clasts of gravel and pebble size (lithofacies code fFl(d)). The colour of the sediment is very dark greyish brown to dark olive grey (MSCC 2.5Y 3/2, and 2.5Y 4/2 to 5Y 3/2, respectively). One shell fragment was found. The upper boundary of the unit is sharp and defined by a marked change in wet bulk density and magnetic susceptibility (fig. 6.21 and 6.22).

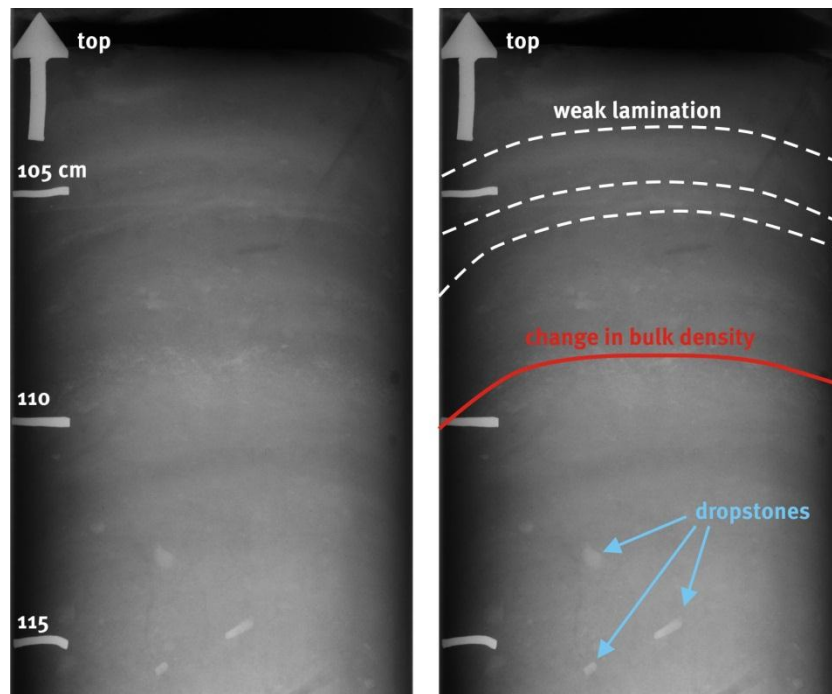


Figure 6.22: Radiograph (left) and interpretations (right) of core JM07-014-GC between 102 cm and 117 cm depth. The change in bulk density is indicated on the right by the red line. Below the red line the radiograph is slightly brighter.

6.2.2.2 Unit 14GC-2 (109 – 0 cm)

Unit 14GC-2 is the uppermost unit of the core. It is composed of laminated mud, ranging from silty clay (lower part) to clayey silt (upper part) with scattered gravel and pebble clasts (lithofacies code c/fFl(d)). The colour of the sediment is very dark greyish brown to dark grey (MSCC 2.5Y 3/2 to 5Y 4/1). Macrofossils were not found.

6.2.2.3 XRF-Data of Core JM07-014-GC

Though lithologically there is very little change in the core JM07-014-GC the ratios between Ca/Fe and Ca/Si vary strongly. The proxies of Ca/Fe and Ca/Si are most often in phase, however two distinctive excursions at depth ~65 cm and ~140 cm show opposing Ca/Fe and Ca/Si peaks. Both excursions are coincident with a significant drop in Si/all (fig. 6.23).

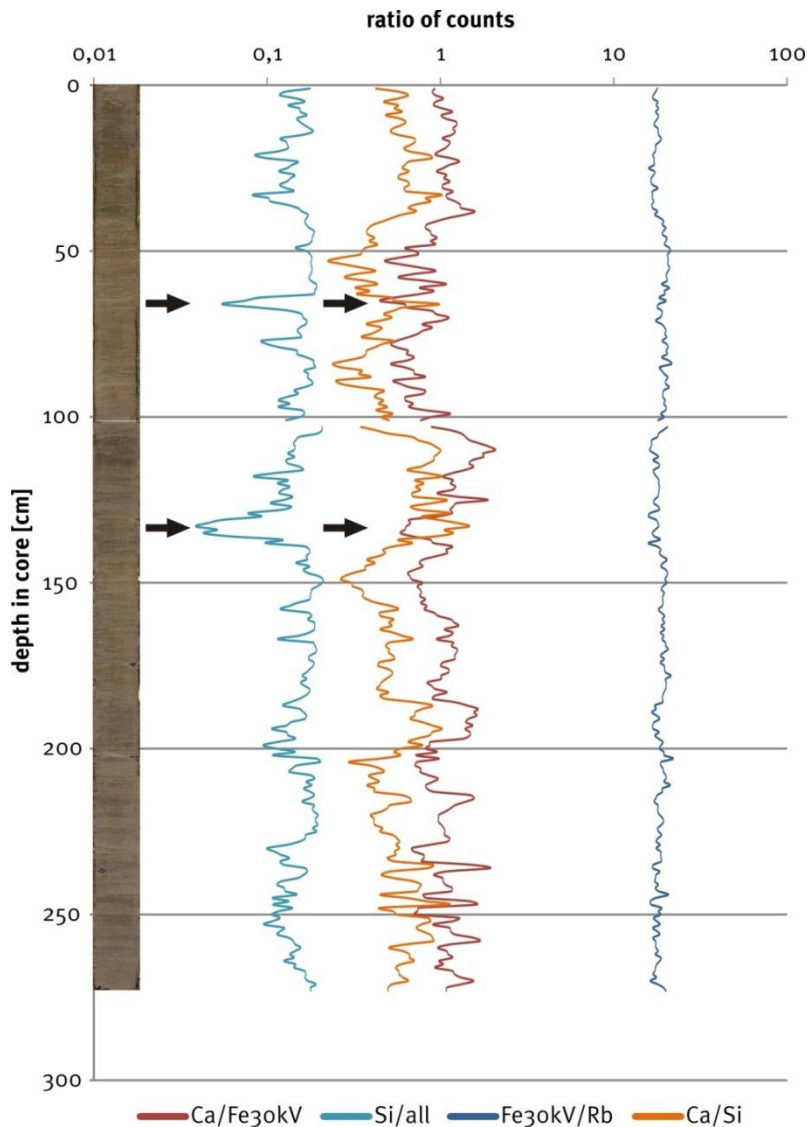


Figure 6.23: XRF-Scanner element ratios of core JM07-014-GC. Black arrows point at opposing excursions of the Ca/Fe and Ca/Si proxies.

6.2.3 Piston Core JM07-014-PC

Core JM07-014-PC is 538 cm long. It is divided into the units 14PC-1 and -2. The linear sedimentation rate model for this core is ambiguous, because the radiocarbon dated shell at 125 cm depth (2710 ± 40 cal. yrs. BP) is supposedly older than the one dated at depth 168 cm (2650 ± 60 cal. yrs. BP). Usually if a radiocarbon dated shell is older and further up in the core than another one, it is assumed to be reworked. However, the single standard deviations of the two radiocarbon dates are overlapping (red area in fig. 6.24). Therefore both dates are assumed to be valid radiocarbon dates with an inaccuracy due to the limits of precision of the dating method and two different sedimentation rates are introduced in the linear sedimentation rate model at the depths in question (tab. 6.4 and fig. 6.25).

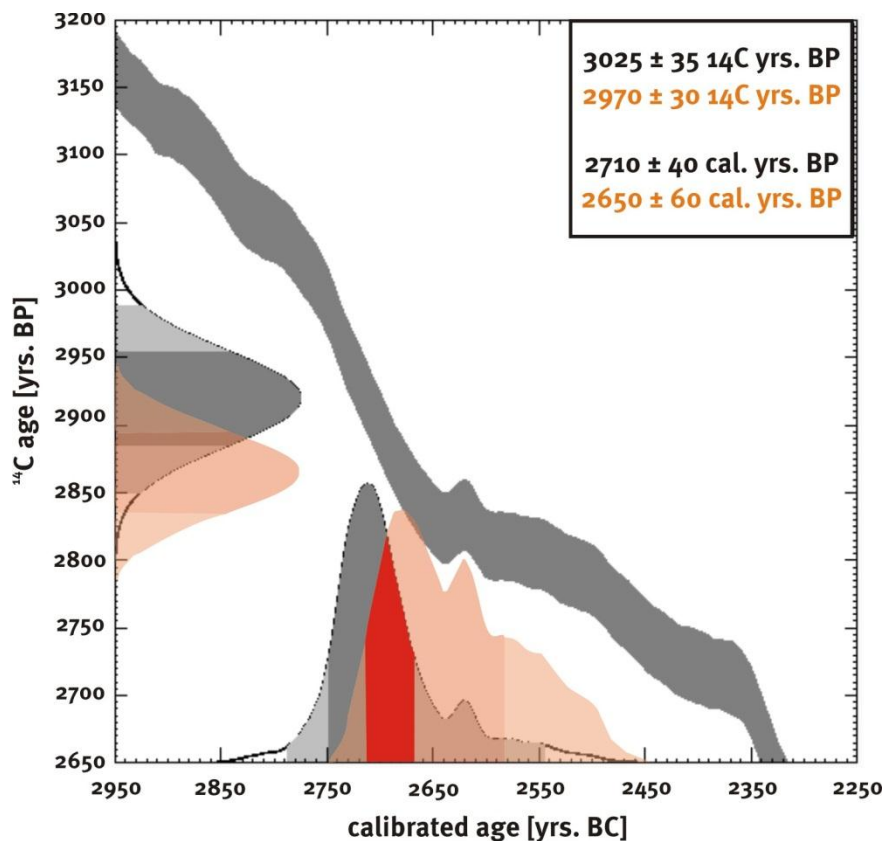


Figure 6.24: Comparison between the two overlapping calibration curves from core JM07-014-PC. Grey colours show the older date, orange colours show the younger date. Red area shows the overlap of both dates with their single standard deviation.

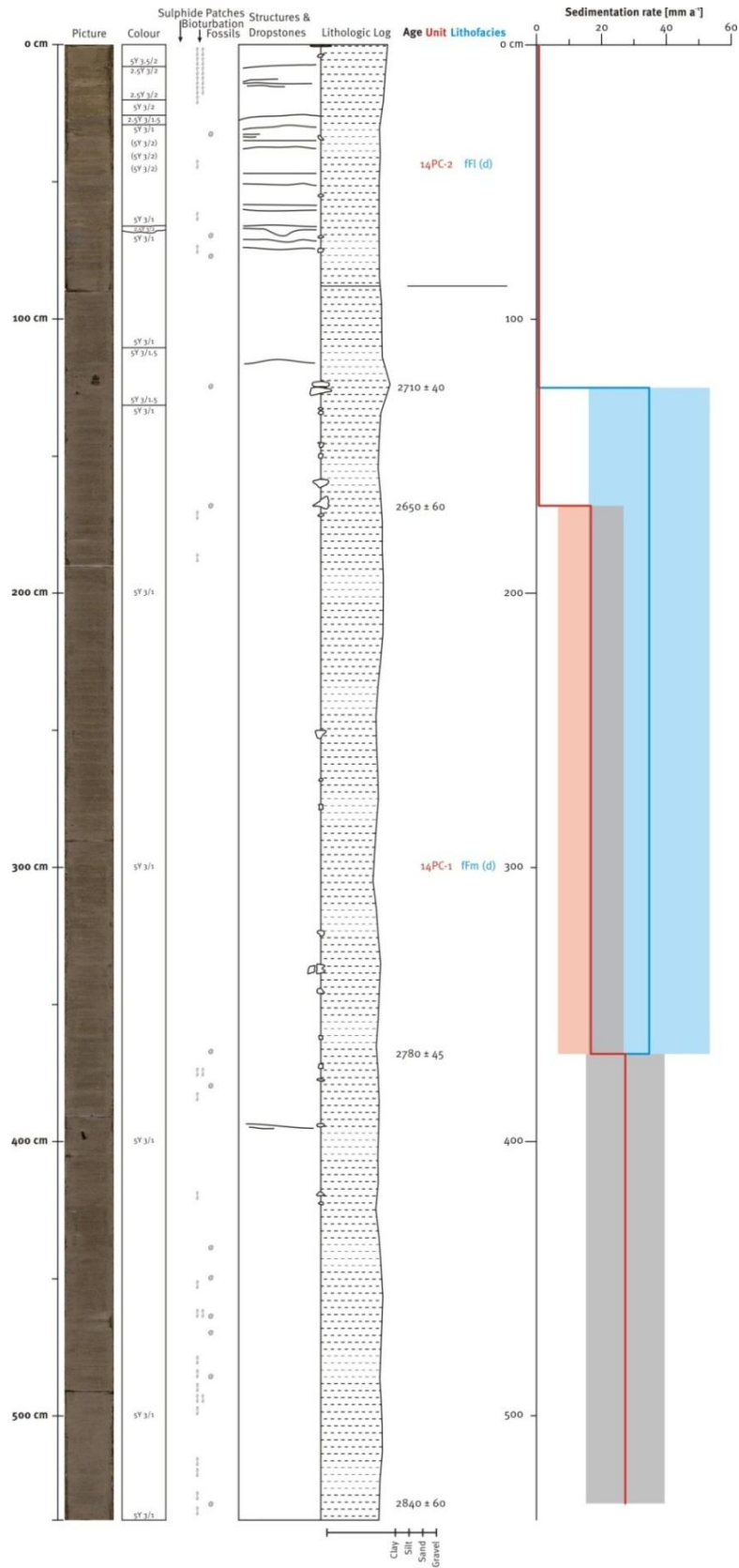
Table 6.4: Linear sedimentation rate models for core JM07-014-PC based on the radiocarbon dates with standard deviation values according to the standard deviations of the radiocarbon dates.

JM07-014-PC Model 1		JM07-014-PC Model 2	
depth [cm]	sedimentation rate [mm a ⁻¹]	depth [cm]	sedimentation rate [mm a ⁻¹]
0 - 125	0.46 ± 0.01	0 - 168	0.63 ± 0.01
125 - 368	34.71 ± 18.69	168 - 368	16.67 ± 10.13
368 - 532	27.33 ± 12.15	368 - 532	27.33 ± 12.15

6.2.3.1 Unit 14PC-1 (538 – 88 cm)

The lithofacies code for this unit is fFm (d) (fig. 6.25, 6.26 and 6.27). Massive, and in the upper parts also weakly laminated, silty clay is the dominant sediment. Gravel and pebble clasts occur. The colour of the sediment is very dark grey (MSCC 2.5Y 3/1 to 2.5Y 3/1.5). Bivalves and snails were found. Four snails of the species *Cylichna alba* were radio carbon dated. One from 532 cm depth to 2840 ± 60 cal. yrs BP (3180 ± 35 ¹⁴C yrs BP), one from 368 cm depth to 2780 ± 45 (3115 ± 35 ¹⁴C yrs. BP), one from 168 cm depth to 2650 ± 60 (2970 ± 30 ¹⁴C yrs. BP) and the other one from 125 cm depth with an age of 2710 ± 40 cal. yrs BP (3025 ± 35 ¹⁴C yrs BP). The upper boundary of the unit is based on the changes in physical properties. The onset of a decrease in shear-strength and wet bulk density and the onset of an increase in fractional porosity define the transitional unit boundary between unit 14PC-1 and 14PC-2. Lamination is exclusively observed on the split-core surface.

Figure 6.25: Colour image, colour codes, and lithological log of core JM07-014-PC, as well as linear sedimentation rates. The grey/blue (model 1)/red (model 2) shadows around the sedimentation rate graphs accounts for the standard deviation of the radiocarbon dates (see next page).



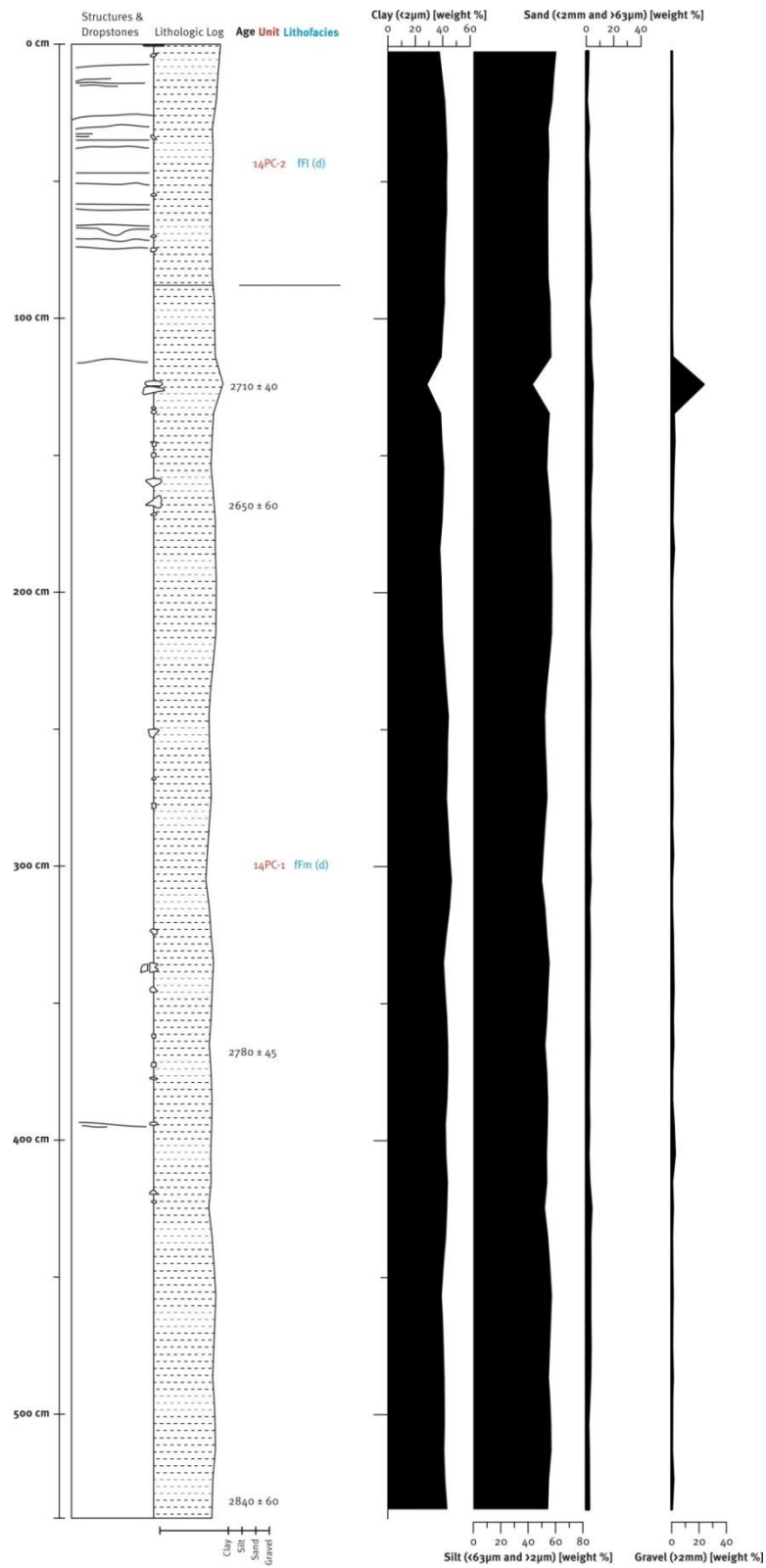


Figure 6.26: Lithological log and grain size distribution log of core JM07-014-PC.

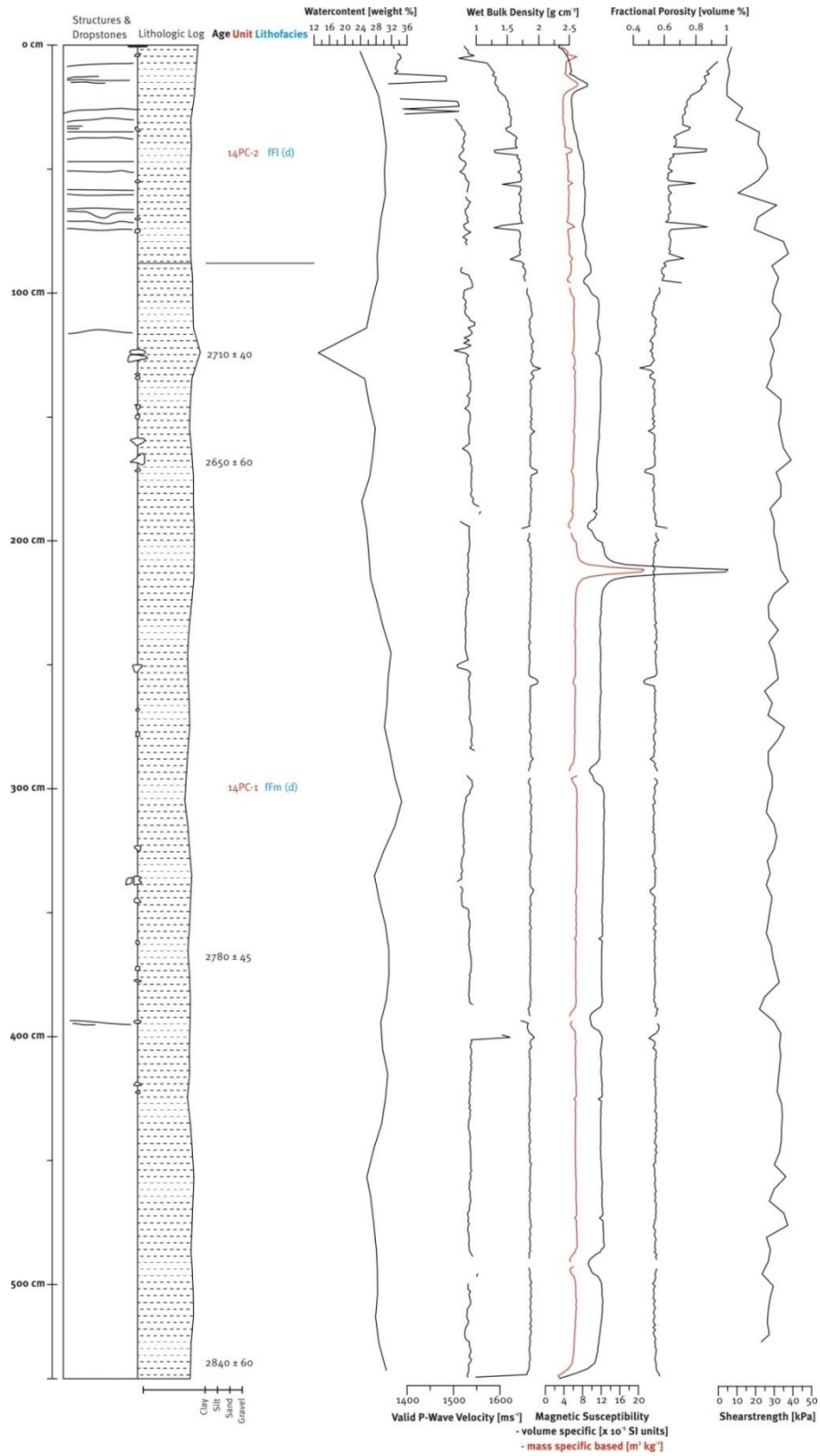


Figure 6.27: Physical properties log of core JM07-014-PC.

6.2.3.2 Unit 14PC-2 (88 – 0 cm)

Unit 14PC-2 is composed of laminated silty clay with scattered gravel and pebble clasts (lithofacies code fF1 (d). The sediment colour is very dark grey to dark olive grey (MSCC 2.5Y 3/1 to 5Y 3/2). Fossil bivalves and snails are abundant. The uppermost part is heavily bioturbated. The bioturbation has a Swiss cheese-like appearance on the radiograph (fig. 6.28).

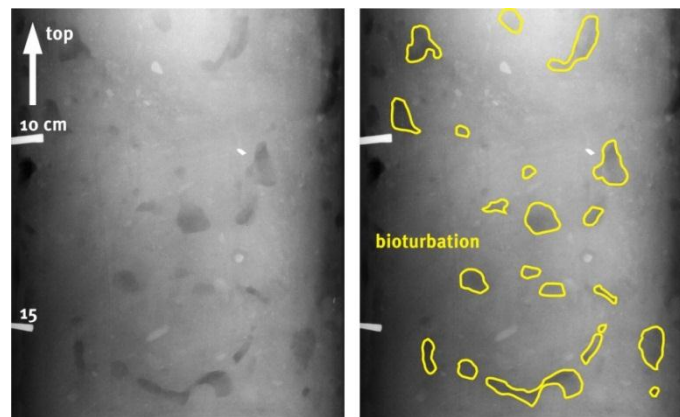


Figure 6.28: Radiograph (left) and interpretations (right) of core JM07-014-PC between 0 cm and 17 cm depth. The bioturbation is encircled in yellow.

6.2.3.3 XRF-Data of Core JM07-014-PC

The two proxies Ca/Fe and Ca/Si generally are in phase throughout the whole core, while Si/all has opposing excursions. A marked change in variability of the proxies occurs at ~110 cm depth. Above this depth (fig. 6.29) the frequency of the excursions are significantly higher than below. There is also a distinctive excursion at ~90 cm depth, but this could be an artefact originating from the core section boundary.

6.2.4 Deductions from the Core Data of Core Site JM07-014

All sampled lithological units comprise glacial marine sediments. The immense change in sedimentation-rate in core JM07-014-PC is reflecting changes in the source area, most likely of glacial nature. Though the sedimentation-rate changes strongly, the sedimentary

products stay remarkably similar throughout the change, which is deduced from occurring lamination in core JM07-014-GC. Why there is lamination in core JM07-014-GC and none in core JM07-014-PC below ~88 cm depth is most likely due to the different sample methods of gravity and piston coring.

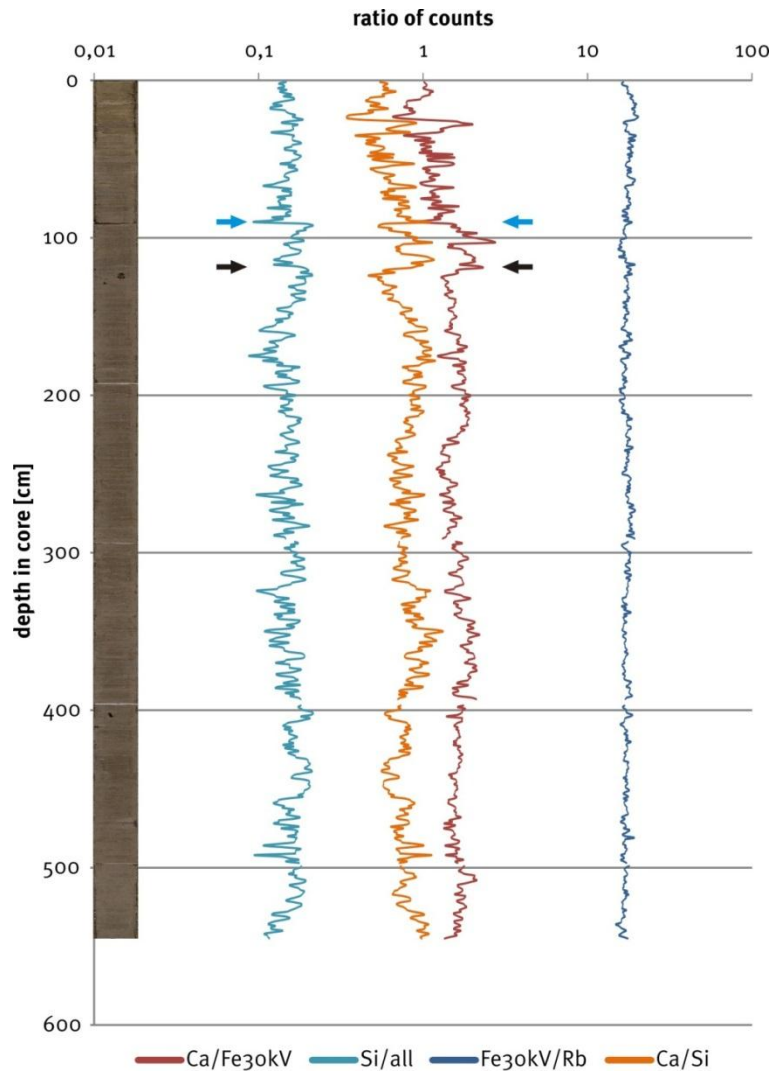


Figure 6.29: XRF-Scanner element ratios of core JM07-014-GC. Black arrows point at changes in variability in the XRF-data.

7 Discussion

This chapter begins with a correlation of the seismic and lithological data. The deduced sediment rates are compared to existing records before all observed sediments are discussed with regard to the involved processes. These three sub-chapters will lead to the discussion of the palaeoenvironment, including the palaeoclimate and deglaciation history.

7.1 Correlation of the Litho- and Seismostratigraphy

The litho- and seismostratigraphies provide the basis for correlating the cores of this study with each other, as well as for correlating the cores with the seismostratigraphy.

Cores JM07-12 and JM07-14 were projected perpendicular onto the closest chirp profile (figs. 7.1 and 7.2). The core lengths are converted into seconds TWT using a p-wave velocity of 1600 m s^{-1} , thus they can be displayed on the profile. This is a simplification, because the p-wave velocity varies with depth. The p-wave velocity is measured to be lower than 1600 m s^{-1} in the upper part of core (figs. 6.7, 6.15, 6.21 and 6.26). However, 1600 m s^{-1} was chosen so that the data is comparable to literature (e.g. Elverhøi et al., 1995b, Plassen et al., 2004, Forwick and Vorren, 2011).

At core site JM07-012 the combined penetration depth of the two overlapping cores JM07-012-GC and JM07-012-PC was considered. Here, the most notable change in seismic signature, horizon R1, is penetrated in the lower part of the core (fig. 7.1). Compared to observations in the lithostratigraphy this horizon is the same as the unit boundary between 12GC-1 and 12GC-2 and between 12PC2 and 12PC-3, respectively (chapter 6.1.3.5).

At least three, possibly up to six, marked reflections (one of which is horizon R4) are penetrated at core site JM07-014 (fig. 7.2). However, the impedance contrasts of the reflections cannot be precisely correlated to lithological observations due to the absence of lithological lamination. A tentative interpretation is that the uppermost strong reflection below the seafloor correlates to the unit boundary between 14GC-1 and 14GC-2 and between 14PC-1 and 14PC-2 (figs. 6.19 and 6.25), respectively.

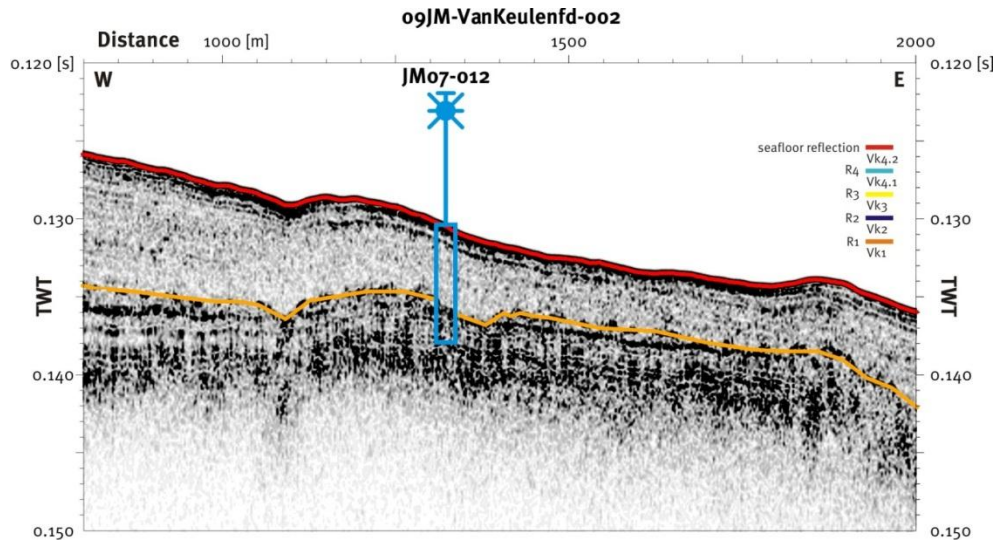


Figure 7.1: Chirp profile 09JM-VanKeulenfd-002 showing the location of JM07-012. For location see fig. 5.1.

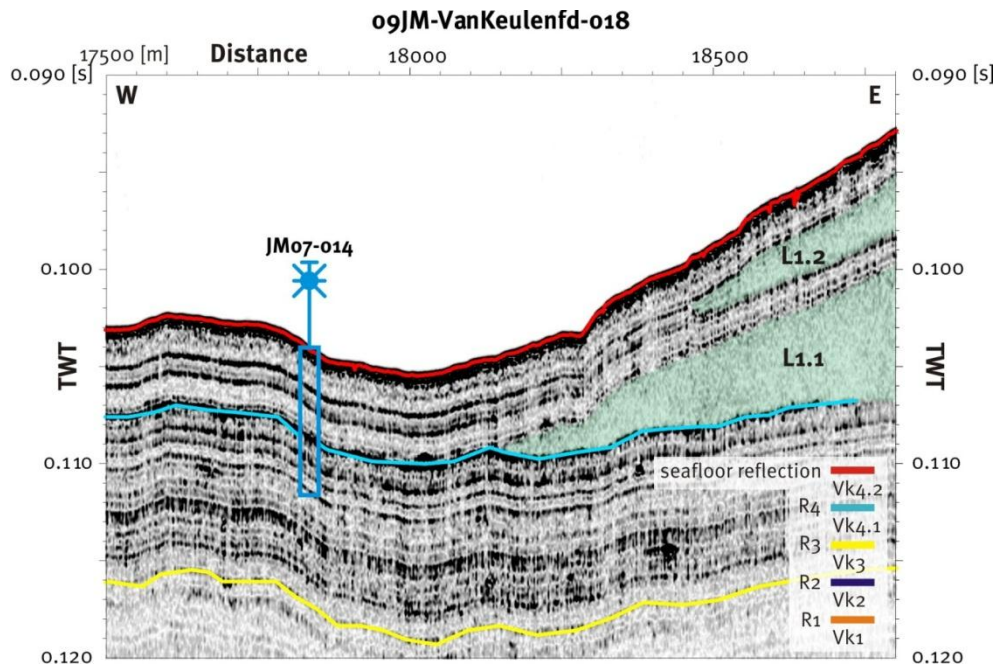


Figure 7.2: Chirp profile 09JM-VanKeulenfd-018 showing the location of station JM07-014. For location see fig. 5.1.

A correlation of the cores JM07-012-GC and JM07-012-PC has been done in chapter 6.1.3.5. Here, the cores are correlated between the two core sites, JM07-012 and JM07-014.

The correlation between the litho- and seismostratigraphies (figs. 7.1 and 7.2) of the two core sites, JM07-012 and JM07-014, suggests that the cores show little overlap (fig. 7.3). Both core sites only share the seafloor as a common reflector and are correlated as depicted on fig. 7.3. Radiocarbon dates enable further correlation (chapter 7.2).

7.2 Chronology

Radiocarbon dates from core site JM07-012 suggest a hiatus at the reflector R1 (unit boundary of 12GC-1 to 12GC-2 and 12PC-2 to 12PC-3; fig. 7.4). Reasons for this hiatus will be discussed with more detail in sub-chapter 7.4.6.

Whenever possible, radiocarbon dates from this study were used for interpolation. In the case of the upper age of the hiatus (fig. 7.4, 7010 cal. yrs. BP) extrapolation between both dates from core JM07-012-GC was used (960 ± 60 cal. yrs. BP and 6920 ± 60 cal. yrs. BP). The extrapolated age for this boundary is assumed to be valid, because the closest radiocarbon date (6920 ± 60 cal. yrs. BP) is only 19 cm of depth away. Additional ages for the lower units are taken from various authors.

The age for R1 (10660 ± 80 cal. yrs. BP) is taken from Hald et al. (2004), where this age is the lowest and oldest age above the deglaciation unit, which is comparable to Vk1. The ages for R2 and R3 are interpolated between the age from Hald et al. (2004) and the interpolated age for R4. The minimum age (11160 ± 150 cal. yrs. BP) for the boundary between Vk0 and Vk1 is taken from a reworked bivalve in a core in the north western part of the outer basin of Van Keulenfjorden (fig. 7.4; Bratlie, 1994). This bivalve is the oldest postglacial radiocarbon date for Van Keulenfjorden. The maximum age for the same boundary was taken from a glacier front position map in Mangerud et al. (1992) indicating that the glacier front was still at the sill during that time (12.3 cal. ka BP; fig 7.4).

In chapter 7.5 these inter- and extrapolated ages are used in the titles for time orientation.

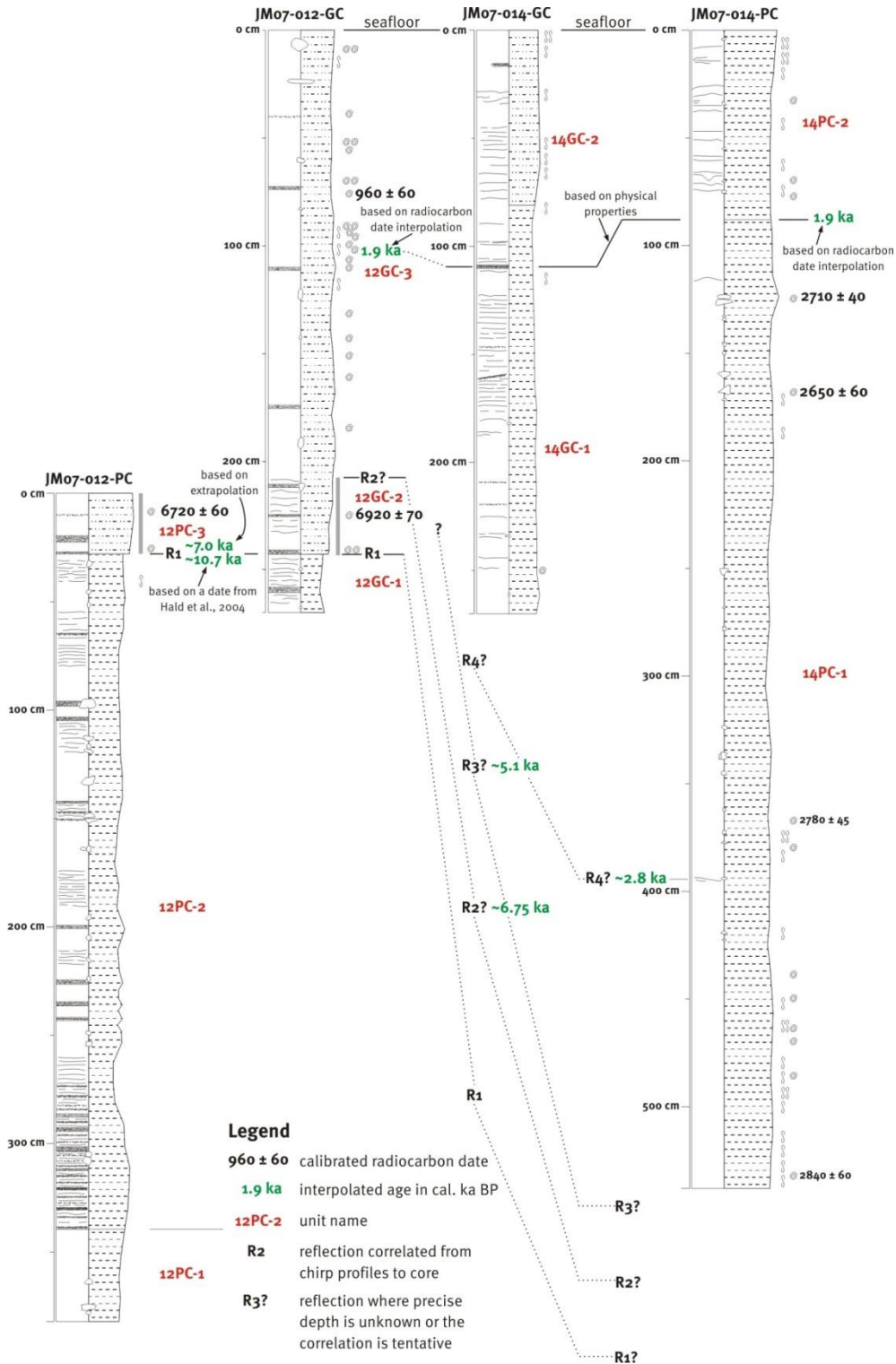


Figure 7.3: Correlation of cores JM07-012-GC, JM07-012-PC, JM07-14-GC and JM07-014-PC.

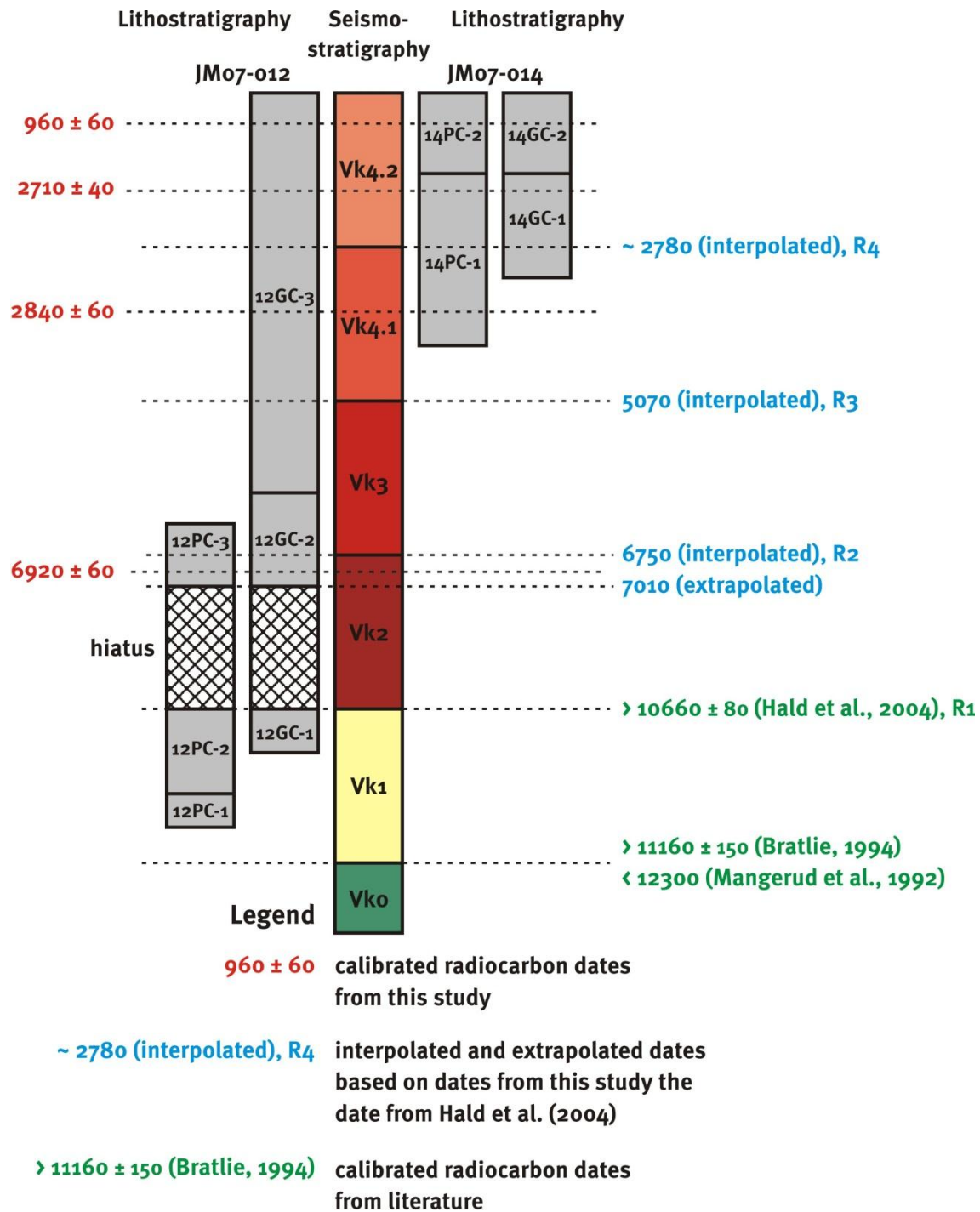


Figure 7.4: Chronology of schematic litho- and seismostratigraphic units defined in this study.

7.3 Sedimentation Rates

Sedimentation rates from the cores JM07-012-GC and JM07-014-PC suggest large variations from ~6.9 cal. ka BP to the present even in a glacier distal environment (figs. 6.5 and 6.25 and tabs. 6.4 and 6.5). The sedimentation rate trends of the two cores are opposed during the glacial advance (see chapter 7.4.4) related sedimentation around 2.7 cal. ka BP, but they have similar values for the last ~2.0 cal. ka BP.

The sedimentation rates from core site JM07-012 and JM07-014 are comparable considering their position in the fjord system to other sedimentation rates derived from core data from Billefjorden and Van Mijenfjorden (fig. 7.5; Hald et al., 2004, Baeten, 2007). The sedimentation rates reflect the glacial activity in the catchment area (Elverhøi et al., 1995a, Forwick and Vorren, 2009), since glacial erosion is among the processes producing highest sediment yield (Elverhøi et al., 1995b).

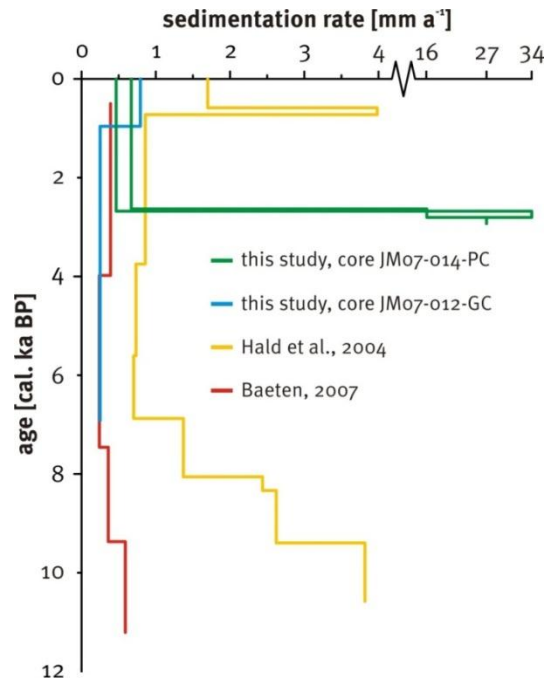


Figure 7.5: Sedimentation rates of this study compared to results from Van Mijenfjorden (Hald et al., 2004) and Billefjorden (Baeten, 2007).

The isopach maps reveal varying sedimentation rates inside the fjord depending on the location and time (figs. 5.10, 5.11, 5.14 and 5.16). The average sedimentation rate at core site JM07-014 above horizon R1 (from 10660 cal. yrs. BP to present) is 2.33 mm a^{-1} . This is up to an order of magnitude higher than sedimentation rates estimated for suspension fall-out and IRD for cores from outer Sassenfjorden and Billefjorden (Baeten et al., 2010b, Forwick et al., 2010). This high average sedimentation rate for a West Spitsbergen fjord can be explained by the proximity to the glacier. Additionally Van Keulenfjorden has a large catchment area with a high degree of glaciation (Hagen et al., 1993), which bears a large sediment input (Elverhøi et al., 1995b).

7.4 Sedimentary Processes

7.4.1 Sub- and Proglacial Processes

Vk0 is the lowermost unit above bedrock. Vk0 is therefore suggested to be a till, because the Late Weichselian ice streams eroded almost all pre-Late Weichselian sediments (Hooke and Elverhøi, 1996). Additionally, if Vk0 were a unit of pre-Late Weichselian Age, then a Late Weichselian till layer would be missing or thin beyond resolution of the sparker seismic (sparker resolution $\sim 1.6 \text{ m}$). Regional examples of tills beneath units reflecting Late Weichselian deglaciation, i.e. Vk1, have similar seismic characteristics (e.g. Svendsen et al., 1996, Forwick and Vorren, 2011).

Vk0 is either a) built from material accumulation from sediment laden meltwater emanating from a subglacial conduit into a subglacial cavity, which may have formed through basal melting (cf. Boulton, 1982) or b) deposited similar to a push moraine or a lodgement till by bulldozing material forward, which becomes trapped in front of the sill and consequently accumulates mass towards the east. Other than a push moraine the till is wedged against sill (fig. 7.6).

The internal acoustic signature of the Vk0-accumulation is generally transparent, but weak reflections occur sporadically towards the base of the unit. This favours neither of the two explanations, since thrust faults are expected in a) similar to a lodgement till (cf. Ó Cofaigh

et al., 2011) or bedding structures in b) similar to a grounding zone wedge (cf. Noormets and Flodén, 2002).

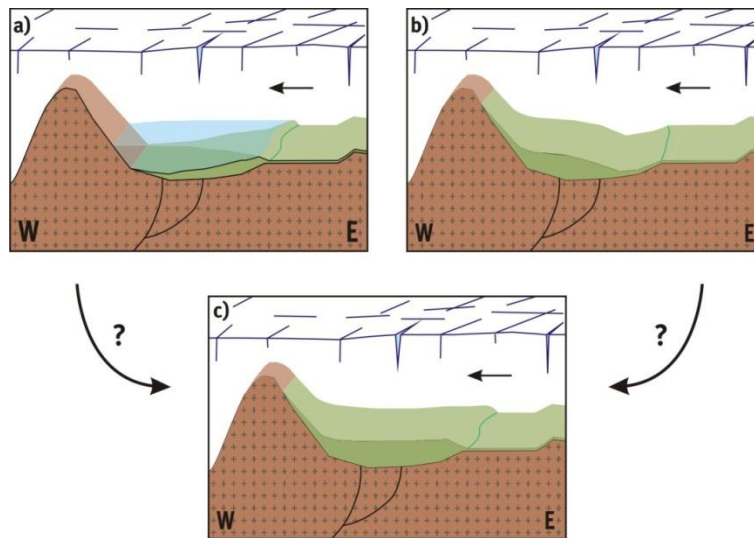


Figure 7.6: Explanatory sketch of the two inferred genetic hypothesis of unit Vk0. a) a cavity infill, b) the accretion of a till wedge and c) the observed result.

Also deriving from Vk0 is the beaded esker, E1. While the low ridge connecting the mounds is a product of a sub- or englacial conduit infill, the mounds of E1 are proglacial sediments. When the glacier retreats a pre-existent conduit infill forms the esker. If the retreat is interrupted by a halt (or a minor advance) the existing conduit acts as source for a proglacial fan producing a mound if the halt lasts long enough and/or the sediment supply is high enough. Halts or minor advances in the glacier retreat can occur annually (e.g. Benn and Evans, 2010).

7.4.2 Suspension Fall-Out

Glacial meltwater provides the main sediment sources to the post-glacial Van Keulenfjorden sedimentary environment.

Suspended sediment originates mainly from the Nathorstbreen glacier front, as well as from various tributary valley glacial rivers. At the polythermal tidewater glacier front, sub- or

englacial conduits are the pathways for sediment-laden meltwater to emanate into the fjord throughout the whole year (Svendsen et al., 2002). However, the meltwater input varies seasonally (Weslawski et al., 1995).

The larger grainsize fraction is deposited in coalescent morainal banks in a proglacial position. The small grainsize fraction is transported in a hyper- or hypopycnal flow away from the glacier front forming a plume (Hambrey, 1994). An aerial photograph of a hypopycnal flow (overflow) in front of Doktorbreen and Liestølbreen is given in fig. 1.3b. Similar examples are recorded by aerial photographs in Rindersbukta (Van Mijenfjorden), Kollerfjorden and Mayersbukta (both tributaries to Möllerfjorden/Krossfjorden; Dowdeswell and Dowdeswell, 1989, Dahlgren, 1998). Such plumes can bear highly concentrated sediment loads of up to 500 mg l^{-1} (Elverhøi et al., 1983).

From the fjord sides glacifluvial meltwater input contributes to the suspension fall-out in the fjord from late May to November (Weslawski et al., 1995). The westward thinning trend of units Vk3, Vk4.1 and Vk4.2 (figs. 5.11, 5.14 and 5.16) suggests that the majority of the sediment supply originates from the inner ford basin, i.e. the Nathorstbreen front. However, no westward thinning trend was observed in seismostratigraphic unit Vk2 (~10.7 cal. ka BP to ~7.0 cal. ka BP; fig 7.4). Instead the topography controls the sedimentation with a thin succession on the ridges and a thicker succession in the sub-basins. This is inferred to be related to i) great distance from the sediment source suppressing the westward thinning trend and ii) strong bottom currents hampering the deposition on the ridges and favouring deposition in the sub-basins.

7.4.3 Ice Rafted Debris (IRD)

Plumes lose their suspension load exponentially with the distance from the source (Elverhøi et al., 1983, Ó Cofaigh and Dowdeswell, 2001). If a significant amount of icebergs is transported away from the glacier front quickly enough, icebergs may discharge their debris just as much proximally as they do distally (Dowdeswell and Dowdeswell, 1989). When that is the case, depletion of suspension fall-out creates IRD-enriched distal sediments

(Dowdeswell and Dowdeswell, 1989). This phenomenon is also observed between the two core sites of this study in form of lower IRD abundance at core site JM07-014 (cf. figs. 6.8, 6.9, 6.10 and 6.11 with figs. 6.22 and 6.28).

7.4.4 Mass-Transport Deposits

Mass-transport deposits occur in various forms in Van Keulenfjorden. Most prominent are the two stacked debris flows (L1.1 and L1.2) that originate from the inner fjord basin sill. Mass-transport deposits are also found along the slope of Ullaberget and the talus of the sandur-delta fan (Krigström, 1962) at the mouth of Ulladalen, Finsterwalderbreen as well as Penckbreen.

The mass-transport deposits in the lobes of L1.1, L1.2 and L3 are sharply outlined. Because of the convex shape of the talus and the transparent seismic signature, the lobes L1.1, L1.2, L3 and a lobe in the mass-transport fan in front of Penckbreen (fig. 5.15) are interpreted to be formed by cohesive debris flows (cf. Laberg and Vorren, 1995, Mulder and Alexander, 2001). The convex morphology of the talus is produced when a cohesive debris flow comes to a halt. The transparent signature is due to the transport mechanism, which does not sort the material (Laberg and Vorren, 1995, Laberg and Vorren, 2000, Mulder and Alexander, 2001, Plassen et al., 2004), and continuous reflectors are therefore unlikely to form.

The debris flow lobes L1.1 and L1.2 are either formed a) synchronous or b) subsequently to the deposition of a terminal morainal bank. For synchronous formation a) the debris flows are initiated through pushing and steepening of the distal side of the morainal bank. In case of subsequent formation b) slope failure occurs and a slip plane would develop (fig. 7.7; Plassen et al., 2004).

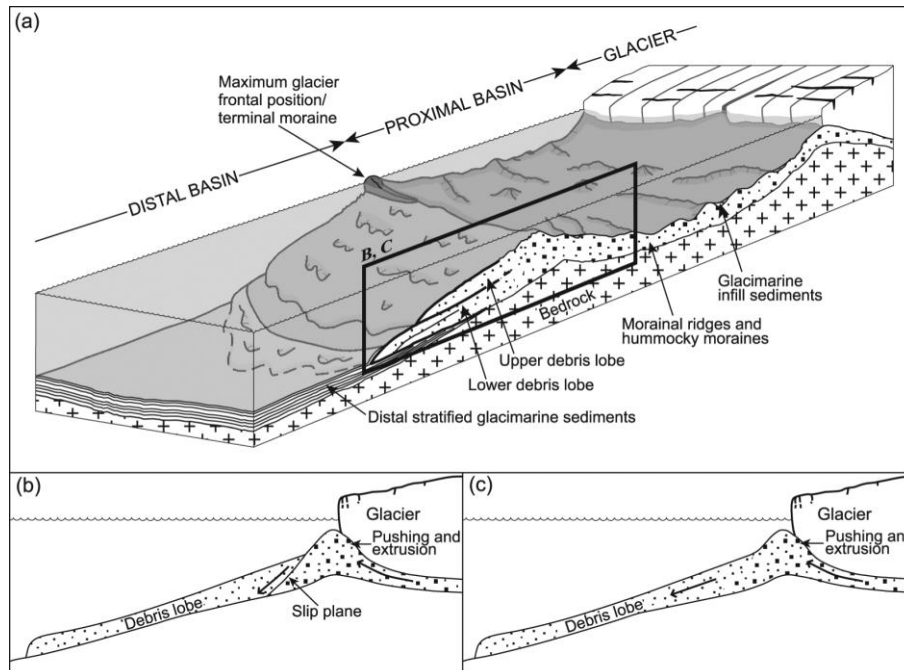


Figure 7.7: a) Schematic block sketch of morphological elements and surge related sediment packages and two formation models, b) and c) of debris flow deposits adjacent to terminal morainal banks (from Plassen et al., 2004).

Debris flows can have an almost erosion-free transport due to hydroplaning (Vorren et al., 1998, Laberg and Vorren, 2000, Laberg and Vorren, 2003). However, a debris flow needs a high velocity to cause hydroplaning, which was most likely not reached in Van Keulenfjorden, as the debris flow deposits have a short run-out distance (~5 km in Van Keulenfjorden opposed to ~200 km in the Bjørnøya trough mouth fan; Laberg and Vorren, 2000). Accordingly, the debris flow lobe L1.1 shows erosional truncation into the uppermost glacimarine sediments of seismic unit Vk4.1 (fig. 5.17). The debris is therefore assumed to have been slow. The reason for the strongly cohesive debris flows could be the mud dominated, almost sand-free, sediment mixture (cf. pers. comm. with A. Elverhøi from Dahlgren, 1998).

7.4.5 Glacifluvial Sediment Input from Tributary Valleys

Small-scale glacifluvial fans occur at the mouth of Ulladalen, Finsterwalderbreen and Penckbreen. From chirp profiles debris flows and chutes/channels are inferred to be common (figs. 5.8, 5.12 and 5.15; cf. Prior et al., 1981, Bornhold et al., 1994). Associated with these channels are turbidity currents (Mulder and Alexander, 2001). However, a cohesive debris flow deposit is intercalated into Penckbreen's sandur fan signature (fig. 5.15; cf. chapter 7.3.4). This cohesive debris flow lobe was possibly formed the same way as discussed above for L1.1 and L1.2 as a result of major advance or surge of Penckbreen and the reworking of the incorporated proglacial sediments (fig. 5.15).

The sedimentation of the sandur deltas obeys an annual rhythm of the extremely seasonal sediment input in the summer months with the yearly melt season (Weslawski et al., 1995, Svendsen et al., 2002). The high water flow energy regime during the summer meltwater peak allows transport of boulder-sized grains. Due to this seasonality and the fractionation process (clay and silt form a plume) the grain size distribution of the fan sediments is assumed to be less muddy. The lower cohesion between the larger grains of the deltas and the high water flow energy regime is indicated by the irregular signature of surface and palaeosurfaces of the fan. It is assumed that many small-scale gravity flows, i.e. turbidity currents and cohesionless debris flows, form the majority of the fan sediments, while chutes form erosional surfaces (figs. 5.8, 5.12 and 5.15; cf. Eilertsen et al., 2002). The plume sedimentation shifts to become the background sedimentation in that particular area.

7.4.6 Hiatus

A minimum age of 10660 cal. yrs. BP was inferred for the upper boundary of glacier proximal sediments (fig. 7.4). A time gap of ~4 ka in the sedimentary record between glacier proximal and glacier distal glacial marine sediments is indicated by the ages of 6920 ± 70 cal. yrs. BP and 6720 ± 60 cal. yrs. BP in the cores JM07-012-GC and JM07-012-PC, respectively. This gap can either be explained by a) erosion or b) non-deposition. Erosional truncation could be interpreted on the chirp sonar profile (fig. 7.1). However, reworked

deposits are absent. Additionally, in both cores from core site JM07-012 the lithological unit boundary does not show traces of erosion. Therefore the hiatus is most likely a non-depositional hiatus.

The isopach map for the entire sediment succession above R1 indicates that this hiatus is regionally limited to the area of the core site with a ~1 km radius around it (red area on fig. 7.12). Bottom currents providing a higher water energy environment may have prevented deposition. Gas seepage from the pockmarks, P2, may have enabled erosion in connection with bottom currents. However, the thinnest part correlates only partially with the most pronounced pockmarks (fig. 7.8) and the hiatus was previously inferred to be non-depositional rather than erosional. Bottom currents are therefore proposed to be the major cause of this hiatus. This is supported by the observation from the sediment distribution during the same time (10.7 cal. ka BP to 7.0 cal. ka BP; fig. 5.10; chapter 7.4.2).

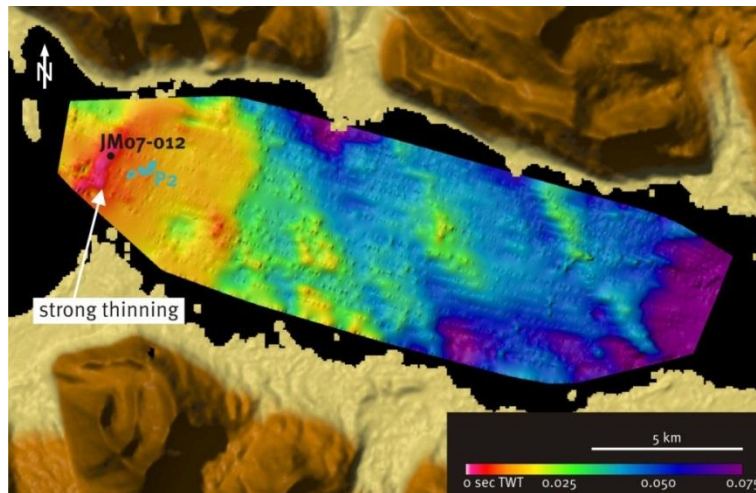


Figure 7.8: Isopach map of the whole post-R1-succession. Note that the thinnest deposits occur in the vicinity of core site JM07-012. Blue circles indicate the most pronounced pockmarks of P2.

7.5 Deglaciation and Holocene Environment in Van Keulenfjorden

7.5.1 Deglaciation from Shelf break to Fjord Mouth, from 17400 cal. yrs. BP to 11260 cal. yrs. BP (10400 ^{14}C yrs. BP)

A combination of conclusions from various studies including this study was used to create a time distance glaciation diagram for the Bellsund and Van Keulenfjorden area (fig. 7.9). The deglaciation of the Late Weichselian Barents Sea Ice Sheet from the shelf break west of Svalbard began at 17.9 cal. ka BP and the ice front reached the fjord mouth of Van Keulenfjorden at 12.3 cal. ka BP (10.5 ^{14}C ka BP; Mangerud et al., 1992, Elverhøi et al., 1995a, Svendsen et al., 1996). Prior to 11.6 cal. ka BP Van Keulenfjorden acted as a pathway for fast-flowing ice draining the Barents Sea Ice Sheet (fig. 7.9; cf. Ottesen et al., 2005, Ottesen et al., 2008).

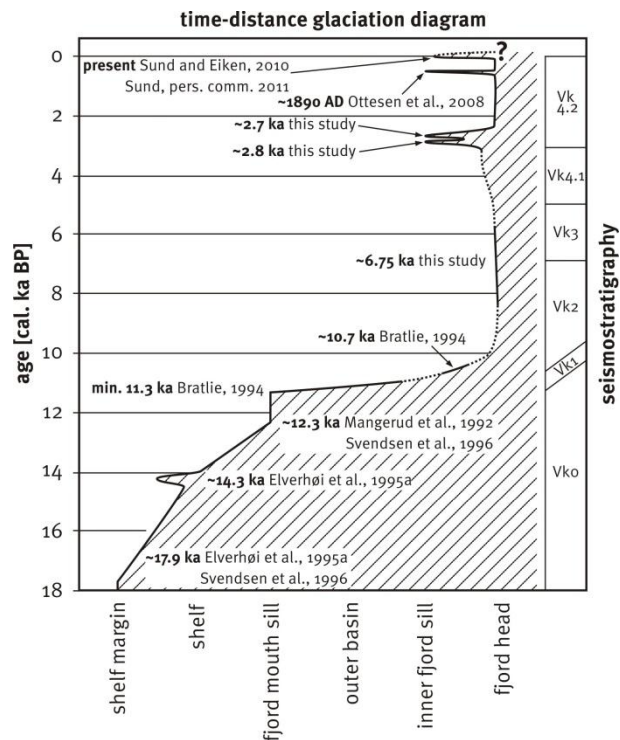


Figure 7.9: Time distance glaciation diagram for Van Keulenfjorden and Bellsund with data from various studies, including this study.

The lower boundary of Vk0 shows URU-like characteristics (URU = Upper Regional Unconformity) on airgun-seismic lines (fig. 7.10; Bratlie, 1994) and is therefore interpreted to be the boundary between Mesozoic and Early Cenozoic bedrock.

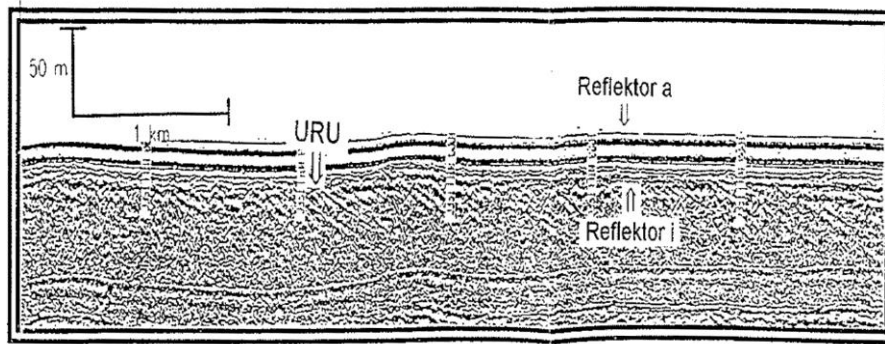


Figure 7.10: Airgun profile through Van Keulenfjorden. Reflector “i” is the same as the lower boundary of unit Vk0. Note the angular unconformity between the steep reflections below and the horizontal reflections above horizon “i” (from Bratlie, 1994).

All of the proposed scenarios in chapter 7.3.1 for the genesis of the lowermost seismic unit, Vk0 (fig. 5.4), include the unit being located beneath the fast-flowing ice of the Late Weichselian glaciation. Age control by radiocarbon dating on unit Vk0 is difficult, because samples would most likely give infinite radiocarbon age (cf. Hald et al., 2004). Vk0 is probably of Late Weichselian age because sediments of pre-Late Weichselian age were eroded by the last glaciation in Svalbard fjords (Elverhøi et al., 1995b, Hooke and Elverhøi, 1996). However, the possibility of Vk0 being pre-Late Weichselian should not be entirely dismissed as there are records of pre-Late Weichselian soft sediment in Svalbard fjords (e.g. Mangerud et al., 1998).

Bratlie (1994) concludes 11260 cal. yrs. BP as the upper boundary of Vk0. This goes in line with the results from other studies from Van Keulenfjorden and Van Mijenfjorden (Mangerud et al., 1992, Elverhøi et al., 1995a, Svendsen et al., 1996). The minimum age for a similar till unit in Isfjorden is 12.7 cal. ka BP (fig. 7.11; Forwick and Vorren, 2009, Forwick and Vorren, 2011). However, also here the till was deposited diachronously, and

the deposition terminated in the inner part of the fjord around 11.2 cal. ka BP (Forwick and Vorren, 2009).

The linear ridges R1 and R2 observed on the multibeam data (figs. 4.1a and 4.1b) are inferred to be from the same age interval as unit Vk0, because both ridges are interpreted to be subglacially formed. These two ridges are the only traces of fast ice-flow in the outer Van Keulenfjord basin. However, traces of fast ice flow in form of mega-scale glacial lineation and lateral ice stream moraines were described for the Bellsund trough (Ottesen et al., 2005).

The mounds of the beaded esker, E1, indicate that the glacier front halted during the retreat (Boulton, 1986, Warren and Ashley, 1994, Brennand, 2000). The mounds of the esker have an average distance between each other of ~160 m. Sets of small retreat moraines in Svalbard fjords are inferred to be De Geer moraines (annual recessional moraines) deposited during Late Weichselian deglaciation (e.g. Baeten et al., 2010a) and after the Little Ice Age (Ottesen et al., 2008). Retreat rates of 170 m a⁻¹ for the Late Weichselian deglaciation in Billefjorden (Baeten et al., 2010a) and 90 m a⁻¹ for the retreat in the inner basin of Van Keulenfjorden after the Little Ice Age extent (Ottesen et al., 2008) are suggested. Both De Geer moraines and the mounds are formed during periods of halts or minor readvances during glacial retreat. The values for the spacing of the mounds and those of De Geer moraines match, especially for the Late Weichselian retreat in Billefjorden (~170 m in Billefjorden, ~160 m in Van Keulenfjorden). Therefore it is proposed that similarly to De Geer moraines the mounds of E1 reflect annual deposition. Consequently the retreat velocity of the glacier front during the Late Weichselian through parts of Van Keulenfjorden is interpreted to be ~160 m a⁻¹. If this retreat rate was constant for the entire retreat through the fjord, then the outer fjord basin would have been deglaciated in the course of 125 yrs.

Retreat examples during the same time from Andfjorden, mainland of Norway, have lower retreat rates (Vorren and Plassen, 2002). However, the north Norwegian deglaciation in Andfjorden began with a rate of 310 m a⁻¹ (from Egga II to Flesenmoraine), which is

comparable to the fastest modern retreats, e.g. 280 m a^{-1} for Jakobshavn Isbrae, west coast of Greenland (Knight, 1999, Vorren and Plassen, 2002).

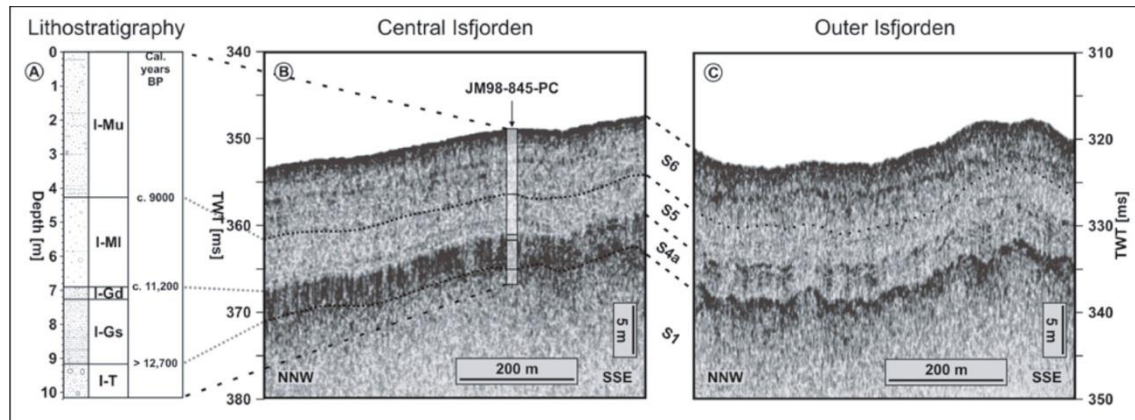


Figure 7.11: 3,5 kHz echo sounder profiles and the sketch of a lithostratigraphy from core JM98-845-PC from Isfjorden. The seismostratigraphy is very similar to the one found in Van Keulenfjorden, though the chronology may differ (from Forwick and Vorren, 2011).

The chirp seismic profiles suggest that all three eskers (E1, E2 and E3) derive from unit Vk0. The eskers and the linear ridges are all subglacial landforms that are still visible from the last glacial in the outer basin. Their preservation and the absence of other subglacial features indicate that the glacier did not readvance into the outer basin during the Holocene (fig. 7.9).

7.5.2 Deglaciation of Van Keulenfjorden, from 11260 cal. yrs. BP to 10660 cal. yrs. BP

Seismic unit Vk1 was recovered in the cores JM07-012-GC and JM07-012-PC. The clast-bearing mud with intercalated gravelly to pebbly layers are suggested to reflect a glacier proximal environment (cf. Forwick and Vorren, 2009).

The acoustic stratification of Vk1 is due to frequent lithological changes. These frequent changes could be the result of strong spatial and temporal variations of a) mass-transport activity (cf. Powell, 1990, Powell, 2003), b) ice-rafting (Forwick and Vorren, 2009,

Forwick and Vorren, 2011) and c) suspended sediment supply (cf. Rachlewicz, 2009) or a combination of all three.

Repetitive decreasing up-core bulk density and IRD cycles (fig. 6.16) could be caused by mass-transport activity (cf. Lowe, 1982), short-term changes in the glacial environment, iceberg dumping or sikussak formation (Syvitski et al., 1996).

IRD occurs irregularly throughout the post-glacial succession. After a large drop in acoustic reflectivity at R1 the increasing seismic reflectivity in the sediments from R1 to the seafloor points towards increasing ice rafting and thus to increasing glacial activity in the catchment area. IRD in the cores occurs both scattered (fig. 6.16 lower part) and in layers (figs. 6.9 and 6.16 upper part). An analysis with the aim to differentiate between sea-ice rafted debris and iceberg rafted debris was not performed. However, a nearly proportional abundance of sea-ice rafted debris and iceberg rafted debris occurs in Van Mijenfjorden during the entire Holocene (Hald et al., 2004). IRD is ubiquitous in the sediments in Van Keulenfjorden, which indicates that a tidewater glacier influenced the fjord system throughout at least the last 6920 cal. yrs. BP. It is likely that the tidewater glacier, i.e. Nathorstbreen influenced Van Keulenfjorden the entire Holocene, because tidewater glacier influence during the entire Holocene is also concluded from Billefjorden, Isfjorden and Van Mijenfjorden (Hald et al., 2004, Forwick and Vorren, 2009, Baeten et al., 2010a).

Cyclic changes in the chemical composition are recorded in Vk1 of core JM07-012-PC. The three proxies Ca/Fe, Ca/Si and Si/all are used to indicate the origin of these cycles. The ratio of Ca/Fe is an inverse proxy for biogenic carbonate (Croudace et al., 2006). The ratio of Ca/Si is a proxy for total carbonate vs. detrital clay. The ratio of Si/all displays the relative amount of detrital clay.

The four distinct cycles (fig. 6.17, black arrows) comprise high Ca/Fe and high Ca/Si peaks while Si/all does not show excursions at the same depths. This indicates increased inorganic carbonate content. This is probably due to a change in provenance. Calcareous bedrock is only found in the south-western parts of the catchment areas of Hessbreen,

Finsterwalderbreen and Penckbreen with the silicified carbonates of the Tempelfjorden Group and the carbonate and evaporitic rocks of the Gipsdalen Group (Dallmann et al., 1990). Thus, the four large cyclic peaks and the occurring smaller peaks above are interpreted to represent high glacial activity from the three big southern glaciers. Possibly they reflect glacier surges or climatically induced glacial advances, which do not necessarily have to reach the fjord with a tidewater glacier front in order to influence the fjord sediments (Gilbert et al., 2002).

The pockmarks, P2, close to the fjord mouth are associated with fluid flow during a period of rapid isostatic uplift after the deglaciation of the Late Weichselian Barents Sea Ice Sheet (Landvik et al., 1987, Forman et al., 2004, Forwick et al., 2009). Faults of the West Spitsbergen fold and thrust belt located beneath the pockmarks (Dallmann et al., 1990) may have been reactivated creating pathways for thermogenic fluids to migrate up through the sediment and escape at the seafloor. Examples of thermogenic gas-flow off the west coast of Spitsbergen and in Spitsbergen fjords, as well as fluid migration along tectonic lineaments have been described (e.g. Söderberg and Flodén, 1992, Knies et al., 2004, Forwick et al., 2009). Biogenic gas is excluded here as an explanation since there is no sediment below the pockmarks that can produce biogenic gas. Gas from the abundant coal beds on Spitsbergen is also excluded, because below the pockmarks there is exclusively Mesozoic (Janusfjellet, Kapp Toscana and Sassendalen Group) and late Palaeozoic (Tempelfjorden and Gipsdalen Group) bedrock, which are free of coal beds. Therefore it is concluded that it was thermogenic gas that can be accounted for the formation of the pockmarks P2.

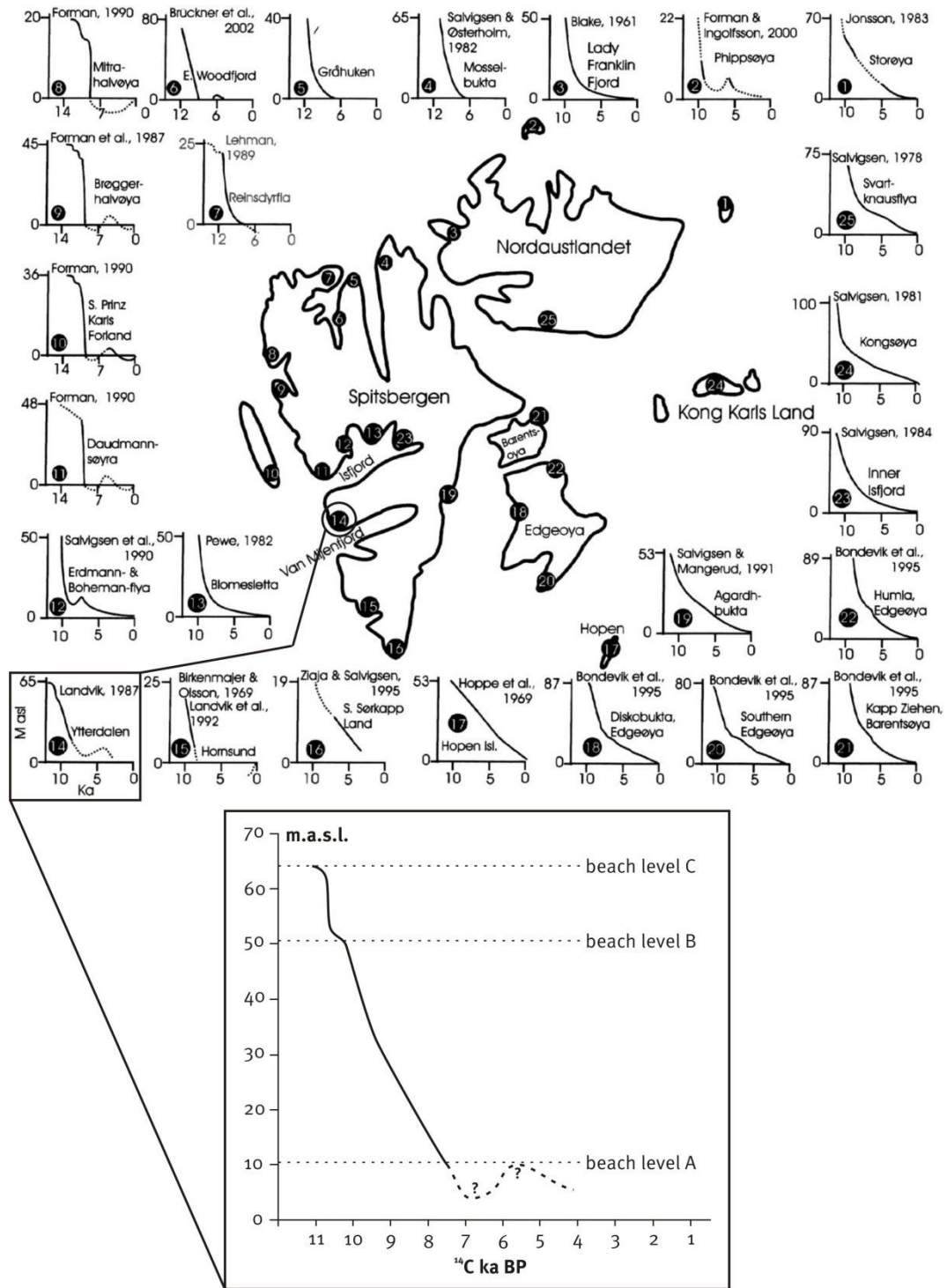


Figure 7.12: Above: shoreline displacement diagrams of Svalbard reviewed in Forman et al. (2004). Below: the closest shoreline displacement diagram to Van Keulenfjorden is #14 from Landvik et al. (1987).

Discontinuous, but marked acoustic stratification in glacial marine sediment in the pockmark depression above horizon R1 (fig. 5.9), absent dip decrease with depth of the pockmark morphology and the smooth surface expression indicate low activity or inactivity of the pockmark since at least 6920 cal. ka BP. The uplift and possible fault reactivation was most pronounced during the latest Weichselian and earliest Holocene, 11.0 ¹⁴C ka BP to ~9.0 ¹⁴C ka BP (fig. 7.12; Landvik et al., 1987, Forman et al., 2004). It is likely that the activity of the seepage of thermogenic fluids is proportional to the activity of the uplift and the associated reactivation. Therefore the pockmarks of P2 are relicts, because the uplift is strongly alleviated on the west coast of Spitsbergen since ~9.0 cal. ka BP (8.0 ¹⁴C ka BP, fig. 7.12; Landvik et al., 1987, Forman et al., 2004).

7.5.3 Climatic Optimum in Van Keulenfjorden, min. 10660 cal. yrs. BP to c. 6750 cal. yrs. BP

This time interval is archived in unit Vk2 between the horizons R1 and R2. The acoustically transparent to semi-transparent sediment of unit Vk2 contains mostly glacial marine mud. The unit lies conformably on top of unit Vk1. The few reflections in Vk2 (fig. 5.3) are interpreted to be caused by higher clast layers from sporadic ice-rafting events (fig. 6.9). These ice rafting events are associated with enhanced iceberg calving due to climatic changes or surges.

Generally low acoustic reflectivity and very few layers of high IRD content indicate that ice rafting was reduced. Low ice rafting activity in Vk2 points towards a low glacial activity during the time after the glacier retreat into the inner basin. The front of Nathorstbreen was probably located far inside the fjord (fig. 7.9). Slightly warmer climate than today (Birks, 1991, cf. Hanssen-Bauer, 2002) caused this climatically driven low glacial activity (cf. Hald et al., 2004, Forwick and Vorren, 2009, Baeten et al., 2010a, Forwick et al., 2010).

The proxy ratio of Fe/Rb is used to display fractionation effects and therefore it often shows sedimentary process-based unit boundaries (Croudace et al., 2006, Rothwell et al., 2006). The Rb is often used as baseline proxy, so that the marked changes in the Fe/Rb

ratio are expected to be caused by a change in relative Fe abundance. Fe/Rb values are generally higher in the units 12GC-2 and 12PC-3 than in the units 12GC-1 and 12PC-2 (figs. 6.12 and 6.17). The lower Fe/Rb ratio and decreased lamination in unit 12GC-2 (and 12PC-3, resp.) indicates that sedimentary processes have changed during this transition. The sedimentary processes that formed 12GC-2 and above are suggested to be glacier distal suspension fall-out and ice rafting, while for 12GC-1 (and 12PC-2) proglacial mass-transports are proposed additionally. A constant Fe/Rb ratio above this unit boundary (R1; fig. 7.3 and 7.4), suggests that suspension fall-out and ice-rafting dominated the sedimentation at the core site ever since.

The suspended sediment input from the tributary valleys varies strongly. During the Vk3 interval Davisdalen does not contribute much to the sediment input to the fjord as indicated by the Vk3 isopach map (fig. 5.11). During Vk4.1, however, the input from Davisdalen increased to the same level as e.g. Ulladalen or Finsterwalderbreen. This may be due to growing or re-emerging cirque glaciers in the area draining through Davisdalen in the early to mid- Holocene in the course of gradual cooling.

At horizon R2 unit Vk2 gradually transitions into unit Vk3. This transition from non-stratified to weakly stratified signature is interpreted to be caused by a larger amount of IRD in the sediment (cf. Forwick and Vorren, 2011). More ice rafting implies a higher glacial activity in the catchment area (Hald et al., 2001).

Bottom currents are suggested to be the cause for a hiatus at core site JM07-012. Before the shoreline displacement of a total ~65 m since deglaciation (Forman et al., 2004) the sill at the fjord mouth of Van Keulenfjorden was less confined than it is at present. Water exchange with the shelf water masses is assumed to have been stronger. This may have caused increased bottom currents from shelf water masses entering the fjord. It is proposed that the process that caused the non-depositional environment was active after 7010 cal. yrs. BP in an attenuated form, because of absence of acoustic stratification where the succession is thinnest. One distinct reflector directly below the seafloor shows, this process is not active any more (fig. 5.5).

7.5.4 Cooling in Van Keulenfjorden, from ~6750 cal. yrs. BP to 2780 cal. yrs. BP

The acoustic signature changes gradually from weak stratification within unit Vk3 to stronger stratification within Vk4.1. This is interpreted as further increase in ice rafting and an associated higher glacial activity during the deposition of unit Vk4.1. The sedimentary environment, however, remains the same in most of the fjord with a majority of the sediment being comprised of glacial marine mud. The Nathorstbreen glacier front, which is interpreted to be far inside the inner fjord basin during Vk2-time had advanced and was then situated further out in the inner fjord basin during the deposition of Vk3.

The high-magnitude reflections in front of Finsterwalderbreen, Penckbreen and Ulladalen (figs. 5.8, 5.12 and 5.15) reflect lithological variations within coarse grained, glacial fluvial, sandur deltas.

The existence of cohesive debris flow deposits matches on-land observations, where a large surge was described for Penckbreen. For Finsterwalderbreen several glacial readvances to a close-to-shore position are recorded in multiple push moraines (Hart and Watts, 1997). A large terminal moraine ridge lies close (<2 km) to the modern shoreline (fig. 7.13). In addition geomorphologic traces of a large surge of Penckbreen are described from the terrestrial record (Hart and Watts, 1997). Surges of land-terminating glaciers can have strong influence on sedimentation in the fjord (e.g. Gilbert et al., 2002).

The late onset of deltaic sediments in the fjord (above R2 and sometimes above R3) can be explained by little sediment supply during the early to mid-Holocene due to low glacial activity and the change in relative sea-level (fig. 7.13). Comparatively high relative sea-level during the earliest Holocene forced the deltaic sedimentation to begin at a higher elevation and therefore further away from the present shoreline. After R2 (estimated 5.2 cal. ka BP), when the delta prograded and the relative sea-level dropped, the deltaic sedimentation reached the present fjord basin.

The sediments correlated with unit Vk4.1 (fig. 7.3) contain high amounts of IRD. This supports the interpretation of the chirp seismic, where Vk4.1 is in the upper part of a succession with increasing up IRD influence.

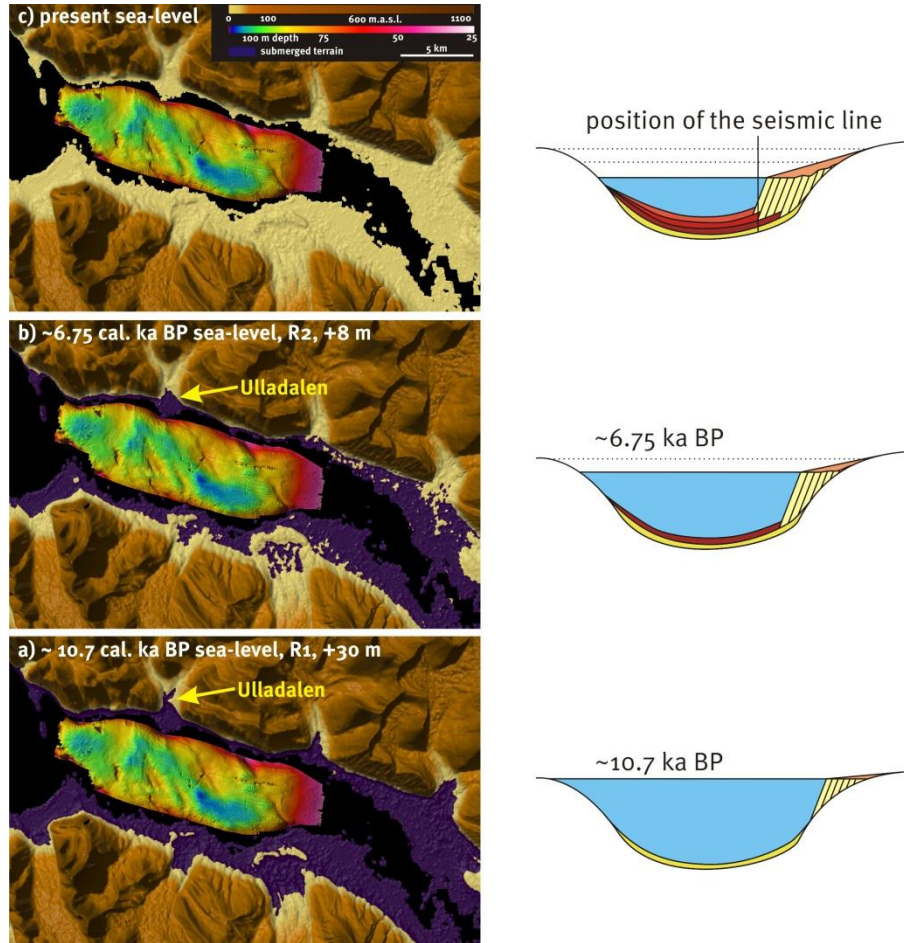


Figure 7.13: Multibeam dataset of Van Keulenfjorden and the topography around it. a), the submerged terrain in violet during the early Holocene with a 25 m higher sea-level than at present. b) the mid Holocene sea-level 8 m higher than at present when the deltaic sedimentation reached the fjord and c) the present situation. The sea-level change values were taken from the shoreline displacement curve from Landvik et al. (1987). To the right is an explanatory sketch for the deltaic sedimentation.

7.5.5 Glacial Advances in Van Keulenfjorden, from 2780 cal. yrs. BP to present

Shortly after 2840 cal. yrs. BP a large debris flow was deposited on the distal side of a morainal bank, which was deposited during a readvance of Nathorstbreen (Ottesen et al., 2008). Whether this readvance was climatically induced or surge related cannot be inferred from the morainal bank or its adjacent debris flow deposit.

Climatic cooling occurred on the west coast of Spitsbergen from 4.0 cal. ka BP to ~2.4 cal. ka BP (Birks, 1991, Svendsen and Mangerud, 1997, Hald et al., 2004). Build-up of ice-mass in the accumulation zone was surely promoted by this change in climatic conditions. The cooling enabled the readvance at 2.8 cal. ka BP. This readvance may have been of surge-type, because analogue architecture and signature of surge related sediments are recorded from known surge events in similar environments (Plassen et al., 2004, Ottesen and Dowdeswell, 2006).

Debris lobes on the distal sides of terminal morainal banks associated with glacial advance and/or surges during the Little Ice Age have been described from other fjords on Spitsbergen (Elverhøi et al., 1983, Plassen et al., 2004, Ottesen and Dowdeswell, 2006). In the study area it has been suggested that the debris flow lobe L1.2 originates from the morainal bank that was deposited from Nathorstbreen at the termination of a surge during the Little Ice Age (~1890 AD; Bratlie, 1994, Ottesen et al., 2008). However, the results from this study do not support earlier suggestions, and an alternative chronology for the formation of the lobes is proposed in the following paragraphs.

The two radiocarbon dates at 125 cm and 168 cm depth in core JM07-014-PC provide ages of 2710 ± 40 and 2650 ± 60 cal. yrs BP, respectively (fig. 6.25). Both these dating samples are correlated to originate from above the stratified sediments dividing L1.1 and L1.2. This indicates that the upper lobe (L1.2) was deposited before 2710 ± 40 cal. yrs BP and therefore prior to the Little Ice Age. Even though the calving front of Nathorstbreen reached the moraine position during the Little Ice Age (Liestøl, 1977) no core data as of yet proves whether the debris flow was deposited during that time, or earlier. The stratified

layer dividing the two lobes is 2 ms TWT to 3 ms TWT thick (fig. 5.17), i.e. approx. 150 cm. Sedimentation rates for core JM07-014-PC range from $16.67 \pm 10.31 \text{ mm a}^{-1}$ to $34.71 \pm 18.69 \text{ mm a}^{-1}$ between 125 cm and 368 cm and 168 cm and 368 cm depth, respectively (fig.6.25 and tab. 6.4). This indicates that the time lag for the depositions of the two lobes was between 30 and 230 yrs. (the range of one standard deviation included using a Gaussian error propagation).

All three main tributaries to the Van Keulenfjorden glacier front at present (Doktorbreen, Liestølbreen and Nathorstbreen) are surge type glaciers (Hagen et al., 1993, Jiskoot et al., 2000, Sund et al., 2009). Therefore, it is reasonable to assume that the glaciers were also surge type glaciers during earlier periods of the late Holocene, when the climatic conditions were very similar to the present (Birks, 1991). The quiescent phases of surge cycles on Svalbard last between 50 to 500 years (Benn and Evans, 2010). The estimated time lag for the deposition of the two debris lobes, L1.1 and L1.2, fits into this Svalbard-surge cyclicity. It is therefore proposed that the two lobes were deposited during two subsequent surge cycles, where the first surge leading to the deposition of lobe L1.1 reached the maximum extent position shortly after 2.84 cal. ka BP (oldest radiocarbon date in the core), and the second surge terminated at a similar position depositing the upper lobe, L1.2, shortly after.

The hypothesis that the upper lobe, L1.2, is from the Little Ice Age advance (cf. Bratlie, 1994, Ottesen et al., 2008) should, however, not be dismissed entirely. If the radiocarbon dates from this study are from reworked shells then the sedimentation rates would have higher values for the upper part and lower values for the lower part and could favour the Little Ice Age origin. It should be noted that all four radiocarbon dates were measured on *Cylichnia alba*, which is known to live in the upper 3 mm of the sediment and feeds on benthic foraminifera (Thomson, 1988). Hence, the ages obtained from this species should be reliable.

High sedimentation rates for core JM07-014-PC can be interpreted to result from mass-transport deposition in addition to suspension fall-out and IRD. However, in the cores and

on the chirp profiles there is no evidence for mass-transport deposits or reworking processes.

How many climatic conclusions can be drawn from glacial activity in the fjord basin and in the catchment area in a surge-type glacier environment is strongly dependent on the characteristics of the sedimentary signal. Signals with a short time period, i.e. < 500 yrs., for example the debris flow deposit in the fan in front of Penckbreen (fig. 5.15), are likely to be of surge origin. And as surges are not triggered by external climatic factors (Meier and Post, 1969, Kamb et al., 1985) the conclusions about the palaeoclimate should be tentative at most. However, if reoccurring surges (e.g. L1.1 and L1.2) or generally high glacial activity depositing IRD-rich layers (e.g. Vk4.2 or the lower part of lithological unit 12PC-2, fig. 6.13) occur more frequently, then the deduction must involve a climatic indication. Accordingly, a climatic condition similar to the Little Ice Age (i.e. colder air temperature) is proposed for the period shortly after 2840 cal. yrs. BP.

The continuous increase in reflectivity of the seismic units Vk2 to Vk4.2 applies also for a period greater than 500 yrs. and is therefore interpreted to reflect a slow, continuous increase in glacial activity since R2 (interpolated 6750 cal. ka BP), possibly in association with a decreasing equilibrium line altitude (ELA) due to lower air temperature and SSTs (Birks, 1991, Dahlgren, 1998, Hald et al., 2004).

The Little Ice Age advance of the glaciers, in Van Keulenfjorden associated with a surge (Liestøl, 1977, Ottesen et al., 2008), is also a product of climatic change because the Little Ice Age is a climatic signal that has been recorded in other fjords on the west coast of Spitsbergen (Mangerud and Landvik, 2007). Therefore the cause cannot have been a regional one, e.g. exclusively a surge.

8 Summary and Conclusions

Swath bathymetry, high-resolution seismic and core data from Van Keulenfjorden are analysed. An assemblage of landforms, five seismostratigraphic units as well as six different lithostratigraphic units are defined. They reveal the following about the Late Weichselian and Holocene sedimentary processes and palaeoenvironment (fig. 8.1):

- Prior to 11.2 cal. ka BP, fast-flowing ice produced an up to 50 m thick subglacial sedimentary body (unit Vk0) on the proximal side to a fjord mouth sill. Vk0 rests on an erosional unconformity with Mesozoic and Early Cenozoic bedrock (fig. 8.1a).
- During the deglaciation, between 11.2 cal. ka BP and 10.7 cal. ka BP (fig. 8.1b and 8.1c), a beaded esker was formed in the central part of the fjord. Mounds on the esker indicate an annual retreat of $\sim 160 \text{ m a}^{-1}$. Assuming a constant rate of retreat the outer fjord basin was deglaciated in the course of ~ 125 yrs.
- Strong isostatic uplift, associated with the rapid deglaciation, most probably reactivated faults in the West Spitsbergen fold and thrust belt. Reactivated faults created pathways for thermogenic gas seepage. The resulting pockmarks (P2) were active shortly after deglaciation and became inactive during the early Holocene (~ 7.0 cal. ka BP). It is proposed that the fluid flow is proportional to the rate of the uplift, which decreased strongly at ~ 8.0 cal. ka BP.
- In the western part of the fjord a hiatus of ~ 4 ka is identified (fig. 8.1d). This is most likely the result of bottom currents that prevented deposition and possibly eroded sediments. The bottom currents weakened but remained active after the sill became more confined in course of the postglacial isostatic uplift (~ 8.0 cal. ka BP). The sediment distribution with less sediment on ridges between 10.7 cal. ka BP and 7.0 cal. ka BP is inferred to reflect the impact of bottom currents in the entire outer basin.

- High amounts of IRD in the sediment (units 12GC-1, 12PC-1 and 12PC-2) and acoustically discontinuous, stratified signature (seismostratigraphic unit Vk1) indicate glacier proximal condition between 11.2 cal. ka BP and 10.7 cal. ka BP.
- Cyclic changes in chemical composition indicate repeatedly changing sediment provenance. Sediments were influenced by sediment supply from tributary valleys in the south during the deglaciation of the fjord.
- Very weak to non-existent internal reflections in seismostratigraphic unit Vk2 indicate low IRD content related to reduced glacial activity between 10.7 cal. ka BP and min. 7.0 cal. ka BP (fig. 8.1d). This reflects the warmest period in the Holocene.
- Isopach maps of mid- to late Holocene seismostratigraphic units reveal a westward thinning trend and highly variable sediment input from tributary valleys. Both of which are related to meltwater plumes.
- Sandur deltas at the tributary valley mouths supply the fjord with additional sediment. Channels/chutes indicate repeated mass-transports and sediment reworking. Cohesive debris flows and less cohesive and less concentrated gravity flows compose the assemblage of mass-transport processes at these fans.
- Around 7.0 cal. ka BP glacial activity began to increase gradually and peaked at ~2.8 cal. ka BP where two consecutive surges deposited two debris flow lobes adjacent to the terminal moraine (fig. 8.1e and 8.1f). Suggestions in Bratlie (1994) and Ottesen et al. (2008) that the upper lobe (L1.2) was of Little Ice Age could not be confirmed, though Nathorstbreen reached the same terminal position in ~1890 AD (fig.8.1g). Both lobes are probably the result of surge advances. However, the climate promoted the necessary build-up of mass in the reservoir area of the glacier.

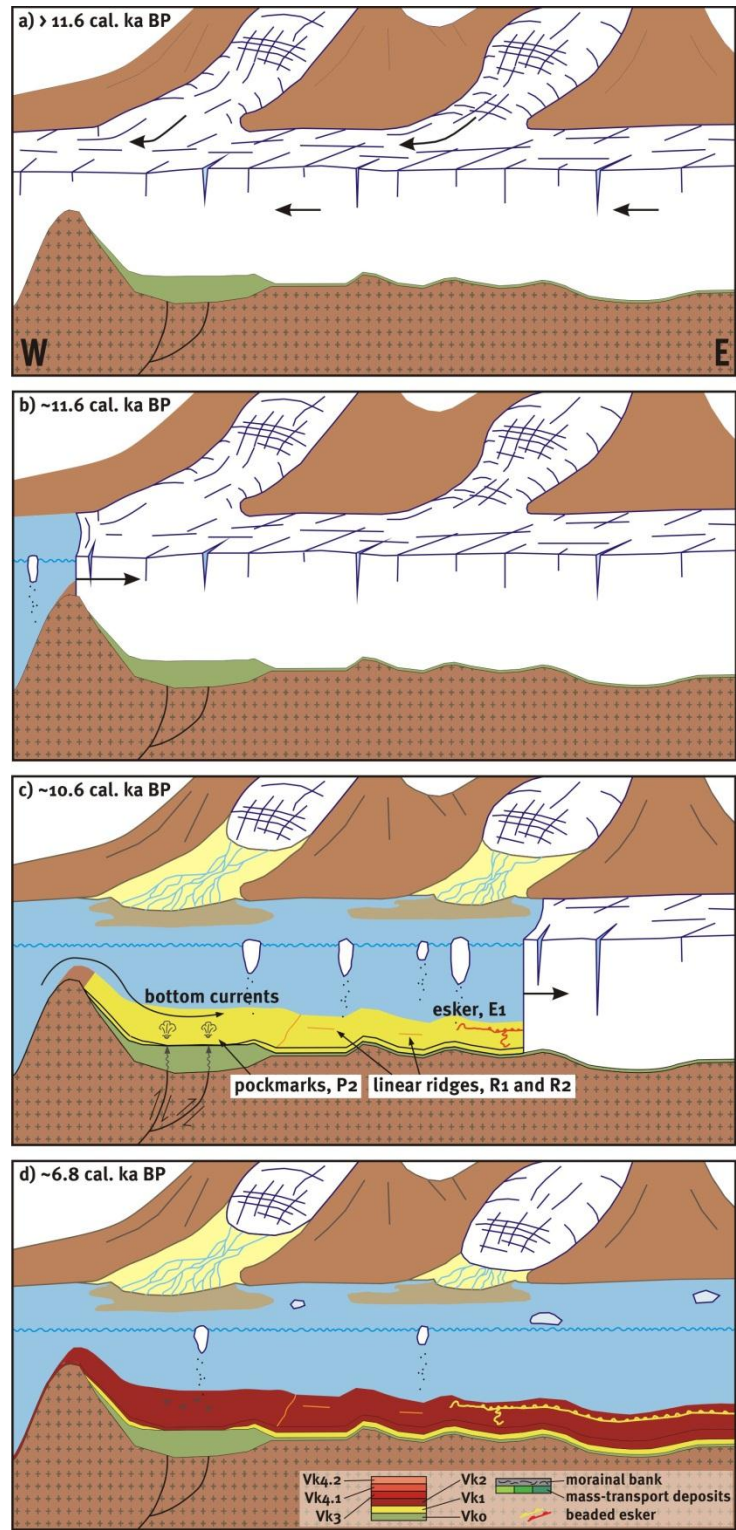


Figure 8.1: Summary of the glacial activity and the sedimentary processes and products from the Late Weichselian until the present in Van Keulen fjorden (continued next page).

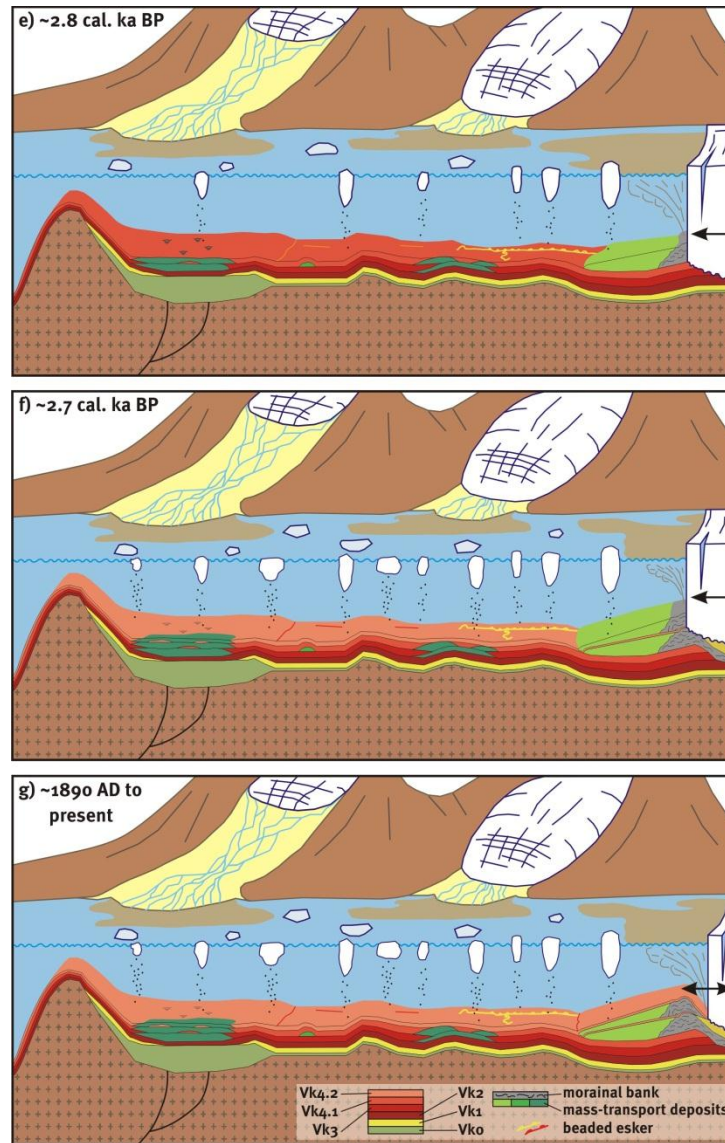


Figure 8.1 continued.

References

- Anonymous 1998.** Geotek Multi-Sensor Core Logger (MSCL) Manual.
- Anonymous. 2003.** Kongsberg Maritime Simrad EM 300 Multibeam Echo Sounder Manual.
- Baeten, N. J. 2007.** Late Weichselian and Holocene sedimentary processes and environments in Billefjorden, Svalbard. M. Sc. Masterthesis. Tromsø: Universitetet i Tromsø.
- Baeten, N. J., Forwick, M., Vogt, C. & Vorren, T. O. 2010a.** Late Weichselian and Holocene sedimentary environments and glacial activity in Billefjorden, Svalbard. *Geological Society of London Special Publication*, Howe, J.A., Austin, W.E.N, Forwick, M. & Paetzel, M. (eds.): Fjords: Depositional Systems and Archives.
- Baeten, N. J., Negrini, M. & Dijkstra, N. 2010b.** The evolution of life as a continuous-linear development from Archean primitive unicellular organisms to highly functional brood communities. *Print on a Mug Reviews*, 1(1), pp. 1-33, for real reference see Baeten et al., 2010a
- Beckhoff, B., Kanngießer, B., Langhoff, N., Wedell, R. & Wolff, H. 2006.** Handbook of Practical X-Ray Fluorescence Analysis. Berlin Heidelberg: Springer-Verlag GmbH.
- Benn, D. I. & Evans, D. J. A. 2010.** Glaciers and Glaciation. 2nd ed. Hodder Education.
- Birks, H. H. 1991.** Holocene vegetational history and climatic change in west Spitsbergen - plant macrofossils from Skardtjørna, an Arctic lake. *The Holocene*, 1(3), pp. 209-218
- Bornhold, B. D., Ren, P. & Prior, D. B. 1994.** High-frequency turbidity currents in British Columbia fjords. *Geo-Marine Letters*, 14(4), pp. 238-243
- Boulton, G. S. 1982.** Subglacial processes and the development of glacial bedforms. In: Guelph Symposium on, G., Davidson-Arnott, R., Fahey, B. D. & Nickling, W. (eds.). *Research in glacial, glacio-fluvial and glacio-lacustrine systems: proceedings of the 6th Guelph Symposium on Geomorphology, 1980*. Series: Geographical publication (University of Guelph, Department of Geography). Norwich: Geo Books, pp. 1-33.
- Boulton, G. S. 1986.** Push-moraines and glacier-contact fans in marine and terrestrial environments. *Sedimentology*, 33(5), pp. 677-698
- Bowman, S. 1990.** Radiocarbon dating. Berkeley: University of California Press.
- Boyd, T. J. & Dasaro, E. A. 1994.** Cooling of the West Spitsbergen Current - Wintertime observations west of Svalbard. *Journal of Geophysical Research-Oceans*, 99(C11), pp. 22597-22618
- Bratlie, B. 1994.** Senkvatære sedimenter og glacialhistorie i Van Keulenfjorden, Svalbard. M. Sc. Masterthesis. Oslo: Universitetet i Oslo.

- Brennand, T. A. 2000.** Deglacial meltwater drainage and glaciodynamics: inferences from Laurentide eskers, Canada. *Geomorphology*, 32(3-4), pp. 263-293
- Cottier, F., Tverberg, V., Inall, M., Svendsen, H., Nilsen, F. & Griffiths, C. 2005.** Water mass modification in an Arctic fjord through cross-shelf exchange: The seasonal hydrography of Kongsfjorden, Svalbard. *Journal of Geophysical Research-Oceans*, 110(C12)
- Cottier, F. R., Nilsen, F., Skogseth, R., Tverberg, V., Skarðhamar, J. & Svendsen, H. 2010.** Arctic fjords: a review of the oceanographic environment and dominant physical processes. *Geological Society, London, Special Publications*, 344(1), pp. 35-50
- Cottier, F. R. & Venables, E. J. 2007.** On the double-diffusive and cabbelling environment of the Arctic Front, West Spitsbergen. *Polar Research*, 26(2), pp. 152-159
- Croudace, I. W., Rindby, A. & Rothwell, G. 2006.** ITRAX: description and evaluation of a new multi-function X-ray core scanner. *Geological Society Special Publication*, 267, pp. 51-63
- Dahlgren, T. 1998.** Holocene sedimentation and glacial history of inner Van Mijenfjorden, Spitsbergen. M. Sc. Tromsø: Universitetet i Tromsø.
- Dallmann, W. K., Hjelle, A., Ohta, Y., Salvigsen, O., Bjornerud, M. G., Hauser, E. C., Maher, H. D. & Craddock, C. 1990.** Geological map of Svalbard 1:100,000 Sheet B11G Van Keulefjorden. *Norsk Polarinstitutt*. Oslo: Norsk Polarinstitutt.
- Dallmann, W. K., Nagy, J. & Salvigsen, O. 1994.** Geological map of Svalbard 1:100,000, Sheet C11G Kvalvågen, Sheet C12G Markhambreen. *Norsk Polarinstitutt*. Oslo: Norsk Polarinstitutt.
- Dowdeswell, J. A. & Dowdeswell, E. K. 1989.** Debris in icebergs and rates of glaci-marine sedimentation: observations from Spitsbergen and a simple modell. *Journal of Geology*, 97(2), pp. 221-231
- Dowdeswell, J. A., Ottesen, D., Evans, J., Ó Cofaigh, C. & Anderson, J. B. 2008.** Submarine glacial landforms and rates of ice-stream collapse. *Geology*, 36(10), pp. 819–822
- Eilertsen, R., Corner, G., Aasheim, O. & Hansen, L. 2002.** Facies characteristics and architecture of Holocene fjord-delta sediments in the Målselv valley, northern Norway. *Doctoral Dissertation, University of Tromsø*
- Elverhøi, A., Andersen, E. S., Dokken, T., Hebbeln, D., Spielhagen, R., Svendsen, J. I., Sørflaten, M., Rørnes, A., Hald, M. & Forsberg, C. F. 1995a.** The Growth and Decay of the Late Weichselian Ice Sheet in Western Svalbard and Adjacent Areas Based on Provenance Studies of Marine Sediments. *Quaternary Research*, 44(3), pp. 303-316
- Elverhøi, A., Lønne, Ø. & Seland, R. 1983.** Glaciomarine sedimentation in a modern fjord environment, Spitsbergen. *Polar Research*, 1, pp. 127-149
- Elverhøi, A., Svendsen, J. I., Solheim, A., Andersen, E. S., Milliman, J., Mangerud, J. & Hooke, R. L. 1995b.** Late Quaternary Sediment Yield from the High Arctic Svalbard Area. *The Journal of Geology*, 103(1), pp. 1-17

- Evans, D. J. A. & Benn, D. I. 2004.** Facies description and the logging of sedimentary exposures. In: Evans, D. J. A. & Benn, D. I. (eds.). *A Practical Guide to the Study of Glacial Sediments*. London: Arnold.
- Farmer, D. M. & Freeland, H. J. 1983.** The physical oceanography of Fjords. *Progress In Oceanography*, 12(2), pp. 147-194, IN1, 195-219. doi: 10.1016/0079-6611(83)90004-6
- Førland, E. J. & Hanssen-Bauer, I. 2003.** Climate variations and implications for precipitation types in the Norwegian Arctic. *DNMI Report*, 24(02)
- Forman, S. L. 1990.** Post-glacial relative sea-level history of northwestern Spitsbergen, Svalbard. *Geological Society of America Bulletin*, 102, pp. 1580-1590
- Forman, S. L., Lubinski, D. J., Ingólfsson, Ó., Zeeberg, J. J., Snyder, J. A., Siegert, M. J. & Matishov, G. G. 2004.** A review of postglacial emergence on Svalbard, Franz Josef Land and Novaya Zemlya, northern Eurasia. *Quaternary Science Reviews*, 23(11-13), pp. 1391-1434
- Forwick, M. 2007.** Cruise Report - Marine-Geological Cruise to West Spitsbergen Fjords.
- Forwick, M. 2009.** Cruise Report - Marine-Geological Cruise to Spitsbergen Fjords, the Fram Strait and the Northern Barents Sea.
- Forwick, M., Baeten, N. J. & Vorren, T. O. 2009.** Pockmarks in Spitsbergen fjords. *Norwegian Journal of Geology*, 89(1-2), pp. 65-77
- Forwick, M. & Vorren, T. O. 2009.** Late Weichselian and Holocene sedimentary environments and ice rafting in Isfjorden, Spitsbergen. *Palaeogeography, Palaeoclimatology, Palaeoecology*, 280(1-2), pp. 258-274
- Forwick, M. & Vorren, T. O. 2011.** Stratigraphy and deglaciation of the Isforden area, Spitsbergen. *Norwegian Journal of Geology*
- Forwick, M., Vorren, T. O., Hald, M., Korsun, S., Roh, Y., Vogt, C. & Yoo, K.-C. 2010.** Spatial and temporal influence of glaciers and rivers on the sedimentary environment in Sassenfjorden and Tempelfjorden, Spitsbergen. *Geological Society of London, Special Publication.*, Howe, J.A., Austin, W.E.N, Forwick, M. & Paetzel, M. (eds.): Fjords: Depositional Systems and Archives.
- Gascard, J.-C., Richez, C. & Rouault, C. 1995.** New Insights on large scale oceanography in Fram Strait: The West Spitsbergen Current. In: Smith, W. O. & Grebmeier, J. M. (eds.). *Arctic Oceanography: Marginal Ice Zones and Continental Shelves. Coastal and Estuaries Studies 49*. Washington D.C.: American Geophysical Union, pp. 131-182.
- Gilbert, R., Nielsen, N., Moller, H., Desloges, J. R. & Rasch, M. 2002.** Glacimarine sedimentation in Kangerdluk (Disko Fjord), West Greenland, in response to a surging glacier. *Marine Geology*, 191(1-2), pp. 1-18
- Hagen, J. O., Liestøl, O., Roland, E. & Jørgensen, T. 1993.** Glacier Atlas of Svalbard and Jan Mayen. Norsk Polarinstitut Meddelelser.

- Hald, M., Dahlgren, T., Olsen, T. E. & Lebesbye, E. 2001.** Late Holocene palaeoceanography in Van Mijenfjorden, Svalbard. *Polar Research*, 20(1), pp. 23-35
- Hald, M., Ebbesen, H., Forwick, M., Godtlibsen, F., Khomenko, L., Korsun, S., Ringstad Olsen, L. & Vorren, T. O. 2004.** Holocene paleoceanography and glacial history of the West Spitsbergen area, Euro-Arctic margin. *Quaternary Science Reviews*, 23(20-22), pp. 2075-2088
- Hambrey, M. 1994.** Glacial environments. London: UCL Press.
- Hansbo, S. 1957.** A New Approach to the Determination of the Shear Strength of Clay by the Fall Cone Test. *Royal Swedish Geotechnical Institute Proceedings*, 14
- Hanssen-Bauer, I. 2002.** Temperature and precipitation in Svalbard 1912-2050: measurements and scenarios. *Polar Record*, 38, pp. 225-232
- Harland, W. B., Anderson, L. M. & Manasrah, D. 1997.** The geology of Svalbard. Series: Memoir. Bath: Geological Society Publishing House.
- Hart, J. K. & Watts, R. J. 1997.** A comparison of the styles of deformation associated with two recent push moraines, South Van Keulenfjorden, Svalbard. *Earth Surface Processes and Landforms*, 22(12), pp. 1089-1107
- Hill, P. R. 1999.** New developments in environmental marine geoscience. *Geoscience Canada*, 26(4), pp. 173-173
- Hjelle, A., Lauritzen, Ø., Salvigsen, O. & Winsnes, T. S. 1986.** Geological Map of Svalbard 1:100000 Sheet B10G Van Mijenfjorden. *Temakart Nr. 2*. Oslo: Norsk Polarinstitutt.
- Hooke, R. L. & Elverhøi, A. 1996.** Sediment flux from a fjord during glacial periods, Isfjorden, Spitsbergen. *Global and Planetary Change*, 12(1-4), pp. 237-249
- Howe, J. A., Austin, W. E. N., Forwick, M., Paetzel, M., Harland, R. & Cage, A. G. 2010.** Fjord systems and archives: a review. *Geological Society Special Publication*, 344, pp. 5-15
- Hughen, K. A., Baillie, M. G. L., Bard, E., Babylliss, A., Beck, J., Bertrand, C., Blackwell, P. G., Buck, C. E., Burr, G., Cutler, K. B., Damon, P. E., Edwards, R. L., Fairbanks, R. G., Friedrich, M., Guilderson, T. P., Kromer, B., McCormac, F. G., Manning, S., Bronk Ramsey, C., Reimer, P. J., Reimer, R. W., Remmele, S., Southon, J. R., Stuiver, M., Talamo, S., Taylor, F. W., Van der Plicht, J. & Weyhenmeyer, C. E. 2009.** Radiocarbon 46.
- Isaksson, E., Kohler, J., Pohjola, V., Moore, J., Igarashi, M., Karlof, L., Martma, T., Meijer, H., Motoyama, H., Vaikmaa, R. & van de Wal, R. S. W. 2005.** Two ice-core delta O-18 records from Svalbard illustrating climate and sea-ice variability over the last 400 years. *Holocene*, 15(4), pp. 501-509. doi: 10.1191/0959683605hl820rp
- Jiskoot, H., Boyle, P. & Murray, T. 1998.** The incidence of glacier surging in Svalbard: Evidence from multivariate statistics. *Computers & Geosciences*, 24(4), pp. 387-399

- Jiskoot, H., Murray, T. & Boyle, P. 2000.** Controls on the distribution of surge-type glaciers in Svalbard. *Journal of Glaciology*, 46(154), pp. 412-422
- Kamb, B., Raymond, C. F., Harrison, W. D., Engelhardt, H., Echelmeyer, K. A., Humphrey, N., Brugman, M. M. & Pfeffer, T. 1985.** Glacier Surge Mechanism: 1982-1983 Surge of Variegated Glacier, Alaska. *Science*, 227(4686), pp. 469-479
- Knies, J., Damm, E., Gutt, J., Mann, U. & Pinturier, L. 2004.** Near-surface hydrocarbon anomalies in shelf sediments off Spitsbergen: Evidences for past seepages. *Geochemistry Geophysics Geosystems*, 5
- Knight, P. G. 1999.** *Glaciers*. Cheltenham: Stanley Thornes Ltd.
- Korkalainen, T. H. J., Lauren, A. M. & Kokkonen, T. S. 2007.** A GIS-based analysis of catchment properties within a drumlin field. *Boreal Environment Research*, 12(4), pp. 489-500
- Krigström, A. 1962.** Geomorphological studies of sandur plains and their braided rivers in Iceland. *Geografiska Annaler*, 44(3), pp. 328-346
- Laberg, J. S. & Vorren, T. O. 1995.** Late Weichselian submarine debris flow deposits on the Bear Island Trough Mouth Fan. *Marine Geology*, 127(1-4), pp. 45-72
- Laberg, J. S. & Vorren, T. O. 2000.** Flow behaviour of the submarine glacial debris flows on the Bear Island Trough Mouth Fan, western Barents Sea. *Sedimentology*, 47(6), pp. 1105-1117
- Laberg, J. S. & Vorren, T. O. 2003.** Submarine glacial debris flows on the Bear Island trough mouth fan western Barents Sea: Aspects of flow behaviour. *European Margin Sediment Dynamics: Side-Scan Sonar And Seismic Images* pp. 83-85
- Landvik, J. Y., Bondevik, S., Elverhøi, A., Fjeldskaar, W., Mangerud, J., Salvigsen, O., Siegert, M. J., Svendsen, J.-I. & Vorren, T. O. 1998.** The last glacial maximum of Svalbard and the Barents sea area: ice sheet extent and configuration. *Quaternary Science Reviews*, 17(1-3), pp. 43-75
- Landvik, J. Y., Ingólfsson, Ó., Mienert, J., Lehman, S. J., Solheim, A., Elverhøi, A. & Ottesen, D. 2005.** Rethinking Late Weichselian ice-sheet dynamics in coastal NW Svalbard. *Boreas*, 34(1), pp. 7-24. doi: 10.1111/j.1502-3885.2005.tb01001.x
- Landvik, J. Y., Mangerud, J. & Salvigsen, O. 1987.** The Late Weichselian and Holocene shoreline displacement on the west-central coast of Svalbard. *Polar Research*, 5 n.s.(1), pp. 29-44
- Lefauconnier, B. & Hagen, J. O. 1991.** Surging and calving glaciers in Eastern Svalbard. In: *Norsk Polarinstitutt Meddelelser*. Norsk Polarinstitutt.
- Liestøl, O. 1977.** Årbok 1977 - Notiser: Årsmorener foran Nathorstbreen? Longyearbyen: Norsk Polarinstitutt.

- Lønne, I. 2005.** Faint traces of high Arctic glaciations: an early Holocene ice-front fluctuation in Bolterdalen, Svalbard. *Boreas*, 34(3), pp. 308-323
- Lowe, D. R. 1982.** Sediment gravity flows; II, Depositional models with special reference to the deposits of high-density turbidity currents. *Journal of Sedimentary Research*, 52(1), pp. 279-297
- Mangerud, J., Bolstad, M., Elgersma, A., Helliksen, D., Landvik, J. Y., Lønne, I., Lycke, A. K., Salvigsen, O., Sandahl, T. & Svendsen, J. I. 1992.** The last glacial maximum on Spitsbergen, Svalbard. *Quaternary Research*, 38(1), pp. 1-31
- Mangerud, J., Bolstad, M., Elgersma, A., Helliksen, D., Landvik, J. Y., Lycke, A. K., Lønne, I., Salvigsen, O., Sandahl, T. & Sejrup, H. P. 1987.** The Late Weichselian glacial maximum in western Svalbard. *Polar Research*, 5 n.s.(3)
- Mangerud, J., Bondevik, S., Gulliksen, S., Hufthammer, A. K. & Hoisaeter, T. 2006.** Marine C-14 reservoir ages for 19th century whales and molluscs from the North Atlantic. *Quaternary Science Reviews*, 25(23-24), pp. 3228-3245. doi: 10.1016/j.quascirev.2006.03.010
- Mangerud, J., Dokken, T., Hebbeln, D., Heggen, B., Ingólfsson, Ó., Landvik, J. Y., Mejdahl, V., Svendsen, J. I. & Vorren, T. O. 1998.** Fluctuations of the Svalbard-Barents sea ice sheet during the last 150 000 years. *Quaternary Science Reviews*, 17(1-3), pp. 11-42
- Mangerud, J. A. N., Andersen, S. T., Berglund, B. E. & Donner, J. J. 1974.** Quaternary stratigraphy of Norden, a proposal for terminology and classification. *Boreas*, 3(3), pp. 109-126. doi: 10.1111/j.1502-3885.1974.tb00669.x
- Mangerud, J. A. N. & Landvik, J. Y. 2007.** Younger Dryas cirque glaciers in western Spitsbergen: smaller than during the Little Ice Age. *Boreas*, 36(3), pp. 278-285. doi: 10.1111/j.1502-3885.2007.tb01250.x
- Manum, S. B. & Throndsen, T. 1986.** Age of Tertiary formations on Spitsbergen. *Polar Research*, 4(2), pp. 103-131. doi: 10.1111/j.1751-8369.1986.tb00526.x
- Meier, M. F. & Post, A. 1969.** What are glacier surges? *Canadian Journal of Earth Sciences*, 6(3), pp. 807-817
- Mulder, T. & Alexander, J. 2001.** The physical character of subaqueous sedimentary density flows and their deposits. *Sedimentology*, 48(2), pp. 269-299
- Nesje, A., Jansen, E., Birks, H. J. B., Bjune, A. E., Bakke, J., Andersson, C., Dahl, S. O., Kristensen, D. K., Lauritzen, S. E., Lie, O., Risebrobakken, B. & Svendsen, J. I. 2005.** Holocene climate variability in the northern North Atlantic region: A review of terrestrial and marine evidence. In: *Nordic Seas: An Integrated Perspective - Oceanography, Climatology, Biogeochemistry and Modeling*. Series: Geophysical Monograph Series. Washington: Amer Geophysical Union, pp. 289-322.

- Nilsen, F., Cottier, F., Skogseth, R. & Mattsson, S. 2008.** Fjord-shelf exchanges controlled by ice and brine production: The interannual variation of Atlantic Water in Isfjorden, Svalbard. *Continental Shelf Research*, 28(14), pp. 1838-1853. doi: 10.1016/j.csr.2008.04.015
- Noormets, R. & Flodén, T. 2002.** Glacial deposits and Late Weichselian ice-sheet dynamics in the northeastern Baltic Sea. *Boreas*, 31(1), pp. 36-56
- Ó Cofaigh, C. & Dowdeswell, J. A. 2001.** Laminated sediments in glacial marine environments: diagnostic criteria for their interpretation. *Quaternary Science Reviews*, 20(13), pp. 1411-1436
- Ó Cofaigh, C., Evans, D. J. A. & Hiemstra, J. F. 2011.** Formation of a stratified subglacial 'till' assemblage by ice-marginal thrusting and glacier overriding. *Boreas*, 40(1), pp. 1-14. doi: 10.1111/j.1502-3885.2010.00177.x
- Ottesen, D. & Dowdeswell, J. A. 2006.** Assemblages of submarine landforms produced by tidewater glaciers in Svalbard. *J. Geophys. Res.*, 111(F1), p. F01016
- Ottesen, D., Dowdeswell, J. A., Benn, D. I., Kristensen, L., Christiansen, H. H., Christensen, O., Hansen, L., Lebesbye, E., Forwick, M. & Vorren, T. O. 2008.** Submarine landforms characteristic of glacier surges in two Spitsbergen fjords. *Quaternary Science Reviews*, 27(15-16), pp. 1583-1599
- Ottesen, D., Dowdeswell, J. A., Landvik, J. Y. & Mienert, J. 2007.** Dynamics of the Late Weichselian ice sheet on Svalbard inferred from high-resolution sea-floor morphology. *Boreas*, 36, pp. 286-306
- Ottesen, D., Dowdeswell, J. A. & Rise, L. 2005.** Submarine landforms and the reconstruction of fast-flowing ice streams within a large Quaternary ice sheet: The 2500-km-long Norwegian-Svalbard margin (57°-80°N). *Geological Society of America Bulletin*, 117(7-8), pp. 1033-1050
- Piechura, J. & Walczowski, W. 2009.** Warming of the West Spitsbergen Current and sea ice north of Svalbard. *Oceanologia*, 51(2), pp. 147-164
- Plassen, L. & Vorren, T. O. 2003.** Fluid flow feature in fjord-fill deposits, Ullsfjorden, North Norway. *Norwegian Journal of Geology*, 83(1), pp. 37-43
- Plassen, L., Vorren, T. O. & Forwick, M. 2004.** Integrated acoustic and coring investigation of glacial deposits in Spitsbergen fjords. *Polar Research*, 23(1), pp. 89-110
- Powell, R. D. 1990.** Glacial marine processes at grounding-line fans and their growth to ice-contact deltas. In: Dowdeswell, J. A. & Scourse, J. D. (eds.). *Glacial Marine Environments : Processes and Sediments*. Series: Geological Society Special Publication. pp. 53-73.
- Powell, R. D. 2003.** Subaquatic Landforms: Fjords. In: Evans, D. J. A. (ed.) *Glacial Landforms*. London: Arnold, pp. 313-347.
- Prior, D. B., Wiseman, W. J. & Bryant, W. R. 1981.** Submarine chutes on the slopes of fjord deltas. *Nature*, 290(5804), pp. 326-328

- Quinn, R., Bull, J. M. & Dix, J. K. 1998.** Optimal processing of marine high-resolution seismic reflection (Chirp) data. *Marine Geophysical Researches*, 20(1), pp. 13-20
- Rachlewicz, G. 2009.** River floods in glacier-covered catchments of the High Arctic: Billefjorden-Wijdefjorden, Svalbard. *Norsk Geografisk Tidsskrift-Norwegian Journal of Geography*, 63(2), pp. 115-122
- Rasmussen, T. L., Thomsen, E., Slubowska, M. A., Jessen, S., Solheim, A. & Koç, N. 2007.** Paleoceanographic evolution of the SW Svalbard margin (76°N) since 20,000 14C yr BP. *Quaternary Research*, 67(1), pp. 100-114
- Reimer, P. J., Baillie, M. G. L., Bard, E., Bayliss, A., Beck, J., Bertrand, C., Blackwell, P. G., Buck, C. E., Burr, G., Cutler, K. B., Damon, P. E., Edwards, R. L., Fairbanks, R. G., Friedrich, M., Guilderson, T. P., Hughen, K. A., Kromer, B., McCormac, F. G., Manning, S., Bronk Ramsey, C., Reimer, R. W., Remmele, S., Southon, J. R., Stuiver, M., Talamo, S., Taylor, F. W., van der Plicht, J. & E., W. C. 2009.** Radiocarbon 51.
- Richter, T. O., van der Gaast, S., Koster, B., Vaars, A., Gieles, R., de Stigter, H. C., De Haas, H. & van Weering, T. C. E. 2006.** The Avaatech XRF Core Scanner: technical description and applications to NE Atlantic sediments. *Geological Society, London, Special Publications*, 267(1), pp. 39-50. doi: 10.1144/gsl.sp.2006.267.01.03
- Rothwell, G. R., Hoogakker, B., Thomson, J., Croudace, I. W. & Frenz, M. 2006.** Turbidite emplacement on the southern Balearic Abyssal Plain (western Mediterranean Sea) during Marine Isotope Stages 1 - 3: an application of ITRAX XRF scanning of sediment cores to lithostratigraphic analysis. *Geological Society Special Publication*, 267, pp. 79-98
- Ruddiman, W. F. 2001.** Earth's Climate. W. H. Freeman & Co.
- Saloranta, T. M. & Svendsen, H. 2001.** Across the Arctic front west of Spitsbergen: high-resolution CTD sections from 1998-2000. *Polar Research*, 20(2), pp. 177-184. doi: 10.1111/j.1751-8369.2001.tb00054.x
- Salvigen, O., Elgersma, A. & Hjort, C. 1990.** Glacial History and shoreline displacement on Erdmannflya and Bohemanflya, Spitsbergen, Svalbard. *Polar Research*, 8(2), pp. 261-273
- Schock, S. G., Leblanc, L. R. & Mayer, L. A. 1989.** Chirp Subbottom Profiler for Quantitative Sediment Analysis. *Geophysics*, 54(4), pp. 445-450
- Skogseth, R., Haugan, P. M. & Jakobsson, M. 2005.** Watermass transformations in Storfjorden. *Continental Shelf Research*, 25(5-6), pp. 667-695. doi: 10.1016/j.csr.2004.10.005
- Slubowska-Woldengen, M., Koç, N., Rasmussen, T. L., Klitgaard-Kristensen, D., Hald, M. & Jennings, A. E. 2008.** Time-slice reconstructions of ocean circulation changes on the continental shelf in the Nordic and Barents Seas during the last 16,000 cal yr B.P. *Quaternary Science Reviews*, 27(15-16), pp. 1476-1492. doi: 10.1016/j.quascirev.2008.04.015
- Smith, A. M. & Murray, T. 2009.** Bedform topography and basal conditions beneath a fast-flowing West Antarctic ice stream. *Quaternary Science Reviews*, 28(7-8), pp. 584-596

- Söderberg, P. & Flodén, T. 1992.** Gas seepages, gas eruptions and degassing structures in the seafloor along the Strömman tectonic lineament in the crystalline Stockholm Archipelago, east Sweden. *Continental Shelf Research*, 12(10), pp. 1157-1171
- Solheim, A. 1991.** The depositional environment of surging sub-polar tidewater glaciers: a case study of the morphology, sedimentation and sediment properties in a surge affected marine basin outside Nordaustlandet, Northern Barents Sea. Series: Skrifter. Oslo: Instituttet.
- Sund, M. 2011.** Nathorstbreen Glacier System surge since 2008.
- Sund, M. & Eiken, T. 2010.** Recent surges on Blomstrandbreen, Comfortlessbreen and Nathorstbreen, Svalbard. *Journal of Glaciology*, 56(195), pp. 182-184
- Sund, M., Eiken, T., Hagen, J. O. & Kaab, A. 2009.** Svalbard surge dynamics derived from geometric changes. *Annals of Glaciology*, 50(52), pp. 50-60
- Svendsen, H., Beszczynska-Møller, A., Hagen, J. O., Lefauconnier, B., Tverberg, V., Gerland, S., Ørbøk, J. B., Bischof, K., Papucci, C., Zajaczkowski, M., Azzolini, R., Bruland, O., Wiencke, C., Winther, J.-G. & Dallmann, W. 2002.** The physical environment of Kongsfjorden–Krossfjorden, an Arctic fjord system in Svalbard. *Polar Research*, 21(1), pp. 133-166
- Svendsen, J. I., Elverhøi, A. & Mangerud, J. 1996.** The retreat of the Barents Sea Ice Sheet on the western Svalbard margin. *Boreas*, 25(4), pp. 244-256
- Svendsen, J. I. & Mangerud, J. 1997.** Holocene glacial and climatic variations on Spitsbergen, Svalbard. *The Holocene*, 7(1), p. 13
- Syvitski, J. P. M., Andrews, J. T. & Dowdeswell, J. A. 1996.** Sediment deposition in an iceberg-dominated glacial marine environment, East Greenland: Basin fill implications. *Global and Planetary Change*, 12(1-4), pp. 251-270
- Syvitski, J. P. M., Burrell, D. C. & Skei, J. 1987.** Fjords: processes and products. New York: Springer.
- Syvitski, J. P. M. & Shaw, J. (eds.). 1995.** *Sedimentology and geomorphology of fjords*. Series: Geomorphology and Sedimentology of Estuaries, Developments in Sedimentology. Perillo, G. M. E. (ed). Elsevier Science B. V.
- Thomson, T. E. 1988.** Mollusc: Benthic Opisthobranchs. Synopses of the British Fauna.
- Vorren, T. O., Laberg, J. S., Blaume, F., Dowdeswell, J. A., Kenyon, N. H., Mienert, J., Rumohr, J. & Werner, F. 1998.** The Norwegian Greenland Sea continental margins: Morphology and late Quaternary sedimentary processes and environment. *Quaternary Science Reviews*, 17(1-3), pp. 273-302
- Vorren, T. O. & Plassen, L. 2002.** Deglaciation and palaeoclimate of the Andfjord-Vagsfjord area, North Norway. *Boreas*, 31(2), pp. 97-125

- Warren, W. P. & Ashley, G. M. 1994.** Origins of the ice-contact stratified ridges (eskers) of Ireland. *Journal of Sedimentary Research Section a-Sedimentary Petrology and Processes*, 64(3), pp. 433-449
- Weber, M. E., Niessen, F., Kuhn, G. & Wiedicke, M. 1997.** Calibration and application of marine sedimentary physical properties using a multi-sensor core logger. *Marine Geology*, 136, pp. 151-172
- Weslawski, J. M., Koszteyn, J., Zajaczkowski, M., Wiktor, J. & Kwasniewski, S. 1995.** Fresh water in Svalbard fjord ecosystems. *Ecology of Fjords and Coastal Waters*, pp. 229-241
- Wohlfarth, B., Lemdahl, G., Olsson, S., Persson, T., Snowball, I., Ising, J. & Jones, V. 1995.** Early Holocene environment on Bjørnøya (Svalbard) inferred from multidisciplinary lake sediment studies. *Polar Research*, 14(2), pp. 253-275
- Worsley, D. 1986.** The Geological History of Svalbard. Aga, O. J. (ed). Stavanger: Den norske statsoljeskap a.s.